INSTITUT FÜR INFORMATIK

UND PRAKTISCHE MATHEMATIK

Hypercomplex Spectral Signal Representations for the Processing and Analysis of Images

Thomas Bülow

Bericht Nr. 9903
August 1999

CHRISTIAN-ALBRECHTS-UNIVERSITÄT

KIEL

Institut für Informatik und Praktische Mathematik der
Christian-Albrechts-Universität zu Kiel
Olshausenstr. 40
D – 24098 Kiel

Hypercomplex Spectral Signal Representations for the Processing and Analysis of Images

Thomas Bülow

Bericht Nr. 9903
August 1999

e-mail: tbl@ks.informatik.uni-kiel.de

"Dieser Bericht gibt den Inhalt der Dissertation wieder, die der Verfasser
im Dezember 1998 bei der Technischen Fakultät der
Christian-Albrechts-Universität zu Kiel eingereicht hat.
Datum der Disputation: 28. April 1999"

Zusammenfassung

In der vorliegenden Arbeit werden *hyperkomplexe spektrale* Methoden für die Bildverarbeitung und -analyse eingeführt. Die Arbeit gliedert sich in drei Hauptkapitel. Im **ersten Hauptkapitel** wird die quaternionische Fouriertransformation (QFT) für 2D Signale definiert, und ihre wichtigsten Eigenschaften werden untersucht. Die QFT ist mit der 2D Fourier- und der 2D Hartleytransformation verwandt; Gemeinsamkeiten und Unterschiede dieser drei Transformationen werden unter besonderer Berücksichtigung der Symmetrieeigenschaften analysiert. Als n-dimensionale Verallgemeinerung wird die Clifford-Fouriertransformation eingeführt. Das **zweite Hauptkapitel** beschäftigt sich mit dem Konzept der Phase eines Signals. Wir unterscheiden die *globale*, *momentane* und die *lokale* Phase. Es wird gezeigt, wie diese eindimensionalen Konzepte der Phase mittels der QFT auf zweidimensionale Signale verallgemeinert werden können. Zur Verallgemeinerung der momentanen Phase wird das quaternionische analytische Signal eingeführt; zur Verallgemeinerung der lokalen Phase definieren wir quaternionische Gabor-Filter. Der in 1D bekannte Zusammenhang zwischen der lokalen Phase und der lokalen Signalstruktur wird mittels der quaternionischen Phase auf 2D erweitert. Im **dritten Hauptkapitel** werden zwei Anwendungen der vorgestellten Methoden untersucht. Sowohl zur Disparitätsschätzung als auch zur Textursegmentierung existieren Methoden, die auf der Verwendung der (komplexen) lokalen Phase basieren. Diese Methoden werden mittels der quaternionischen lokalen Phase erweitert. In beiden Fällen bleiben bestehende Eigenschaften der Methoden erhalten und werden durch die quaternionische Phase erweitert.

Abstract

In the present work *hypercomplex spectral* methods of the processing and analysis of images are introduced. The thesis is divided into three main chapters. **First** the quaternionic Fourier transform (QFT) for 2D signals is presented and its main properties are investigated. The QFT is closely related to the 2D Fourier transform and to the 2D Hartley transform. Similarities and differences of these three transforms are investigated with special emphasis on the symmetry properties. The Clifford Fourier transform is presented as nD generalization of the QFT. **Secondly** the concept of the phase of a signal is considered. We distinguish the *global*, the *local* and the *instantaneous* phase of a signal. It is shown how these 1D concepts can be extended to 2D using the QFT. In order to extend the concept of *global phase* we introduce the notion of the quaternionic analytic signal of a real signal. Defining quaternionic Gabor filters leads to the definition of the local quaternionic phase. The relation between signal structure and local signal phase, which is well-known in 1D, is extended to 2D using the quaternionic phase. In the **third** part two application of the theory are presented. For the image processing tasks of disparity estimation and texture segmentation there exist approaches which are based on the (complex) local phase. These methods are extended to the use of the quaternionic phase. In either case the properties of the complex approaches are preserved while new features are added by using the quaternionic phase.

1. Gutachter	Prof. Dr. Gerald Sommer (Kiel)
2. Gutachter	Prof. Dr. Ulrich Heute (Kiel)
3. Gutachter	Prof. Dr. Bernd Jähne (Heidelberg)

Datum der mündlichen Prüfung:	28. April 1999

Acknowledgment

The making of this thesis would not have been possible without the support of a lot of helpful people. It is a pleasure for me to take the opportunity to thank them here.

First of all I thank my supervisor Professor Gerald Sommer, head of the cognitive systems group at the Christian Albrechts University of Kiel, whose scientific vision was a guiding light for me during the past few years. He suggested me to work on the subject of hypercomplex algebras in signal processing, and supervised and guided this work through many stimulating and critical discussions and remarks. I am grateful to him also for having given me the opportunity of presenting my work at many conferences, starting at an early stage of my PhD studies. By this he gave me the chance to discuss my work in the community and to improve it by that.

I also thank the Co-referees Professor B. Jähne and Professor U. Heute for pointing me to possible improvements and for giving hints which found their way into the final version of the text.

Professor Hahn, whose work on complex signals with single orthant spectra inspired major parts of chapter 3 of this thesis, suggested several modifications on the occasion of a personal meeting in Warsaw.

I thank Professor Kostas Daniilidis for his interest in my work and several discussions on the subject. He was and is a steady source of motivation.

I appreciated the work with my former student Dipl.-Ing. Michael Felsberg who developed and implemented the fast QFT algorithm.

The "Studienstiftung des deutschen Volkes" provided me with a scholarship during my Phd studies. They also were always generous and gave additional financial support such that I could join the "conference tourism".

Dr. Gregory Baratoff helped to improve the language of this thesis. I want to thank him for taking on the hard and time-consuming task of correcting my English. (It is not necessary to note that I account for the bunch of remaining mistakes.)

Indispensable for surviving even the hard periods in the life of a PhD student is the atmosphere in the institute. I am happy to thank my colleagues for providing a friendly and helpful ambiance. I am grateful to our secretary Francoise Maillard for providing help in all clerical matters and especially for being the good spirit of the institute.

I owe the biggest gratitude to my wife Olga who did not see much of me during the final months of finishing this thesis. I thank her for her love, understanding and moral support. Special thanks to my son Jan Nikolai, who was born two days after I submitted the thesis, for waiting patiently for this work to end.

Finally, I thank my parents for being confident about my ability to finish this work successfully. Their confidence gave me the necessary self assurance not only for this part of my life.

Contents

Chapter 1

Introduction

1.1 Motivation

The methods presented in this thesis belong to low level image processing[1], which comprises the first processing steps in any image recognition or computer vision task. The characterization of these methods is that they transform raw image data into a first pre-symbolic representation. The data considered are discrete gray-value images, i.e. matrices of real numbers in mathematical terms. However, in this thesis most of the methods will first be defined for continuous signals. Afterwards discretized versions of these methods are applied to the discrete data.

Spectral signal representations are of high importance in image processing. The power of the Fourier transform, which yields a spectral representation of a given signal, is well-known. It provides a powerful tool for the manipulation as well as for the analysis of signals. In image processing we are often interested in local spectral properties. Sometimes this is expressed in the question: **What is where?** [97, 98]. One of the most prominent tools for local spectral image processing and analysis is the Gabor filter. Gabor filters are simultaneously optimally localized in the spatial and in the frequency domain. Thus, spatial and frequency properties are optimally analyzed at the same time by Gabor filters. In the 80's this resolved the question whether spatial or spectral features are more important in the mammalian visual system [28], since the profiles of cortical receptive fields were found to strongly resemble the impulse responses of Gabor filters.

[1] In the general n-dimensional case we will also use the term *signal processing* instead of *image processing* which is restricted to 2D.

Gabor filters are linear shift invariant (LSI) filters, which makes it very convenient to use them: LSI-filters can be applied by simply convolving the signal with the impulse response of the filter. In this thesis we often use the term *filter* as an abbreviation of *impulse response of a linear shift-invariant filter* when no confusion is possible.

Our interest in Gabor filters is based on their property of giving access to the local phase of a signal. The local phase of a real signal is defined as the angular phase of its complex filter response. It has been shown that there is a close correspondence between the local structure of a signal and its local phase [47, 45]. This correspondence has been used in different fields of image analysis and computer vision, such as texture analysis [11] and disparity estimation [42]. The relation between structure and phase was first established for one-dimensional signals and later extended to signals of higher dimension. However, the way of extension is not satisfactory in all respects. The impulse responses of complex Gabor filters of any dimension are Gaussian functions with a complex modulation with respect to one spatial orientation. Thus, complex Gabor filters can only capture signal variations along this one orientation. As a consequence the local phase is related merely to intrinsically one-dimensional signal structure, such that the local phase makes only sense for intrinsically one-dimensional[2] (or *simple*) signals [45].

An important aim of this thesis is to provide a concept of local phase which can be derived from linear filter responses, and is related to the intrinsically two-dimensional local structure of an image. A complex Gabor filter can be regarded as consisting of two symmetry components: a real, even component and an imaginary, odd component. These two components are not sufficient for capturing non-simple structures. This leads to **the main idea** of this thesis: we introduce filters which consist of more then two components of different symmetry. More exactly, in nD, there are 2^n components of different reflectional symmetry, with respect to the n coordinate axes. Thus, we will introduce filters consisting of 2^n components. In order not to loose the concept of *one* filter, these filters will take values in 2^n-dimensional algebras. This corresponds exactly to the one-dimensional case where Gabor filters with values in the two-dimensional algebra of complex numbers are used.

Complex Gabor filters are closely related to the Fourier transform. Actually, the impulse response of a Gabor filter is equal to the integral kernel of the Fourier transform for some frequency u, multiplied with a Gaussian function centered at the origin. While Gabor filters analyze the *local* spectral properties of a signal, the

[2] A mathematical definition of intrinsic dimensionality will be given in the following section.

Fourier transform decomposes a signal into its *global* spectral components. The Fourier transform can be considered the basis upon which Gabor filters were introduced. Thus, if one is interested in the development of Gabor filters with values in higher-dimensional algebras it is a theoretical necessity to develop and analyze the corresponding generalization of the Fourier transform.

While above we talked about local symmetry, the Fourier transform separates a real signal into two components which differ in their global symmetry. This is expressed in the well-known theorem that the Fourier transform of a real signal is hermitian. Thus, the signal is decomposed into two components of different specular symmetry with respect to the origin. Analogously to the local filter construction principle we will define an extension of the complex Fourier transform which decomposes an n-dimensional signal into its 2^n components of different specular symmetry with respect to the n coordinate axes. Again, this will be accomplished by replacing the algebra of complex numbers by a 2^n-dimensional algebra. An important task will be to check whether the main properties of the Fourier transform such as the existence of an inverse transform, the Rayleigh theorem, the convolution theorem, and the shift and modulation theorems are fulfilled or how they have to be modified.

The local phase as indicated above is related to the instantaneous phase of a real signal which is evaluated as the angular phase of its complex-valued analytic signal. While the analytic signal results from a real signal roughly speaking by suppressing the negative frequency components, leaving the positive frequency components untouched, Gabor filters have a single passband in one half of the frequency domain.[3] Since the analytic signal is most easily constructed in the frequency domain, there is a close linkage to the Fourier transform. As a third main subject of this thesis we will consider the definition of the analytic signal of a multidimensional signal. Up to now there exists no unique definition of the analytic signal of a multidimensional signal. We will analyze frequency domain constructions of analytic signal definitions. Especially, we will use the frequency domain reached by the newly defined Fourier transforms in 2^n-dimensional algebras.

[3]Actually, Gabor filters have a certain amount of their energy in the other half of the frequency domain. However, this amount is negligible in most practical applications.

1.2 Related Work

The notion *intrinsic dimensionality of a signal* mentioned above, was used by Krieger and Zetzsche [72]. They use the following definition. An n-dimensional signal f is called intrinsically m-dimensional at position $\mathbf{x} \in \mathbb{R}^n$ if it is constant with respect to $n - m$ orthogonal orientations in a neighborhood of $\mathbf{x}$ (see figure 1.1). Formally, a signal $f : \mathbb{R} \to \mathbb{R}^n$ is of intrinsic dimension m at $\mathbf{x} \in \mathbb{R}^n$ if it can be expressed in a neighborhood of $\mathbf{x} \in \mathbb{R}^n$ as

$$f(\mathbf{x}) = f(\mathbf{A}\mathbf{x}),$$

for some real $m \times n$ matrix $\mathbf{A}$ and no other $l \times n$ matrix with $l < m$.

Intrinsic dimensionality is a local signal property. Of course, the intrinsic dimensionality m can never exceed the dimension n of the signal domain. Zetzsche et al. [99] proved that it is not possible to construct linear filters which respond exclusively to signals which are locally of intrinsic dimension greater than 1.

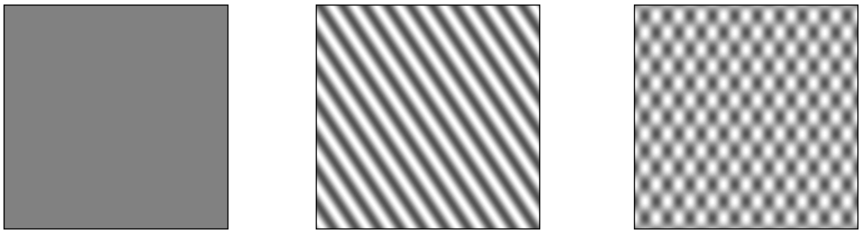

Figure 1.1: From left to right: an intrinsically 0D, 1D and 2D signal. Note, that intrinsic dimensionality is a *local* property. Each of the shown images is of constant intrinsic dimensionality.

In order to avoid confusion we mention that the notion *intrinsic dimensionality* is also used in another context. A set of data points in an n-dimensional vector space is said to have intrinsic dimension m if m is the minimum number of parameters needed to describe the set of points. An example of estimating the intrinsic dimensionality of a sequence of images is given in [17]. Assume, that the discretized images are of size N^2, each frame of the sequence is represented by a point in the N^2-dimensional signal space.

The two definitions of the intrinsic dimensionality apply to different domains. According to Zetzsche's definition intrinsic dimensionality is a local property of a function with continuous domain. Considering signals this is a property of *one signal* in the *spatial domain*. According to the second definition, intrinsic dimensionality is a geometric property of a (discrete) set of points lying within an n-dimensional vector space, i.e. a property of a *set of signals* in the *signal domain*

Throughout this thesis the first definition will be used, since we are dealing with signals. A signal which is intrinsically one-dimensional is sometimes called a *simple signal* .

Haglund [47] has proposed a definition of the local phase of n-dimensional signals. In his work he used the intrinsic one-dimensional phase in direction of the dominant signal orientation. This can be measured using the orientation tensor [45]. The phase is then given by a vector, containing the dominant orientation as well as the intrinsically one-dimensional phase with respect to this orientation. This definition is reasonable for locally simple signals.

A discretized version of the generalized Fourier transform to be introduced in this thesis has been used by Chernov [24]. His aim was to construct optimized fast algorithms for calculating the complex Fourier transform of n-dimensional signals. Ell [34, 35] used a transform similar to our definition for the analysis of linear partial differential systems. Based on this work Sangwine proposed the use of generalized Fourier transforms for the processing of color images [85].

A recent attempt to the generalization of the analytic signal of multidimensional signals has been made by Hahn [48, 49]. He defines an analytic signal as a signal with single orthant spectrum. This approach suffers from the fact that the original signal is not contained in its analytic signal. Most of the abovementioned literature will be reviewed in more detail in the appropriate sections of this thesis.

The work presented in this thesis is one component of a project initiated and guided by Sommer at the Institute of Computer Science of the University of Kiel, Germany[4]. The project is concerned with the design of behavior-based systems on the basis of the fusion of perception and action into the so-called perception-action cycle (PAC). The main interest lies in the algebraic embedding of PAC systems. It is desired to embed the different tasks of a PAC system such as signal processing, computer vision, neural computation and learning, and robotics using one unifying algebraic frame. The algebraic frame proposed by Sommer [89] is the geometric algebra. Geometric algebras are Clifford algebras in a geometric interpretation introduced by Hestenes et al. [56]. First results can be found e.g. in [9, 8, 26] (computer vision, robotics) and [7] (neural networks). For a more complete overview of the project see Sommer [89].

[4]This project is supported by the DFG grant So 320-2-1 under the title *Geometric Algebra, a Representation Frame of the Perception-Action Cycle.*

The results obtained in the field of signal processing are presented in this thesis. Since PAC systems have to deal with multidimensional signals, the ideas developed in this thesis fit into the project outlined here. Especially, it will turn out that among the 2^n-dimensional algebras used in this thesis there are mainly Clifford algebras.

1.3 Structure of the Thesis

Following the motivation given above we structure the thesis as follows. Besides this introduction and a final conclusion there are three chapters.

The subject of **chapter 2** are global harmonic transforms. Besides reviewing existing transforms, namely the Hartley transform and the complex Fourier transform, we introduce the 2D quaternionic Fourier transform (QFT). For this reason, we review the algebra of quaternions and introduce some new concepts, namely the *angular phase* of a unit quaternion and the notion of a *quaternionic hermitian* function. The latter is the appropriate extension of the notion of complex hermitian functions, since it turns out that the QFT of a real signal is quaternionic hermitian. As an extension of the QFT the n-dimensional Clifford Fourier transform is defined. This transform is compared to another class of hypercomplex harmonic transforms introduced here, which is based on *commutative* hypercomplex algebras, in contrast to the non-commutative Clifford algebras.

Chapter 3 is devoted to the concept of phase. We distinguish three different types of phase: *Global* or *Fourier phase*, *instantaneous phase* and *local phase*. In order to extend the local phase concept we first review existing approaches to the definition of a two-dimensional analytic signal. This leads in a natural way to a new definition which is based on the QFT. The quaternionic extension of the instantaneous phase and quaternionic Gabor filters are introduced. These filters are intrinsically two-dimensional, hence they fulfill the requirement posed above. Evaluating the angular phase of the quaternionic filter response gives the local quaternionic phase of a two-dimensional signal. We will establish a relation between this phase and the intrinsically two-dimensional structure of a signal.

Furthermore, we will investigate whether the two following properties of complex Gabor filters can be extended to quaternion-valued Gabor filters. First, complex Gabor filters approximate derivatives of the Gaussian function. We will examine whether quaternion-valued Gabor filters approximate partial derivatives of the two-dimensional Gaussian function as well. Second, we will test quaternionic Gabor filters for the optimal fulfillment of the two-dimensional uncertainty principle.

In **chapter 4** the theory developed in chapters 2 and 3 is applied to the two image processing tasks of *disparity estimation* and *texture segmentation*. Disparity estimation is the problem of estimating the field of displacement vectors between two given gray-value images of the same scene taken under different viewing conditions. Since the local phase is equivariant with the spatial position in the image, it is possible to estimate the disparity based on the local phase. Phase-based approaches to disparity estimation which use complex Gabor filters exist in the literature.

Texture segmentation deals with textured image. The task is to segment the images into regions of different texture. Also in this field there exist approaches using Gabor amplitude and Gabor phase. In both applications we extend known approaches which use the complex Gabor phase to the use of quaternionic Gabor filters.

At the end of each chapter we summarize the main results. It will be clear from the text, which definitions and theorems are original contributions of this work[5] and which ones are taken from the literature. Among the definitions and theorems the ones which have not occurred in the literature before are: definitions 2.4, 2.6, 2.7, 2.14, 2.16, 2.17, 3.10, 3.11, and 3.14, and the theorems 2.2, 2.6, 2.9, 2.11, 2.13, 2.16, 3.1, 3.2, and 3.3.

[5] *This work* means: this thesis, the articles [18, 19, 20, 21, 22] on which the thesis is based, or, in few cases, the student project [39] and the master's thesis [40] which were supervised by the author.

Chapter 2

Hypercomplex Harmonic Transforms

Harmonic transforms play a crucial role in signal processing. The most prominent example is the Fourier transform which is a complex transform defined for signals of arbitrary dimension. Closely related to the Fourier transform is the Hartley transform, which is a real transform. In this chapter we show that in 1D the Hartley transform and the Fourier transform can be viewed as the two levels of a hierarchy of harmonic transforms where the hierarchical order is given by the degree of symmetry-selectivity of the transform. In 2D, the Hartley transform and the Fourier transform are only the *first two levels* of a three level hierarchy, the third level of which is the quaternionic Fourier transform (QFT), first introduced by Ell [35] and Bülow and Sommer [18], independently. If we consider n-dimensional signals we end up with an $(n + 1)$-level hierarchy with the n-dimensional Clifford Fourier transform as the highest level.

The structure of this section is as follows: first, we restrict ourselves to 2D harmonic transforms. These are the topic of the following section, where we start with an introduction of the quaternion algebra. Based on this the QFT is introduced. For real applications a discrete version of the QFT is needed. Thus, we introduce the DQFT as an analogue to the DFT. Fast algorithms for computing the DQFT exist, and are presented in section 2.2.3.

Since reviews on the Fourier transform and its meaning for image processing can be found in many textbooks we will only give a very brief review of this transform and present the Hartley transform a little bit more detailed. In section 2.4 the three 2D transforms are compared and the abovementioned hierarchy is explained.

In section 2.5 the n-dimensional extension of the QFT, namely the Clifford Fourier transform (CFT) is introduced. The multiplication in Clifford algebras is not commutative which makes it sometimes difficult to work with the Clifford Fourier transform. However, it is possible to replace the Clifford algebra by a commutative algebra without changing the main properties of the transform, when applied to real-valued signals. The introduction of the commutative algebras, the corresponding transforms, and the comparison between the 2D CFT and the 2D commutative transform closes this chapter. **Note**, that if not stated otherwise, the term *algebra* always means $\mathbb{R}$-algebra in the following.

2.1 The Quaternion Algebra

In this section we review the main definitions and properties of the quaternion algebra and introduce a magnitude/phase-representation for quaternions in section 2.1.2. This representation is used throughout the rest of the thesis. For a more complete review of quaternions see e.g. [64, 36, 10]. The quaternion algebra was introduced by Hamilton in 1843 [50]. It is a four-dimensional algebra which is denoted by $\mathbb{H}$, in honor of Hamilton. The motivation for introducing quaternions was the aim to extend the geometrical meaning of *complex numbers* in the plane to 3D space through a system of *hypercomplex numbers*.

Definition 2.1 (Quaternions) *Consider the set of numbers* $q = q_0 + iq_1 + jq_2 + kq_3$, *with* $q_l \in \mathbb{R}$, $l \in \{0, 1, 2, 3\}$ *and the elements* i, j *and* k *obey the multiplication rules*

$$ij = -ji = k \quad \textit{and} \quad i^2 = j^2 = k^2 = -1. \tag{2.1}$$

Together with component-wise addition and the associative multiplication generated by (2.1) this set is an $\mathbb{R}$*-algebra, denoted by* $\mathbb{H}$ *and called the quaternion algebra.*

For the components of a quaternion q we sometimes write

$$q_0 = \mathcal{R}q, \quad q_1 = \mathcal{I}q, \quad q_2 = \mathcal{J}q, \quad q_3 = \mathcal{K}q.$$

Explicitly, these operations can be expressed as

$$\mathcal{R}q = \frac{1}{4}(q - iqi - jqj - kqk) \tag{2.2}$$

$$\mathcal{I}q = \frac{1}{4}(q - iqi + jqj + kqk) \tag{2.3}$$

$$\mathcal{J}q = \frac{1}{4}(q + iqi - jqj + kqk) \tag{2.4}$$

$$\mathcal{K}q = \frac{1}{4}(q + iqi + jqj - kqk). \tag{2.5}$$

The symbols $\mathfrak{i}$, $\mathfrak{j}$ and k are imaginary units. The full multiplication table of $\mathbb{H}$ is given in table 2.1.

	1	i	j	k
1	1	i	j	k
i	i	-1	k	$-j$
j	j	$-k$	-1	i
k	k	j	$-i$	-1

Table 2.1: The multiplication table of $\mathbb{H}$.

The addition and multiplication of two quaternions q and r is defined as follows:

$$\begin{aligned} q + r &= (q_0 + iq_1 + jq_2 + kq_3) + (r_0 + ir_1 + jr_2 + kr_3) \\ &= (q_0 + r_0) + i(q_1 + r_1) + j(q_2 + r_2) + k(q_3 + r_3) \end{aligned} \tag{2.6}$$

$$\begin{aligned} qr &= (q_0 + iq_1 + jq_2 + kq_3)(r_0 + ir_1 + jr_2 + kr_3) \\ &= (q_0r_0 - q_1r_1 - q_2r_2 - q_3r_3) \\ &\quad + i(q_0r_1 + q_1r_0 + q_2r_3 - q_3r_2) \\ &\quad + j(q_0r_2 + q_2r_0 - q_1r_3 + q_3r_1) \\ &\quad + k(q_0r_3 + q_3r_0 + q_1r_2 - q_2r_1). \end{aligned} \tag{2.7}$$

The multiplication rule (2.7) follows uniquely from the multiplication table 2.1. Note that the multiplication of quaternions is *not commutative*, e.g. from the multiplication table we find $ij = -ji = k$.

An interpretation of the multiplication defined by (2.7) can be found by regarding q_0 as the scalar part and $\mathbf{q} := iq_1 + jq_2 + kq_3$ as the vector part of q. A quaternion whose scalar part is equal to zero is called a *pure quaternion*. The product of two pure quaternions $\mathbf{q}$ and $\mathbf{r}$ is

$$\begin{aligned} \mathbf{qr} &= (-q_1r_1 - q_2r_2 - q_3r_3) \\ &\quad + i(q_2r_3 - q_3r_2) \\ &\quad + j(q_3r_1 - q_1r_3) \\ &\quad + k(q_1r_2 - q_2r_1). \end{aligned} \tag{2.8}$$

From (2.8) it follows that the scalar part of $\mathbf{qr}$ is equal to minus the dot product of two three-dimensional vectors and the vector part is equal to the cross product of the vectors. *Thus, the quaternion product combines in itself the two fundamental products defined between three-dimensional vectors.* We can write $\mathbf{qr} = -\mathbf{q} \cdot \mathbf{r} + \mathbf{q} \times \mathbf{r}$.

Like in the algebra of complex numbers we can define the operation of conjugation for quaternions.

Definition 2.2 (Conjugation) *The endomorphism*

$$
\begin{aligned}
\bar{\ }: \mathbb{H} &\rightarrow \mathbb{H} &(2.9)\\
q &\mapsto \bar{q} = -\frac{1}{2}(q + iqi + jqj + kqk) &(2.10)
\end{aligned}
$$

is called conjugation in $\mathbb{H}$.

According to definition 2.2 the conjugate of a quaternion $q = q_0 + iq_1 + jq_2 + kq_3$, is given by

$$\bar{q} = q_0 - iq_1 - jq_2 - kq_3 \quad . \tag{2.11}$$

The *norm* of q is defined as

$$|q| = \sqrt{q\bar{q}} = \sqrt{q_0^2 + q_1^2 + q_2^2 + q_3^2} \quad . \tag{2.12}$$

For any $q \in \mathbb{H}\backslash\{0\}$ a unique multiplicative inverse exists and can be found to be $q^{-1} = \bar{q}/|q|^2$ [76].

The set $\mathbb{H}$ with the addition and multiplication as defined above forms a *skew field*. With an additional multiplication by real numbers $\mathbb{H}$ becomes an *associative division algebra* over $\mathbb{R}$. The associativity can be proven by direct validation of the 27 equalities $(e_l e_m)e_n = e_l(e_m e_n)$, $l, m, n \in \{1, 2, 3\}$ with $e_1, e_2, e_3 \in \{i, j, k\}$ [36]. However, it can also be shown that $\mathbb{H}$ is isomorphic to an algebra of complex 2×2 matrices which directly proves the associativity of $\mathbb{H}$.

It is also possible to regard $\mathbb{H}$ as a four-dimensional real linear space with the basis $\{1, i, j, k\}$. Using vector notation we assign to each basis element a natural basis vector of $\mathbb{R}^4$: $1 = (1, 0, 0, 0)^\top$, $i = (0, 1, 0, 0)^\top$, $j = (0, 0, 1, 0)^\top$, and $k = (0, 0, 0, 1)^\top$. The Euclidean scalar product in this linear space is $\langle q, r\rangle = \frac{1}{2}(q\bar{r} + r\bar{q}) = q_0r_0 + q_1r_1 + q_2r_2 + q_3r_3$. Now the notion of orthogonality of quaternions can be defined: Two quaternions q and r are said to be orthogonal if $\langle q, r\rangle = 0$. The norm of a quaternion as defined by equation (2.12) can be rewritten using the scalar product as $|q| = \sqrt{\langle q, q\rangle}$. We also introduce a scalar product for quaternion-valued functions.

Definition 2.3 (Scalar product and norm of quaternion-valued functions) *Let* V *be the vector space of integrable functions* $f : \mathbb{R}^n \rightarrow \mathbb{H}$. *Then, by the formula*

$$\langle f,\, g\rangle = \frac{1}{2}\int_{\mathbb{R}^n} (f(\mathbf{x})\bar{g}(\mathbf{x}) + g(\mathbf{x})\bar{f}(\mathbf{x}))\, d^n\mathbf{x}$$

we introduce a scalar product in V. *The* L^2*-norm of a function* $f \in V$ *is given by*

$$||f|| = \sqrt{\int_{\mathbb{R}^n} |f(\mathbf{x})|^2 \, d^n\mathbf{x}}.$$

For later use we show how the field of complex numbers can be embedded into $\mathbb{H}$. A subset of $\mathbb{H}$ which consists only of quaternions of the form $q = q_0 + iq_1 + j0 + k0$ is isomorphic to $\mathbb{C}$. These quaternions are called i-quaternions. Analogously j- and k-quaternions can be defined which are also isomorphic to $\mathbb{C}$. Generally, the following is true:

Theorem 2.1 *Any subset of* $\mathbb{H}$ *of the form* $\mathbb{R}\{1, \mathbf{n}\} = \{q | q = a + \mathbf{n}b\} \subset \mathbb{H}$, *where* $\mathbf{n}$ *is a pure unit quaternion, i.e.* $\mathbf{n} = in_1 + jn_2 + kn_3$ *and* $\sqrt{n_1^2 + n_2^2 + n_3^2} = 1$ *is isomorphic to* $\mathbb{C}$.

Proof: We only have to show that $\mathbf{n}$ behaves like the imaginary unit i of the complex numbers.

$$\begin{aligned} \mathbf{n}^2 &= (in_1 + jn_2 + kn_3)^2 \\ &= -n_1^2 - n_2^2 - n_3^2 + i(n_2n_3 - n_3n_2) + j(n_3n_1 - n_1n_3) + k(n_1n_2 - n_2n_1) \\ &= -1, \end{aligned}$$

which completes the proof. □

The operation of conjugation in $\mathbb{C} : z \mapsto z^*$ is a so-called algebra involution, i.e. it fulfills the two following properties: let $z, w \in \mathbb{C} \Rightarrow (z^*)^* = z$ and $(wz)^* = w^*z^*$. In $\mathbb{H}$ there are three nontrivial algebra involutions [24]:

$$\begin{aligned} \alpha(q) &= -iqi = q_0 + iq_1 - jq_2 - kq_3, \\ \beta(q) &= -jqj = q_0 - iq_1 + jq_2 - kq_3, \text{ and} \\ \gamma(q) &= -kqk = q_0 - iq_1 - jq_2 + kq_3, \end{aligned} \tag{2.13}$$

which we will use in order to extend the notion of Hermite symmetry from complex to quaternionic functions. A function $f : \mathbb{R}^n \to \mathbb{C}$ is called *Hermite symmetric* if $f(\mathbf{x}) = f^*(-\mathbf{x})$ for all $\mathbf{x} \in \mathbb{R}^n$. The notion of Hermite symmetry of a function is useful in the context of Fourier transforms since the Fourier transform of a real function has this property.

Definition 2.4 (Quaternionic Hermite symmetry) *A function* $f : \mathbb{R}^2 \to \mathbb{H}$ *is called quaternionic hermitian if:*

$$f(-x, y) = \beta(f(x, y)) \quad \textit{and} \quad f(x, -y) = \alpha(f(x, y)) \quad , \tag{2.14}$$

for each $(x, y) \in \mathbb{R}^2$.

Theorem 2.2 *For a quaternionic hermitian function* f *the relation*

$$f(-x,-y) = \gamma(f(x,y)) \tag{2.15}$$

holds true.

Proof: By definition we have

$$f(-x,y) = \beta(f(x,y)). \tag{2.16}$$

Applying the second equation of (2.14) to (2.16) yields

$$\begin{aligned} f(-x,-y) &= \alpha(\beta(f(x,y))) \\ &= ij(f(x,y))ji = -k(f(x,y))k \\ &= \gamma(f(x,y)). \end{aligned}$$

□

We will make use of the exponential function for quaternions in the definition of the quaternionic Fourier transform. Before defining the exponential function we have to introduce the following lemma.

Lemma 2.1 *For any quaternion* q *the sequence* $\{a_n\}$ *with*

$$a_n = \sum_{k=0}^{n} \frac{q^k}{k!}, \quad n \in \mathbb{N} \tag{2.17}$$

converges to some $r \in \mathbb{H}$*.*

Proof: Since $\mathbb{H}$ is a normed algebra we have $|q^k| = |q|^k$. It is known that the series $\sum_{k=0}^{n} \frac{|q|^k}{k!} = \sum_{k=0}^{n} \frac{|q^k|}{k!}$ converges for $n \to \infty$ since $|q|$ is real. Thus, the sequence $\{a_n\}$ converges absolutely which implies the lemma. □

Definition 2.5 (Exponential function) *The exponential function for quaternions* $\exp : \mathbb{H} \to \mathbb{H}$ *is defined via the series*

$$\exp(q) = \sum_{k=0}^{\infty} \frac{q^k}{k!}, \quad q \in \mathbb{H} \quad . \tag{2.18}$$

Note, that the existence of $\exp(q)$ *is guaranteed for any* $q \in \mathbb{H}$ *by lemma 2.1.*

An important fact to note is that the addition equation

$$\exp(q+r) = \exp(q)\exp(r) \tag{2.19}$$

which is true for real and complex numbers is not generally true for quaternions q and r. Instead (2.19) has to be replaced by the more general relation

$$\exp(h(q,r)) = \exp(q)\exp(r), \tag{2.20}$$

where in general $h(q,r) \neq q+r$. In fact $h(q,r)$ contains the commutator of q and r and higher order commutators. The form of $h(q,r)$ is given by the Campbell-Hausdorff-formula (see e.g. [55]).

For practical applications $\exp(q)$ can be calculated in the following way. Let us write the quaternion q in the form $q = q_0 + \mathbf{q}$, where q_0 and $\mathbf{q}$ denote the scalar part and the vector part of q, respectively. We can then evaluate $\exp(q)$ as

$$\begin{aligned} \exp(q) &= \exp(q_0 + \mathbf{q}) \\ &= \exp(q_0)\exp(\mathbf{q}) \\ &= \exp(q_0)\exp\left(\frac{\mathbf{q}}{|\mathbf{q}|}|\mathbf{q}|\right) \\ &= \exp(q_0)\left(\cos(|\mathbf{q}|) + \frac{\mathbf{q}}{|\mathbf{q}|}\sin(|\mathbf{q}|)\right) \quad . \end{aligned} \tag{2.21}$$

In the first step we used the fact that a real scalar (here q_0) commutes with any quaternion. In the last step we used the fact that the Euler formula

$$\exp(i\phi) = \cos(\phi) + i\sin(\phi)$$

is valid if i is replaced by any pure unit quaternion $\mathbf{n}$

$$\exp(\mathbf{n}\phi) = \cos(\phi) + \mathbf{n}\sin(\phi). \tag{2.22}$$

This follows from the fact that $\mathbb{R}\{1,\mathbf{n}\}$ is isomorphic to $\mathbb{C}$ as stated in theorem 2.1. Representing $\mathbf{n}$ in the polar form $\mathbf{n} = i\cos\phi\sin\theta + j\sin\phi\sin\theta + k\cos\theta$ we get the polar representation of q which is $\tilde{q} = (|q|, \phi, \theta, \psi)$. The components q_i of q can be recovered from $\tilde{q}$ by

$$\begin{aligned} q_0 &= |q|\cos(\psi) \\ q_1 &= |q|\cos(\phi)\sin(\theta)\sin(\psi) \\ q_2 &= |q|\sin(\phi)\sin(\theta)\sin(\psi) \\ q_3 &= |q|\cos(\theta)\sin(\psi) \quad . \end{aligned} \tag{2.23}$$

However, as we demonstrate later, this polar representation of quaternions does not suit our needs. For this reason we introduce another way of defining the quaternionic phase-angles in section 2.1.2.

2.1.1 Geometric Interpretation of $\mathbb{H}$

As mentioned in the beginning of this section the introduction of quaternions was geometrically inspired. As unit complex numbers represent rotations in the plane, it can be shown that unit quaternions represent rotations in $\mathbb{R}^3$. The set of unit quaternions is the 3D unit hyper-sphere

$$S^3 = \{q \in \mathbb{H} \,|\, |q| = 1\}.$$

Let $q \in S^3$ be given by $q = \cos(\phi) + \mathbf{n}\sin(\phi)$, where $\mathbf{n}$ is a pure unit quaternion. Further let $\mathbf{x}$ be a pure quaternion, representing the three-dimensional vector $(x_1, x_2, x_3)^\top$. A rotation about the axis defined by $\mathbf{n}$ through the angle 2ϕ takes $\mathbf{x}$ to $\mathbf{x}' = q\mathbf{x}q^{-1}$. Thus, any unit quaternion q represents a rotation in $\mathbb{R}^3$. However, there is no one-to-one but a two-to-one correspondence between unit quaternions and the group of rotations in $\mathbb{R}^3$ because q and $-q$ represent the same rotation. In other words S^3 is a two-fold covering group of $SO(3)$, that is, $SO(3) \cong S^3/\{1, -1\}$ (see [55]).

2.1.2 The Quaternionic Phase-Angle

Later in this chapter and especially in chapter 3 we demonstrate the usefulness of the signal-phase concept and show how it is related to the angular phase of complex numbers. In order to establish a new kind of signal phase based on a quaternionic signal representation we first need a definition of the angular phase of a quaternion. There is not a unique angular phase. We introduce one possible definition which is based on Euler angles.

For a complex number $z = a+bi$ the *argument* or *phase-angle* is defined as $\text{atan2}(b, a)$, where atan2 is the sign-dependent arctan-function. I.e. if z is written in the form $z = r\exp(i\phi)$ with $r \geq 0$ the argument of z is ϕ. For the function that returns the argument of any given complex number we introduce the notation arg, i.e. $\arg(z) = \phi$. As mentioned in the previous section, the quaternion algebra contains three complex subfields with orthogonal imaginary units. For later use we define three argument functions each picking out one complex subfield:

Definition 2.6 *Let $q = a + bi + cj + dk$ be a quaternion. Then we define the following functions:*

$$\arg_i(q) = \text{atan2}(b, a) \tag{2.24}$$

$$\arg_j(q) = \text{atan2}(c, a) \tag{2.25}$$

$$\arg_k(q) = \text{atan2}(d, a). \tag{2.26}$$

These argument functions project the quaternion q on one complex subfield as indicated by the index i, j or k and evaluate the phase-angle of the resulting complex number.

There are different possibilities of polar representations of quaternions. Since the quaternions constitute a four-dimensional algebra, a magnitude/phase-representation will always lead to a phase which is given by three real numbers. (The magnitude of a quaternion q is always given by the real value $|q| = \sqrt{q\bar{q}}$.)

The representation given by the equations (2.22) has the drawback that it cannot easily be compared to the classic phase concept. This will be clarified when analyzing the shift-theorem of the quaternionic Fourier transform (see section 2.2.2).

We propose another quaternionic phase representation here, which is more closely related to the classical phase concept in a way that will be made clear below.

Theorem 2.3 *Each quaternion* q *can be represented in the form*

$$q = |q| e^{i\phi} e^{k\psi} e^{j\theta} \text{ with } (\phi, \theta, \psi) \in [-\pi, \pi[\times [-\pi/2, \pi/2[\times [-\pi/4, \pi/4]. \tag{2.27}$$

Before proving the theorem we present two lemmas. The first one gives the explicit form of the mapping that maps unit quaternions to the related rotation matrix. This mapping establishes at the same time the isomorphism of $S^3/\{1, -1\}$ to $SO(3)$ which was mentioned in section 2.1.1. The second lemma specifies the form of the two-fold covering of $SO(3)$ by S^3.

Lemma 2.2 *Let* $q = a + bi + cj + dk$ *be a quaternion, and let* $\mathcal{M}$ *be a mapping from the quaternions to the real* 3×3*-matrices in the following way:*

$$\mathcal{M}(q) = \begin{pmatrix} a^2 + b^2 - c^2 - d^2 & 2(bc - ad) & 2(bd + ac) \\ 2(bc + ad) & a^2 - b^2 + c^2 - d^2 & 2(cd - ab) \\ 2(bd - ac) & 2(cd + ab) & a^2 - b^2 - c^2 + d^2 \end{pmatrix}. \tag{2.28}$$

Then

$$\mathcal{M} : \{q | q \in \mathbb{H}, |q| = 1\} \to SO(3) \tag{2.29}$$

is a surjective group homomorphism. $\mathcal{M}(q)$ *is the matrix which represents the same rotation as the quaternion* q.

Proof: See [70]. □

The matrix $\mathcal{M}(q)$ is sometimes called *Rodriguez matrix*.

Lemma 2.3 *Let* q_1 *and* q_2 *be unit quaternions and*

$$\mathcal{M}(q_1) = \mathcal{M}(q_2). \tag{2.30}$$

Then it follows that

$$q_1 = q_2 \quad \textit{or} \quad q_1 = -q_2. \tag{2.31}$$

Proof: Since S^3 is a two-fold covering group of $SO(3)$ there correspond exactly two different quaternions to each rotation matrix. Using (2.28) it is verified that $\mathcal{M}(q) = \mathcal{M}(-q)$ for all $q \in S^3$. $\square$

Proof of theorem 2.3: Each quaternion q can be written as $q = |q|r$ where r is a unit quaternion. According to Lemma 2.2 each unit quaternion represents a rotation in $\mathbb{R}^3$. The matrix $R = \mathcal{M}(r)$ can be factorized into three rotations

$$R = R_x(2\phi)R_z(2\psi)R_y(2\theta), \tag{2.32}$$

where R_x, R_y and R_z represent rotations about the coordinate axes. The angles $2\phi, 2\theta$ and 2ψ are known as Euler angles (see e.g. [70]). Let $q_1 = \exp(i\phi)$, $q_2 = \exp(j\theta)$ and $q_3 = \exp(k\psi)$. Then it can easily be shown that

$$\mathcal{M}(q_1) = R_x(2\phi), \quad \mathcal{M}(q_2) = R_y(2\theta) \quad \text{and } \mathcal{M}(q_3) = R_z(2\psi). \tag{2.33}$$

Since $\mathcal{M}$ is a group homomorphism (lemma 2.2) it follows that

$$\mathcal{M}(q_1)\mathcal{M}(q_3)\mathcal{M}(q_2) = \mathcal{M}(q_1 q_3 q_2) = \mathcal{M}(r). \tag{2.34}$$

From Lemma 2.3 we get $r = q_1q_3q_2$ or $r = -q_1q_3q_2$, which directly leads to the desired representation — up to a possible minus sign, which can be eliminated by replacing ϕ by $\phi + \pi$. Thus, we have

$$q = \pm|q| \exp(i\phi) \exp(k\psi) \exp(j\theta). \tag{2.35}$$

This proves that each quaternion can be expressed in the given polar representation. In the second part of the proof we have to show that the given intervals of ϕ , θ and ψ are sufficient for expressing any quaternion. In fact, it will turn out that the intervals are minimal. The proof will be constructive and yields a formula, that evaluates the magnitude/phase representation for any quaternion q given in Cartesian representation $q = a + bi + cj + dk$. The magnitude is directly evaluated. **From now on $q = a + bi + cj + dk$ will be the normalized quaternion with $|q| = 1$.**

We construct $\mathcal{M}(r)$ according to (2.28). On the other hand, the rotation matrix R can be given in Euler representation:

$$\begin{aligned} R &= R_x(2\phi)R_z(2\psi)R_y(2\theta) \\ &= \begin{pmatrix} \cos(2\psi)\cos(2\theta) & -\sin(2\psi) & \cos(2\psi)\sin(2\theta) \\ \begin{array}{c}\cos(2\phi)\sin(2\psi)\cos(2\theta) \\ +\sin(2\phi)\sin(2\theta)\end{array} & \cos(2\phi)\cos(2\psi) & \begin{array}{c}\cos(2\phi)\sin(2\psi)\sin(2\theta) \\ -\sin(2\phi)\cos(2\theta)\end{array} \\ \begin{array}{c}\sin(2\phi)\sin(2\psi)\cos(2\theta) \\ -\cos(2\phi)\sin(2\theta)\end{array} & \sin(2\phi)\cos(2\psi) & \begin{array}{c}\sin(2\phi)\sin(2\psi)\sin(2\theta) \\ +\cos(2\phi)\cos(2\theta)\end{array} \end{pmatrix} \end{aligned} \tag{2.36}$$

We set $\mathcal{M}(r) = R$ which leads to nine equations which have to be solved for ϕ, θ and ψ. Firstly, ψ is directly evaluated from R_{12} which yields the equation

$$-\sin(2\psi) = 2(bc - ad). \tag{2.37}$$

Thus, ψ can be evaluated uniquely within the interval $[-\frac{\pi}{4}, \frac{\pi}{4}]$ as

$$\psi = -\frac{\arcsin(2(bc - ad))}{2}. \tag{2.38}$$

In order to solve the remaining equations for ϕ and θ we have to distinguish two different cases: The singular case where $\psi = \pm\frac{\pi}{4}$ and the regular case where $\psi \in]-\frac{\pi}{4}, \frac{\pi}{4}[$.

The regular case ($\psi \in]-\frac{\pi}{4}, \frac{\pi}{4}[$): In this case it is easily verified that

$$\phi = -\frac{1}{2}\operatorname{atan2}\left(\frac{-R_{32}}{\cos(2\psi)}, \frac{R_{22}}{\cos(2\psi)}\right) \quad \text{and} \quad \theta = -\frac{1}{2}\operatorname{atan2}\left(\frac{-R_{13}}{\cos(2\psi)}, \frac{R_{11}}{\cos(2\psi)}\right).$$

Since, $\cos(2\psi)$ is always positive in this case, ϕ and θ can be simplified to

$$\phi = \frac{\operatorname{atan2}(R_{32}, R_{22})}{2} \quad \text{and} \quad \theta = \frac{\operatorname{atan2}(R_{13}, R_{11})}{2}. \tag{2.39}$$

The occurring matrix components are expressed in terms of the quaternion q using (2.28):

$$\begin{aligned} R_{11} &= a^2 + b^2 - c^2 - d^2 \\ R_{13} &= 2(bd + ac) \\ R_{22} &= a^2 - b^2 + c^2 - d^2 \\ R_{32} &= 2(cd + ab) \end{aligned}$$

Replacing the components of R in (2.39) by the corresponding expressions of (2.28) and using a compact notation we obtain the final expressions

$$\phi = \frac{arg_i(q\beta(\bar{q}))}{2} \quad \text{and} \quad \theta = \frac{arg_j(\alpha(\bar{q})q)}{2}. \tag{2.40}$$

Thus, ϕ and θ are uniquely determined within $[-\frac{\pi}{2}, \frac{\pi}{2}[$. (Later, the interval of ϕ will have to be extended to $[-\pi, \pi[$.)

The only ambiguity occurs in **the singular case** ($\psi = \pm\pi/4$). In this case the matrix elements R_{11}, R_{13}, R_{22} and R_{32} are zero (see (2.36)). The remaining non-zero matrix components simplify to

$$R_{31} = R_{23} = -\sin(2\phi + 2\theta) \tag{2.41}$$
$$R_{21} = -R_{33} = -\cos(2\phi + 2\theta) \tag{2.42}$$

for $\psi = -\pi/4$ and

$$R_{31} = -R_{23} = -\sin(-2\phi + 2\theta) \tag{2.43}$$
$$-R_{21} = -R_{33} = -\cos(-2\phi + 2\theta) \tag{2.44}$$

for $\psi = \pi/4$. In the regular case ϕ and θ are uniquely defined. In the singular case, in contrast, only the sum (if $\psi = -\pi/4$) or the difference (if $\psi = \pi/4$) of ϕ and θ is unique. Thus, we have the freedom to choose one of the angles. In the theory of Euler matrices this singularity is known as *Gimbal lock* [70]. There are different possibilities to deal with this situation. We choose to set one of the angles equal to zero. If we set $\theta = 0$ we get

$$\phi = \frac{atan2(-R_{23}, R_{33})}{2} \tag{2.45}$$

or, if we choose to set $\phi = 0$,

$$\theta = \frac{atan2(-R_{31}, R_{33})}{2}. \tag{2.46}$$

Again ϕ and θ lie within $[-\frac{\pi}{2}, \frac{\pi}{2}[$. Replacing the symbols R_{ij} by the entries of (2.28) we get

$$\phi = \frac{arg_i(q\gamma(\bar{q}))}{2} \tag{2.47}$$

if we set $\theta = 0$, and

$$\theta = \frac{arg_j(\gamma(\bar{q})q)}{2} \tag{2.48}$$

if we set $\phi = 0$. In these formulas only the quaternion q occurs. Thus, it is not necessary to construct the rotation matrix (2.36) explicitly. We only needed it in order to derive the final expressions for ϕ and θ.

Following the above procedure results in a triple of angles which is given in the interval $(\phi, \theta, \psi) \in [-\pi/2, \pi/2[\times [-\pi/2, \pi/2[\times [-\pi/4, \pi/4]$. As seen above we have

$$r = q_1 q_3 q_2 \quad \text{or} \quad r = -q_1 q_3 q_2.$$

If $e^{i\phi} e^{k\psi} e^{j\theta} = q$ we have found the final result. Otherwise ϕ has to be treated as follows: If $\phi < 0$, then replace ϕ by $\phi + \pi$, else replace ϕ by $\phi - \pi$. This extends the interval of ϕ to $[-\pi, \pi[$ such that we finally get

$$(\phi, \theta, \psi) \in [-\pi, \pi[\times [-\pi/2, \pi/2[\times [-\pi/4, \pi/4].$$

□

Definition 2.7 *Let* $q \in \mathbb{H}$ *be a quaternion. The angular phase of* q *is then defined by*

$$\arg(q) = (\phi, \theta, \psi) \in [-\pi, \pi[\times [-\pi/2, \pi/2[\times [-\pi/4, \pi/4],$$

according to Theorem 2.3.

We summarize the formulas for the quaternionic phase-angle in table 2.2.

<table>
<tr><td colspan="3">$q = a + bi + cj + dk, \quad |q| = 1$</td></tr>
<tr><td colspan="3">$\psi = -\frac{\arcsin(2(bc - ad))}{2}$</td></tr>
<tr><td rowspan="2">if $\psi \in]-\frac{\pi}{4}, \frac{\pi}{4}[$
$\phi = \frac{\arg_i(q\beta(\bar{q}))}{2}$
$\theta = \frac{\arg_j(\alpha(\bar{q})q)}{2}$</td><td colspan="2">if $\psi = \pm\frac{\pi}{4}$
choose</td></tr>
<tr><td>$\phi = 0$
$\theta = \frac{\arg_j(\gamma(\bar{q})q)}{2}$</td><td>or
$\theta = 0$
$\phi = \frac{\arg_i(q\gamma(\bar{q}))}{2}$</td></tr>
<tr><td>if $e^{i\phi} e^{k\psi} e^{j\theta} = -q$
and $\phi \geq 0$
$\phi \to \phi - \pi$</td><td colspan="2">if $e^{i\phi} e^{k\psi} e^{j\theta} = -q$
and $\phi < 0$
$\phi \to \phi + \pi$</td></tr>
</table>

Table 2.2: How to calculate the quaternionic phase-angle representation from a quaternion given in Cartesian representation

2.2 The Quaternionic Fourier Transform

A new transform which is proposed in this thesis as a tool for image processing is the quaternionic Fourier transform (QFT). In the subsequent sections the QFT is defined, and some important theorems are introduced. The discrete QFT is given followed by a discussion of fast algorithms for the QFT. An overview of the literature on the QFT is given in section 2.2.4.

2.2.1 Definition and Properties of the QFT

The QFT is closely related to the 2D complex Fourier transform. In order to make comparable the definition of the QFT with the one of the complex Fourier transform we first review the definition of the complex Fourier transform. Since the complex Fourier transform is a standard tool in signal processing, we refer to textbooks for detailed reviews [12, 58].

Definition 2.8 (Fourier transform) *Let f be a real n-dimensional signal and*

$$\mathbf{x} = (x_1, x_2, \ldots, x_n)^\top \in \mathbb{R}^n \quad \textit{and} \quad \mathbf{u} = (u_1, u_2, \ldots, u_n)^\top \in \mathbb{R}^n$$

elements of the spatial and the frequency domain, respectively. The Fourier transform of f is defined as

$$F(\mathbf{u}) = \int_{\mathbb{R}^n} f(\mathbf{x}) e^{-i2\pi \mathbf{u}\mathbf{x}} d^n\mathbf{x}. \tag{2.49}$$

Theorem 2.4 (Inverse Fourier transform) *The Fourier transform is invertible and the inverse transform is given by*

$$f(\mathbf{x}) = \int_{\mathbb{R}^n} F(\mathbf{u}) e^{i2\pi \mathbf{u}\mathbf{x}} d^n\mathbf{u}. \tag{2.50}$$

Proof: We prove the theorem by inserting (2.49) into (2.50):

$$\begin{aligned} & \int_{\mathbb{R}^n} F(\mathbf{u}) e^{i2\pi \mathbf{u}\mathbf{x}} d^n\mathbf{u} \\ = & \int_{\mathbb{R}^n} \int_{\mathbb{R}^n} f(\mathbf{x}') e^{i2\pi \mathbf{u}(\mathbf{x}-\mathbf{x}')} d^n\mathbf{u} d^n\mathbf{x}' \\ = & \int_{\mathbb{R}^n} f(\mathbf{x}') \delta^n(\mathbf{x}-\mathbf{x}') d^n\mathbf{x}' = f(\mathbf{x}), \end{aligned}$$

where we used the orthogonality of the harmonic exponential functions. □

The QFT was recently introduced in [19, 20] and [35], independently. While Ell used the QFT for the analysis of partial differential systems, we introduced the QFT for the use in image processing and analysis.

Definition 2.9 (QFT) *Let* f *be a quaternion-valued two-dimensional signal and* $\mathbf{x} = (x, y)^\top \in \mathbb{R}^2$ *and* $\mathbf{u} = (u, v)^\top \in \mathbb{R}^2$*. The QFT of* f*, denoted by* F^q*, is then defined as*

$$F^q(\mathbf{u}) = \int_{\mathbb{R}^2} e^{-i2\pi ux} f(\mathbf{x}) e^{-j2\pi vy} \, d^2\mathbf{x} \quad . \tag{2.51}$$

The mapping from f *to* F^q *is denoted by*

$$\mathcal{F}_q : f \mapsto \mathcal{F}_q\{f\} = F^q. \tag{2.52}$$

For simplicity we introduce the notation

$$f \; \circ\!\!\stackrel{\mathbb{H}}{\text{———}}\!\!\bullet \; F^q \quad \textit{or} \quad F^q \; \bullet\!\!\stackrel{\mathbb{H}}{\text{———}}\!\!\circ \; f$$

in order to indicate that F^q *is the quaternionic Fourier transform of* f*.*

Some notes on definition 2.9 have to be made: Firstly, the QFT resembles very much the two-dimensional Fourier transform which can be written as

$$F(\mathbf{u}) = \int_{\mathbb{R}^2} e^{-i2\pi ux} f(\mathbf{x}) e^{-i2\pi vy} \, d^2\mathbf{x}. \tag{2.53}$$

The only difference between the notations of the transforms is that the imaginary unit i in the second exponential function is replaced by j for the QFT. Thus, the QFT maps signals onto a quaternion-valued representation instead of to a complex-valued one.

Secondly, we note that the QFT has been introduced for real, complex or quaternionic signals, which is possible since real and complex numbers can be embedded into $\mathbb{H}$. In this thesis most of the time we deal with real-valued signals. However, we introduce quaternion-valued Gabor filters and evaluate their transfer functions. This involves calculating the QFT of the quaternion-valued Gabor filter responses. Sangwine [85] uses quaternion-valued signals, which represent color images. We will review this work in some more detail in section 2.2.4. If complex signals are to be used — which, to the best of our knowledge, has not been done up to now — one has to choose one of infinitely many possible embeddings of $\mathbb{C}$ into $\mathbb{H}$, i.e. a complex signal can be written as $f = \mathcal{R}\{f\} + i\mathcal{I}\{f\}$ or $f = \mathcal{R}\{f\} + \frac{i+j}{\sqrt{2}}\mathcal{I}\{f\}$ or in some other way (see section 2.1, theorem 2.1). Depending on the choice of embedding, F^q will take a different form. Since in our work complex signals will not be used, we will not analyze this dependence in more detail.

The third note concerns the order of the factors under the integral in (2.51). Since the multiplication of quaternions is not commutative, the order of the exponential functions and the input function (if not real) is fixed. A change of this order would affect the result. Thus, the order of the factors can freely be chosen as part of the definition of the QFT, but it must be kept fixed afterwards. At the end of this chapter we will introduce an alternative transform using a commutative algebra, which is not subject to this restriction.

Symmetry properties play an important role in Fourier theory. Symmetry means here the evenness or oddness of a signal. We call a one-dimensional function f even if $f(x) = f(-x)$ for all x and odd if $f(x) = -f(-x)$. Any function f can be written as the sum of an even and an odd function $f = f_e + f_o$. The meaning of symmetries for Fourier theory lies in the following: In the case of the one-dimensional Fourier transform it is known that the transform of the even part of a signal is even, while the transform of the odd part is odd. Furthermore, the transform of a real (imaginary) even signal is real (imaginary), while the transform of a real (imaginary) odd signal is imaginary (real). Bracewell [12] summarizes these facts in the diagram shown in figure 2.1.

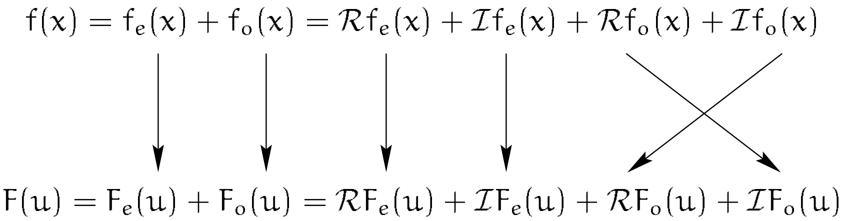

Figure 2.1: Symmetry properties of the one-dimensional Fourier transform.

We will now analyze the symmetry properties of the QFT. A two–dimensional signal can be split into even and odd parts along the x–axis and along the y–axis as well. So, every two–dimensional signal can be written in the form $f = f_{ee} + f_{oe} + f_{eo} + f_{oo}$, where f_{ee} denotes the part of f which is even with respect to x and y, f_{oe} denotes the part which is odd with respect to x and even with respect to y and so on. In order to analyze how the quaternionic Fourier transform deals with these symmetries, we rewrite the QFT as

$$\begin{aligned}
F^q(\mathbf{u}) &= \int_{\mathbb{R}^2} \cos(2\pi ux)\cos(2\pi vy) f(\mathbf{x})\, d^2\mathbf{x} \\
&- i \int_{\mathbb{R}^2} \sin(2\pi ux)\cos(2\pi vy) f(\mathbf{x})\, d^2\mathbf{x} \\
&- j \int_{\mathbb{R}^2} \cos(2\pi ux)\sin(2\pi vy) f(\mathbf{x})\, d^2\mathbf{x} \\
&+ k \int_{\mathbb{R}^2} \sin(2\pi ux)\sin(2\pi vy) f(\mathbf{x})\, d^2\mathbf{x}.
\end{aligned} \tag{2.54}$$

Note, that (2.54) is only valid for real-valued signals. The first summand is even in both orientations and only involves f_{ee}, since the integral kernel is even with respect to both arguments. Analogously the remaining three summands can be examined. For the symmetry properties of the QFT of a quaternion-valued signal we build the diagram shown in figure 2.2.

Figures 2.3 and 2.4 show some of the basis functions of the 2D Fourier transform and of the quaternionic Fourier transform, respectively. The small images show the basis functions in the spatial domain. The frequency parameter is modified from image to image. Only the real parts of the basis functions are shown. In case of the complex Fourier transform each basis function consists actually of two components (real and imaginary), where the imaginary part is shifted in phase against the real part by $\pi/2$. In figure 2.4 each small image represents one basis function consisting of four components. Again, only the real part is shown. The other three components are shifted in phase against the real part by $\pi/2$ in x-direction (i-imaginary component), in y-direction (j-imaginary component) and simultaneously in x- and y-direction (k-imaginary component). It can be seen from figures 2.3 and 2.4 that the basis functions of the complex Fourier transform are intrinsically one-dimensional ("plane waves"). In contrast, the basis functions of the quaternionic Fourier transform are intrinsically two-dimensional, which allows them to capture intrinsically two-dimensional image structure.

2.2.2 Main Theorems

BRACEWELL ([12], p. 391) states that for every theorem about the Fourier transform there is a corresponding Hartley transform theorem. We can claim the same for the correspondence between the two-dimensional Fourier transform and the quaternionic Fourier transform. We will have a look at these correspondences here by stating the important QFT-theorems.

$$
\begin{array}{cccccccc}
f(\boldsymbol{x}) = & \mathcal{R} f_{ee}(\boldsymbol{x}) & + & \mathcal{R} f_{oe}(\boldsymbol{x}) & + & \mathcal{R} f_{eo}(\boldsymbol{x}) & + & \mathcal{R} f_{oo}(\boldsymbol{x}) \\
& \Big\downarrow & & \Big\downarrow & & \Big\downarrow & & \Big\downarrow \\
F^q(\boldsymbol{u}) = & \mathcal{R} F^q_{ee}(\boldsymbol{u}) & + & \mathcal{I} F^q_{oe}(\boldsymbol{u}) & + & \mathcal{J} F^q_{eo}(\boldsymbol{u}) & + & \mathcal{K} F^q_{oo}(\boldsymbol{u})
\end{array}
$$

$$
\begin{array}{cccccccc}
f(\boldsymbol{x}) = & \mathcal{I} f_{ee}(\boldsymbol{x}) & + & \mathcal{I} f_{oe}(\boldsymbol{x}) & + & \mathcal{I} f_{eo}(\boldsymbol{x}) & + & \mathcal{I} f_{oo}(\boldsymbol{x}) \\
& \Big\downarrow & & \Big\downarrow & & \Big\downarrow & & \Big\downarrow \\
F^q(\boldsymbol{u}) = & \mathcal{I} F^q_{ee}(\boldsymbol{u}) & + & \mathcal{R} F^q_{oe}(\boldsymbol{u}) & + & \mathcal{K} F^q_{eo}(\boldsymbol{u}) & + & \mathcal{J} F^q_{oo}(\boldsymbol{u})
\end{array}
$$

$$
\begin{array}{cccccccc}
f(\boldsymbol{x}) = & \mathcal{J} f_{ee}(\boldsymbol{x}) & + & \mathcal{J} f_{oe}(\boldsymbol{x}) & + & \mathcal{J} f_{eo}(\boldsymbol{x}) & + & \mathcal{J} f_{oo}(\boldsymbol{x}) \\
& \Big\downarrow & & \Big\downarrow & & \Big\downarrow & & \Big\downarrow \\
F^q(\boldsymbol{u}) = & \mathcal{J} F^q_{ee}(\boldsymbol{u}) & + & \mathcal{K} F^q_{oe}(\boldsymbol{u}) & + & \mathcal{R} F^q_{eo}(\boldsymbol{u}) & + & \mathcal{I} F^q_{oo}(\boldsymbol{u})
\end{array}
$$

$$
\begin{array}{cccccccc}
f(\boldsymbol{x}) = & \mathcal{K} f_{ee}(\boldsymbol{x}) & + & \mathcal{K} f_{oe}(\boldsymbol{x}) & + & \mathcal{K} f_{eo}(\boldsymbol{x}) & + & \mathcal{K} f_{oo}(\boldsymbol{x}) \\
& \Big\downarrow & & \Big\downarrow & & \Big\downarrow & & \Big\downarrow \\
F^q(\boldsymbol{u}) = & \mathcal{K} F^q_{ee}(\boldsymbol{u}) & + & \mathcal{J} F^q_{oe}(\boldsymbol{u}) & + & \mathcal{I} F^q_{eo}(\boldsymbol{u}) & + & \mathcal{R} F^q_{oo}(\boldsymbol{u})
\end{array}
$$

Figure 2.2: Symmetry properties of the QFT

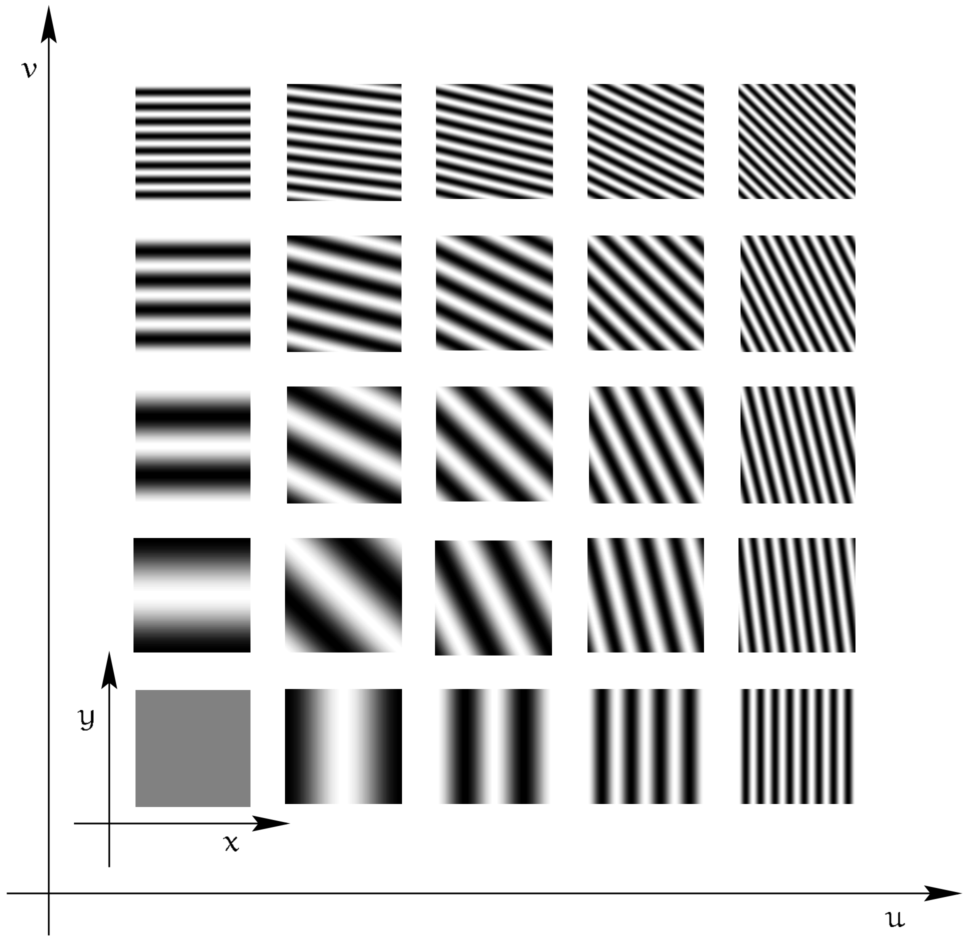

Figure 2.3: Some basis functions of the Fourier transform. The small images are intensity images of the real part of a basis function with fixed frequency $\mathbf{u}_0$. The frequency parameter changes from image to image. One quadrant of the frequency plane is shown.

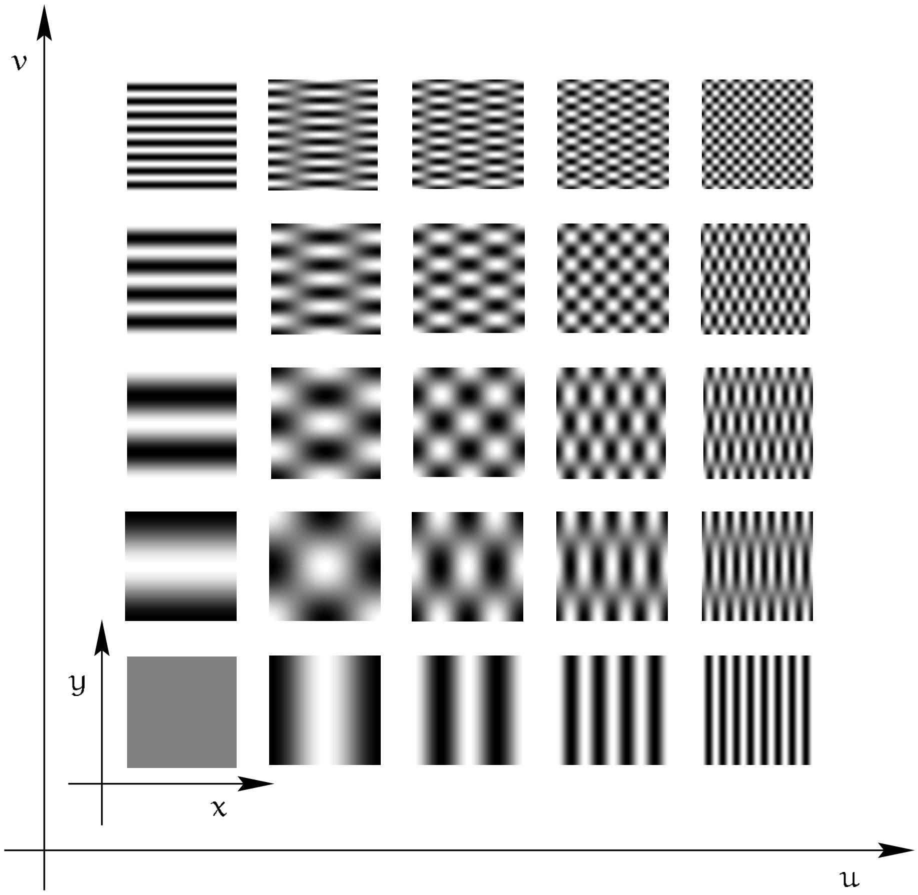

Figure 2.4: Similar to figure 2.3. The images show the real parts of basis functions of the QFT.

Theorem 2.5 (Inverse QFT) *The QFT is invertible. The transform $\mathcal{G}$ given by*

$$\mathcal{G}\{F^q\}(\mathbf{x}) = \int_{\mathbb{R}^2} e^{i2\pi ux} F^q(\mathbf{u}) e^{j2\pi vy} d^2\mathbf{u} \tag{2.55}$$

is the inverse of the QFT.

Proof: By inserting (2.51) into the right hand side of (2.55) we get

$$\mathcal{G}\{F^q\}(\mathbf{x}) = \int_{\mathbb{R}^2}\int_{\mathbb{R}^2} e^{i2\pi ux} e^{-i2\pi ux'} f(\mathbf{x}') e^{-j2\pi vy'} e^{j2\pi vy} d^2\mathbf{u}\, d^2\mathbf{x}'. \tag{2.56}$$

Integrating with respect to $\mathbf{u}$ and taking into account the orthogonality of harmonic exponential functions this simplifies to

$$\begin{aligned} \mathcal{G}\{F^q\}(\mathbf{x}) &= \int_{\mathbb{R}^2} \delta(x - x') f(\mathbf{x}') \delta(y - y') d^2\mathbf{x}' \\ &= f(\mathbf{x}), \end{aligned} \tag{2.57}$$

thus $\mathcal{G} = \mathcal{F}_q^{-1}$. □

The convolution theorem of the Fourier transform states that convolution of two signals in the spatial domain corresponds to their pointwise multiplication in the frequency domain, i.e.

$$f(\mathbf{x}) = (g * h)(\mathbf{x}) \quad \Leftrightarrow \quad F(\mathbf{u}) = G(\mathbf{u})H(\mathbf{u}) \tag{2.58}$$

where f, g and h are two-dimensional signals and F, G and H are their Fourier transforms. We now give the corresponding QFT theorem.

Theorem 2.6 (Convolution theorem (QFT)) *Let f, g and h be real two-dimensional signals and F^q, G^q and H^q their QFT's. Then,*

$$f(\mathbf{x}) = (g * h)(\mathbf{x}) \iff F^q(\mathbf{u}) = G^q_{\cdot e}(\mathbf{u})H^q(\mathbf{u}) + G^q_{\cdot o}(\mathbf{u})\beta(H^q(\mathbf{u})).$$

Here β denotes one of the three nontrivial automorphisms of the quaternion algebra as defined in (2.13). $G_{\cdot e}$ and $G_{\cdot o}$ are the components of G which are even or odd with respect to the second argument.

Proof:

$$\begin{aligned}
F^q(\mathbf{u}) &= \int_{\mathbb{R}^2} e^{-2\pi i x u} \underbrace{\int_{\mathbb{R}^2} (g(\mathbf{x}')h(\mathbf{x}-\mathbf{x}'))d^2\mathbf{x}'}_{=(g*h)(\mathbf{x})} e^{-2\pi j y v} d^2\mathbf{x} \qquad (2.59)\\
&= \int_{\mathbb{R}^2} e^{-2\pi i x' u} g(\mathbf{x}') H^q(\mathbf{u}) e^{-2\pi j y' v} d^2\mathbf{x}'\\
&= \int_{\mathbb{R}^2} e^{-2\pi i x' u} g(\mathbf{x}') \cos(-2\pi y' v) H^q(\mathbf{u}) d^2\mathbf{x}'\\
&\quad + \int_{\mathbb{R}^2} e^{-2\pi i x' u} g(\mathbf{x}') j \sin(-2\pi y' v) \beta(H^q(\mathbf{u})) d^2\mathbf{x}'\\
&= G^q_{\cdot e}(\mathbf{u}) H^q(\mathbf{u}) + G^q_{\cdot o}(\mathbf{u}) \beta(H^q(\mathbf{u})), \qquad (2.60)
\end{aligned}$$

which completes the proof. □

Analogously it can be shown, that

$$\begin{aligned}
f(\mathbf{x}) = (g*h)(\mathbf{x}) \Rightarrow F^q(\mathbf{u}) &= H^q_{\cdot e}(\mathbf{u}) G^q(\mathbf{u}) + H^q_{\cdot o}(\mathbf{u}) \beta(G^q(\mathbf{u})) \qquad (2.61)\\
&= G^q(\mathbf{u}) H^q_{e\cdot}(\mathbf{u}) + \alpha(G^q(\mathbf{u})) H^q_{o\cdot}(\mathbf{u}) \qquad (2.62)\\
&= H^q(\mathbf{u}) G^q_{e\cdot}(\mathbf{u}) + \alpha(H^q(\mathbf{u})) G^q_{o\cdot}(\mathbf{u}). \qquad (2.63)
\end{aligned}$$

In many cases one of the convolving functions is even with respect to at least one of the arguments. In these cases the QFT convolution theorem simplifies to

$$f(\mathbf{x}) = (g*h)(\mathbf{x}) \Rightarrow F^q(\mathbf{u}) = G^q(\mathbf{u}) H^q(\mathbf{u}) \qquad (2.64)$$

which is of the same form as the convolution theorem of the two-dimensional Fourier transform.

The energy of a signal is defined as the integral (or sum in the case of discrete signals) over the squared magnitude of the signal. Rayleigh's theorem states that the signal energy is preserved by the Fourier transform:

$$\int_{\mathbb{R}^2} |f(\mathbf{x})|^2 d^2\mathbf{x} = \int_{\mathbb{R}^2} |F(\mathbf{u})|^2 d^2\mathbf{u} \quad , \qquad (2.65)$$

where $F(\mathbf{u})$ is the Fourier transform of $f(\mathbf{x})$. Rayleigh's theorem is valid for arbitrary integer dimension of the signal. In mathematical terms Rayleigh's theorem states that the L^2-norm of a signal is invariant under the Fourier transform. We will show that the analogous statement for the QFT is true.

Theorem 2.7 (Rayleigh's theorem (QFT)) *The quaternionic Fourier transform preserves the L^2-norm of any real two-dimensional signal $f(\mathbf{x})$:*

$$\int_{\mathbb{R}^2} |f(\mathbf{x})|^2 d^2\mathbf{x} = \int_{\mathbb{R}^2} |F^q(\mathbf{u})|^2 d^2\mathbf{u} \qquad (2.66)$$

where $F^q(\mathbf{u})$ *is the QFT of* $f(\mathbf{x})$.

Proof: We make use of Rayleigh's theorem for the two-dimensional Fourier transform. Thus, we only have to prove that

$$\begin{aligned}
& \int_{\mathbb{R}^2} |F(\mathbf{u})|^2 d^2\mathbf{u} = \int_{\mathbb{R}^2} |F^q(\mathbf{u})|^2 d^2\mathbf{u} \\
\iff & \int_{\mathbb{R}^2} |F(\mathbf{u})|^2 d^2\mathbf{u} - \int_{\mathbb{R}^2} |F^q(\mathbf{u})|^2 d^2\mathbf{u} = 0 \quad . \qquad (2.67)
\end{aligned}$$

Regarding the integrands we find out that

$$|F(\mathbf{u})|^2 = \left(\int_{\mathbb{R}^2} f(\mathbf{x}) \cos(2\pi(ux + vy)) d^2\mathbf{x} \right)^2 \qquad (2.68)$$

$$+ \left(\int_{\mathbb{R}^2} f(\mathbf{x}) \sin(2\pi(ux + vy)) d^2\mathbf{x} \right)^2 \qquad (2.69)$$

while

$$|F^q(\mathbf{u})|^2 = \left(\int_{\mathbb{R}^2} f(\mathbf{x}) \cos(2\pi ux) \cos(2\pi vy) d^2\mathbf{x} \right)^2 \qquad (2.70)$$

$$+ \left(\int_{\mathbb{R}^2} f(\mathbf{x}) \sin(2\pi ux) \cos(2\pi vy) d^2\mathbf{x} \right)^2 \qquad (2.71)$$

$$+ \left(\int_{\mathbb{R}^2} f(\mathbf{x}) \cos(2\pi ux) \sin(2\pi vy) d^2\mathbf{x} \right)^2 \qquad (2.72)$$

$$+ \left(\int_{\mathbb{R}^2} f(\mathbf{x}) \sin(2\pi ux) \sin(2\pi vy) d^2\mathbf{x} \right)^2 . \qquad (2.73)$$

Applying the addition theorems to the sine- and cosine-functions in (2.68) and (2.69) we see that all the terms of $|F^q(\mathbf{u})|^2$ are also contained in $|F(\mathbf{u})|^2$. Only the mixed terms of $|F(\mathbf{u})|^2$ remain such that the left hand side of (2.67) can be evaluated as follows:

$$\int_{\mathbb{R}^2} |F(\mathbf{u})|^2 d^2\mathbf{u} - \int_{\mathbb{R}^2} |F^q(\mathbf{u})|^2 d^2\mathbf{u} \qquad (2.74)$$

$$= -2 \int_{\mathbb{R}^2} \left(\int_{\mathbb{R}^2} f(\mathbf{x}) \cos(2\pi ux) \cos(2\pi vy) d^2\mathbf{x} \times \right. \qquad (2.75)$$

$$\left. \int_{\mathbb{R}^2} f(\mathbf{x}) \sin(2\pi ux) \sin(2\pi vy) d^2\mathbf{x} \right) d^2\mathbf{u}$$

$$+2 \int_{\mathbb{R}^2} \left(\int_{\mathbb{R}^2} f(\mathbf{x}) \sin(2\pi ux) \cos(2\pi vy) d^2\mathbf{x} \times \right. \qquad (2.76)$$

$$\left. \int_{\mathbb{R}^2} f(\mathbf{x}) \cos(2\pi ux) \sin(2\pi vy) d^2\mathbf{x} \right) d^2\mathbf{u}.$$

We introduce the abbreviations

$$A(\mathbf{u}) = \int_{\mathbb{R}^2} f(\mathbf{x})\cos(2\pi ux)\cos(2\pi vy)\,d^2\mathbf{x}\ \times \tag{2.77}$$

$$\int_{\mathbb{R}^2} f(\mathbf{x})\sin(2\pi ux)\sin(2\pi vy)\,d^2\mathbf{x} \tag{2.78}$$

$$B(\mathbf{u}) = \int_{\mathbb{R}^2} f(\mathbf{x})\sin(2\pi ux)\cos(2\pi vy)\,d^2\mathbf{x}\ \times \tag{2.79}$$

$$\int_{\mathbb{R}^2} f(\mathbf{x})\cos(2\pi ux)\sin(2\pi vy)\,d^2\mathbf{x}. \tag{2.80}$$

It is not difficult to see that A and B are odd functions with respect to both arguments: $A(\mathbf{u}) = -A(-u, v) = -A(u, -v)$ and $B(\mathbf{u}) = -B(-u, v) = -B(u, -v)$. Thus, $\int_{\mathbb{R}^2} A(\mathbf{u})d^2\mathbf{u} = \int_{\mathbb{R}^2} B(\mathbf{u})d^2\mathbf{u} = 0$ which completes the proof. □

The shift theorem of the Fourier transform describes how the transform of a signal varies when the signal is shifted. If the signal f is shifted by $\mathbf{d}$, it is known that its Fourier transform is multiplied by a phase factor $\exp(-2\pi i\,\mathbf{d}\cdot\mathbf{u})$. How the QFT of f is affected by the shift is described by the following theorem.

Theorem 2.8 (Shift theorem (QFT)) *Let*

$$F^q(\mathbf{u}) = \int_{\mathbb{R}^2} e^{-i2\pi ux} f(\mathbf{x}) e^{-j2\pi vy}\,d^2\mathbf{x} \tag{2.81}$$

and

$$F^q_T(\mathbf{u}) = \int_{\mathbb{R}^2} e^{-i2\pi ux} f(\mathbf{x}-\mathbf{d}) e^{-j2\pi vy}\,d^2\mathbf{x} \tag{2.82}$$

be the QFT's of a 2D signal f and a shifted version of f, respectively. Then, $F^q(\mathbf{u})$ and $F^q_T(\mathbf{u})$ are related by shift through $\mathbf{d} = (d_1, d_2)^T$.

$$F^q_T(\mathbf{u}) = e^{-i2\pi ud_1} F^q(\mathbf{u}) e^{-j2\pi vd_2}\quad . \tag{2.83}$$

If we denote the phase of $F^q(\mathbf{u})$ by $(\phi(\mathbf{u}), \theta(\mathbf{u}), \psi(\mathbf{u}))^T$, then, as a result of the shift, the first and the second component of the phase undergo a phase-shift

$$\begin{pmatrix} \phi(\mathbf{u}) \\ \theta(\mathbf{u}) \\ \psi(\mathbf{u}) \end{pmatrix} \rightarrow \begin{pmatrix} \phi(\mathbf{u}) - 2\pi ud_1 \\ \theta(\mathbf{u}) - 2\pi vd_2 \\ \psi(\mathbf{u}) \end{pmatrix}. \tag{2.84}$$

Proof: Equation (2.83) follows from (2.81) and (2.82) by substituting $(\mathbf{x}-\mathbf{d})$ with $\mathbf{x}'$. If $F^q(\mathbf{u})$ has the polar representation

$$F^q(\mathbf{u}) = |F^q(\mathbf{u})| e^{i\phi(\mathbf{u})} e^{k\psi(\mathbf{u})} e^{j\theta(\mathbf{u})}$$

we find for the polar representation of $F^q_T(\mathbf{u})$

$$\begin{aligned} F^q_T(\mathbf{u}) &= e^{-i2\pi u d_1} F^q(\mathbf{u}) e^{-j2\pi v d_2} \\ &= e^{-i2\pi u d_1} |F^q(\mathbf{u})| e^{i\phi(\mathbf{u})} e^{k\psi(\mathbf{u})} e^{j\theta(\mathbf{u})} e^{-j2\pi v d_2} \\ &= |F^q(\mathbf{u})| e^{i(\phi(\mathbf{u})-2\pi u d_1)} e^{k\psi(\mathbf{u})} e^{j(\theta(\mathbf{u})-2\pi v d_2)}. \end{aligned}$$

This proves (2.84). □

We have shown that there exist different possibilities of choosing a phase-angle representation for quaternions. The definition we introduced in section 2.1.2 was not motivated so far. The reason for this choice is the shift theorem. A shift of the signal results in a phase shift of the first two components of the quaternionic Fourier phase which is in analogy to the complex Fourier shift theorem. This analogy would not be visible in other phase-angle representations, e.g. in the one introduced in (2.23).

In the shift theorem a shift of the signal in the spatial domain is considered. The effect of such a shift are the modulation factors shown in (2.83). In the following theorem we regard the converse situation: the signal is modulated in the spatial domain, and we ask for the effect in the quaternionic frequency domain.

Theorem 2.9 (Modulation theorem (QFT)) *Let $f(\mathbf{x})$ be a quaternion-valued signal and $F^q(\mathbf{u})$ its QFT. Further, let $f_m(\mathbf{x})$ be a version of $f(\mathbf{x})$ which is modulated by the frequency $\mathbf{u}_0 = (u_0, v_0)^\top$:*

$$f_m(\mathbf{x}) = e^{i2\pi u_0 x} f(\mathbf{x}) e^{j2\pi v_0 y}. \tag{2.85}$$

The QFT of $f_m(\mathbf{x})$ is then given by

$$\mathcal{F}_q\{f_m\}(\mathbf{u}) = F^q(\mathbf{u} - \mathbf{u}_0). \tag{2.86}$$

If $f_m(\mathbf{x})$ is a real modulated version of $f(\mathbf{x})$, i.e.

$$f_m(\mathbf{x}) = f(\mathbf{x}) \cos(2\pi x u_0) \cos(2\pi y v_0), \tag{2.87}$$

the QFT of $f_m(\mathbf{x})$ is given by

$$\begin{aligned} \mathcal{F}_q\{f_m\}(\mathbf{u}) = \frac{1}{4}\big(&F^q(\mathbf{u} + \mathbf{u}_0) + F^q(u - u_0, v + v_0) \\ &+ F^q(u + u_0, v - v_0) + F^q(\mathbf{u} - \mathbf{u}_0)\big). \end{aligned} \tag{2.88}$$

Proof: First, we consider the QFT of

$$f_m(\mathbf{x}) = e^{i2\pi u_0 x} f(\mathbf{x}) e^{j2\pi v_0 y}.$$

By inserting f_m into the definition of the QFT we obtain

$$\begin{aligned} F^q_m(\mathbf{u}) &= \int_{\mathbb{R}^2} e^{-i2\pi ux} f_m(\mathbf{x}) e^{-j2\pi vy} d^2\mathbf{x} \\ &= \int_{\mathbb{R}^2} e^{-i2\pi(u-u_0)x} f(\mathbf{x}) e^{-j2\pi(v-v_0)y} d^2\mathbf{x} \\ &= F^q(\mathbf{u}-\mathbf{u}_0). \end{aligned}$$

For the second part of the proof we introduce the abbreviation

$$\mathfrak{f}(\mathbf{x}) = e^{-i2\pi ux} f(\mathbf{x}) e^{-j2\pi vy}.$$

Further, we use the notation

$$\begin{aligned} I_{ee}(\mathbf{u}_0) &= \int_{\mathbb{R}^2} \cos(2\pi u_0 x)\mathfrak{f}(\mathbf{x})\cos(2\pi v_0 y) d^2\mathbf{x} \\ I_{oe}(\mathbf{u}_0) &= i\int_{\mathbb{R}^2} \sin(2\pi u_0 x)\mathfrak{f}(\mathbf{x})\cos(2\pi v_0 y) d^2\mathbf{x} \\ I_{eo}(\mathbf{u}_0) &= j\int_{\mathbb{R}^2} \cos(2\pi u_0 x)\mathfrak{f}(\mathbf{x})\sin(2\pi v_0 y) d^2\mathbf{x} \\ I_{oo}(\mathbf{u}_0) &= k\int_{\mathbb{R}^2} \sin(2\pi u_0 x)\mathfrak{f}(\mathbf{x})\sin(2\pi v_0 y) d^2\mathbf{x}, \end{aligned}$$

where obviously $I_{ee}(\mathbf{u}_0)$ is even with respect to u_0 and to v_0, $I_{oe}(\mathbf{u}_0)$ is odd with respect to u_0 and even with respect to v_0 and so on. We can then write

$$\begin{aligned} &\frac{1}{4}(F^q(\mathbf{u}+\mathbf{u}_0) + F^q(u-u_0, v+v_0) + F^q(u+u_0, v-v_0) + F^q(\mathbf{u}-\mathbf{u}_0)) \\ =\; &\frac{1}{4}(I_{ee}(\mathbf{u}_0) + I_{oe}(\mathbf{u}_0) + I_{eo}(\mathbf{u}_0) + I_{oo}(\mathbf{u}_0)) \\ &+\frac{1}{4}(I_{ee}(-u_0, v_0) + I_{oe}(-u_0, v_0) + I_{eo}(-u_0, v_0) + I_{oo}(-u_0, v_0)) \\ &+\frac{1}{4}(I_{ee}(u_0, -v_0) + I_{oe}(u_0, -v_0) + I_{eo}(u_0, -v_0) + I_{oo}(u_0, -v_0)) \\ &+\frac{1}{4}(I_{ee}(-\mathbf{u}_0) + I_{oe}(-\mathbf{u}_0) + I_{eo}(-\mathbf{u}_0) + I_{oo}(-\mathbf{u}_0)) \\ =\; &I_{ee}(\mathbf{u}_0) = \mathcal{F}_q\{\cos(2\pi u_0 x) f(\mathbf{x}) \cos(2\pi v_0 y)\}, \end{aligned} \tag{2.89}$$

which completes the proof. □

Theorem 2.10 (Derivative theorem (QFT)) *Let* f *be a real two-dimensional signal,* F^q *its QFT, and* $n = p + r, p, r \in \mathbb{N}$. *Then*

$$\mathcal{F}_q\left\{\frac{\partial^n}{\partial x^p \partial y^r} f\right\}(\mathbf{u}) = (2\pi)^n (iu)^p F^q(\mathbf{u})(jv)^r.$$

Proof: We prove the theorem for $(p, r) = (1, 0)$ and $(p, r) = (0, 1)$.

$$\begin{aligned}
\mathcal{F}_q\left\{\frac{\partial}{\partial x} f\right\}(\mathbf{u}) &= \int_{\mathbb{R}^2} e^{-i2\pi ux}\left(\frac{\partial}{\partial x} f\right)(\mathbf{x}) e^{-j2\pi vy} d^2\mathbf{x} && (2.90)\\
&= \int_{\mathbb{R}}\left[\int_{\mathbb{R}} e^{-i2\pi ux}\left(\frac{\partial}{\partial x} f\right)(\mathbf{x}) dx\right] e^{-j2\pi vy} dy && (2.91)\\
&= -\int_{\mathbb{R}}\left[\int_{\mathbb{R}}\left(\frac{\partial}{\partial x} e^{-i2\pi ux}\right) f(\mathbf{x}) dx\right] e^{-j2\pi vy} dy && (2.92)\\
&= 2\pi i u F^q(\mathbf{u}) && (2.93)
\end{aligned}$$

Here we used integration by parts and the fact that the signal f is assumed to tend to zero for $x \to \infty$. The proof for $(p, r) = (0, 1)$ is performed analogously.

$$\begin{aligned}
\mathcal{F}_q\left\{\frac{\partial}{\partial y} f\right\}(\mathbf{u}) &= \int_{\mathbb{R}} e^{-i2\pi ux}\left[\int_{\mathbb{R}}\left(\frac{\partial}{\partial y} f\right)(\mathbf{x}) e^{-j2\pi vy} dy\right] dx && (2.94)\\
&= -\int_{\mathbb{R}} e^{-i2\pi ux}\left[\int_{\mathbb{R}} f(\mathbf{x})\left(\frac{\partial}{\partial y} e^{-j2\pi vy}\right) dy\right] dx && (2.95)\\
&= 2\pi F^q(\mathbf{u})(jv) && (2.96)
\end{aligned}$$

For general derivatives the theorem follows from successive application of first order derivatives. □

Theorem 2.11 *The QFT of a real two-dimensional signal f is quaternionic hermitian.*

Proof: We have shown before that the QFT of a real signal has the form

$$F^q(\mathbf{u}) = F^q_{ee}(\mathbf{u}) + iF^q_{oe}(\mathbf{u}) + jF^q_{eo}(\mathbf{u}) + kF^q_{oo}(\mathbf{u}).$$

Applying the automorphisms α and β yields

$$\begin{aligned}
\alpha(F^q(\mathbf{u})) &= F^q_{ee}(\mathbf{u}) + iF^q_{oe}(\mathbf{u}) - jF^q_{eo}(\mathbf{u}) - kF^q_{oo}(\mathbf{u})\\
&= F^q_{ee}(u, -v) + iF^q_{oe}(u, -v) + jF^q_{eo}(u, -v) + kF^q_{oo}(u, -v)\\
&= F^q(u, -v) && (2.97)\\
\beta(F^q(\mathbf{u})) &= F^q_{ee}(\mathbf{u}) - iF^q_{oe}(\mathbf{u}) + jF^q_{eo}(\mathbf{u}) - kF^q_{oo}(\mathbf{u})\\
&= F^q_{ee}(-u, v) + iF^q_{oe}(-u, v) + jF^q_{eo}(-u, v) + kF^q_{oo}(-u, v)\\
&= F^q(-u, v), && (2.98)
\end{aligned}$$

which proves the theorem according to definition 2.4. □

It can often happen that a signal undergoes an affine transform in the spatial domain, which can be written as $f(\mathbf{x}) \to f(A\mathbf{x} + \mathbf{b})$, where $\mathbf{b} \in \mathbb{R}^2$ and $A \in Gl(2, \mathbb{R})$.

In these cases it is desirable to know how this transform affects the frequency representation F^q of f. The effect of the shift by $\mathbf{b}$ is already known from the shift theorem. It remains to work out how the frequency representation is transformed under a linear transform of the spatial domain: $f(\mathbf{x}) \to f(A\mathbf{x})$. This is done by the following theorem.

Theorem 2.12 (Affine theorem (QFT))
Let $f(\mathbf{x})$ be a real 2D signal and $F^q(\mathbf{u}) = \mathcal{F}_q\{f(\mathbf{x})\}(\mathbf{u})$ its QFT. Further, let A be the real regular 2×2 matrix

$$A = \begin{pmatrix} a & b \\ c & d \end{pmatrix}, \quad \textit{with} \quad \det(A) = ad - bc \neq 0.$$

The QFT of $f(A\mathbf{x})$ is then given by

$$\begin{aligned} \mathcal{F}_q\{f(A\mathbf{x})\}(\mathbf{u}) = \frac{1}{2\det(A)} & \left(F^q(d'u + c'v, b'u + a'v) + F^q(d'u - c'v, -b'u + a'v) \right. \\ & \left. - kF^q(-d'u + c'v, -b'u + a'v) + kF^q(-d'u - c'v, b'u + a'v) \right), \end{aligned} \tag{2.99}$$

where we introduced the matrix

$$B = \begin{pmatrix} a' & b' \\ c' & d' \end{pmatrix} =: \frac{A}{\det(A)} \quad \Rightarrow \quad \det(B) = \frac{1}{\det(A)}.$$

Proof: The inverse of A is given by

$$A^{-1} = \frac{1}{\det(A)} \begin{pmatrix} d & -b \\ -c & a \end{pmatrix}.$$

For the transformed coordinates we introduce the notation

$$A\mathbf{x} = \mathbf{x}' = \begin{pmatrix} x' \\ y' \end{pmatrix} = \begin{pmatrix} ax + by \\ cx + dy \end{pmatrix} \Rightarrow \begin{pmatrix} x \\ y \end{pmatrix} = \frac{1}{\det(A)} \begin{pmatrix} dx' - by' \\ -cx' + ay' \end{pmatrix}.$$

Now we can express $\mathcal{F}_q\{f(A\mathbf{x})\}(\mathbf{u})$ using the coordinates $\mathbf{x}'$ in the following way:

$$\begin{aligned} \mathcal{F}_q\{f(A\mathbf{x})\}(\mathbf{u}) &= \int_{\mathbb{R}^2} e^{-i2\pi ux} f(A\mathbf{x}) e^{-j2\pi vy} \, dx dy \\ &= \frac{1}{\det(A)} \int_{\mathbb{R}^2} e^{-i2\pi u(d'x' - b'y')} f(\mathbf{x}') e^{-j2\pi v(-c'x' + a'y')} \, dx' dy' \\ &= \frac{1}{\det(A)} \int_{\mathbb{R}^2} e^{-i2\pi u(d'x - b'y)} f(\mathbf{x}) e^{-j2\pi v(-c'x + a'y)} \, dx dy. \end{aligned}$$

In order to complete the proof we still have to show that

$$\begin{aligned} e^{-i2\pi u(d'x-b'y)}e^{-j2\pi v(-c'x+a'y)} &= \frac{1}{2}\big(\, e^{-i2\pi x(d'u+c'v)}e^{-j2\pi y(b'u+a'v)} \\ &\quad + e^{-i2\pi x(d'u-c'v)}e^{-j2\pi y(-b'u+a'v)} \\ &\quad - k e^{-i2\pi x(-d'u+c'v)}e^{-j2\pi y(-b'u+a'v)} \\ &\quad + k e^{-i2\pi x(-d'u-c'v)}e^{-j2\pi y(b'u+a'v)}\,\big)\,. \end{aligned} \tag{2.100}$$

For a more compact form of (2.100) we introduce the notation

$$\alpha = 2\pi v y a', \quad \beta = 2\pi u y b', \quad \gamma = 2\pi v x c', \quad \delta = 2\pi u x d'$$

and get the following expression:

$$\begin{aligned} e^{-i(\delta-\beta)}e^{-j(-\gamma+\alpha)} &= \frac{1}{2}\left(e^{i(-\delta-\gamma)}e^{j(-\beta-\alpha)} + e^{i(-\delta+\gamma)}e^{j(\beta-\alpha)}\right. \\ &\quad \left. -k e^{i(\delta-\gamma)}e^{j(\beta-\alpha)} + k e^{i(\delta+\gamma)}e^{j(-\beta-\alpha)}\right)\,. \end{aligned} \tag{2.101}$$

We evaluate the right-hand side:

$$\begin{aligned} & \frac{1}{2}\left(e^{i(-\delta-\gamma)}e^{j(-\beta-\alpha)} + e^{i(-\delta+\gamma)}e^{j(\beta-\alpha)} - k e^{i(\delta-\gamma)}e^{j(\beta-\alpha)} + k e^{i(\delta+\gamma)}e^{j(-\beta-\alpha)}\right) \\ = \;& \frac{1}{2}\left(e^{i(-\delta-\gamma)}e^{j(-\beta-\alpha)} + e^{i(-\delta+\gamma)}e^{j(\beta-\alpha)} - e^{-i(\delta-\gamma)}k e^{j(\beta-\alpha)} + e^{-i(\delta+\gamma)}k e^{j(-\beta-\alpha)}\right) \\ = \;& \frac{1}{2}e^{-i\delta}\left(e^{-i\gamma}e^{-j\beta} + e^{i\gamma}e^{j\beta} - e^{i\gamma}k e^{j\beta} + e^{-i\gamma}k e^{-j\beta}\right)e^{-j\alpha} \\ = \;& e^{-i\delta}\left(\cos(\gamma)\cos(\beta) + k\sin(\gamma)\sin(\beta) + i\cos(\gamma)\sin(\beta) + j\sin(\gamma)\cos(\beta)\right)e^{-j\alpha} \\ = \;& e^{-i\delta}e^{i\beta}e^{j\gamma}e^{-j\alpha}. \end{aligned}$$

Obviously, this final result equals the left-hand side of (2.101) which completes the proof. □

We can simplify the form of the theorem if we use the following notation. For a given matrix A let $A^\top$ be the transpose of A and A^t the transpose of A according to the minor diagonal:

$$A = \begin{pmatrix} a & b \\ c & d \end{pmatrix} \Rightarrow A^\top = \begin{pmatrix} a & c \\ b & d \end{pmatrix}, \quad A^t = \begin{pmatrix} d & b \\ c & a \end{pmatrix}.$$

Besides that, we use the fact that the QFT of a real signal is a quaternionic hermitian function in order to write the theorem in the form

$$\begin{aligned} \mathcal{F}_q\{f(A\mathbf{x})\}(\mathbf{u}) = \frac{1}{2\det(A)} \quad & \big(\quad F^q(\det(B)B^{-1\top}\mathbf{u}) + F^q(B^{\top t}\mathbf{u}) \\ & + \quad i(F^q(\det(B)B^{-1\top}\mathbf{u}) - F^q(B^{\top t}\mathbf{u}))j\ \big)\,. \end{aligned} \tag{2.102}$$

Example 1: As an example we will demonstrate the effect of a rotation of the original signal. The transformation matrix A is then given by

$$A = \begin{pmatrix} \cos(\phi) & -\sin(\phi) \\ \sin(\phi) & \cos(\phi) \end{pmatrix} \Rightarrow \det(A) = 1, \quad B = A^t = A, \tag{2.103}$$

$$A^T = A^{-1} = \begin{pmatrix} \cos(\phi) & \sin(\phi) \\ -\sin(\phi) & \cos(\phi) \end{pmatrix}. \tag{2.104}$$

$$\mathcal{F}_q\{f(A\mathbf{x})\}(\mathbf{u}) = \frac{1}{2} \Big(F^q(A\mathbf{u}) + F^q(A^{-1}\mathbf{u}) + i(F^q(A\mathbf{u}) - F^q(A^{-1}\mathbf{u}))j \Big). \tag{2.105}$$

Example 2: Here we regard a pure dilation of the original signal with different scaling factors for the x-axis and the y-axis. In this case the transformation matrix takes the form:

$$A = \begin{pmatrix} a & 0 \\ 0 & b \end{pmatrix} \Rightarrow \det(A) = ab, \tag{2.106}$$

$$B = B^T = \begin{pmatrix} 1/b & 0 \\ 0 & 1/a \end{pmatrix}, \quad B^t = \frac{1}{ab}B^{-1} = \begin{pmatrix} 1/a & 0 \\ 0 & 1/b \end{pmatrix}. \tag{2.107}$$

$$\mathcal{F}_q\{f(A\mathbf{x})\}(\mathbf{u}) = \frac{1}{2ab}\left(F^q\left(\frac{u}{a}, \frac{v}{b}\right) + F^q\left(\frac{u}{a}, \frac{v}{b}\right)\right. \tag{2.108}$$

$$\left. + i\left(F^q\left(\frac{u}{a}, \frac{v}{b}\right) - F^q\left(\frac{u}{a}, \frac{v}{b}\right)\right)j\right) \tag{2.109}$$

$$= \frac{1}{ab}F^q\left(\frac{u}{a}, \frac{v}{b}\right). \tag{2.110}$$

This result has the same form as the analogue result for the 2D Fourier transform. The affine theorem of the Hartley transform [14] is like the version for the QFT more complicated than the affine theorem of the Fourier transform.

2.2.3 DQFT and FQFT

The QFT has been defined for continuous signals so far. For implementation and application to sampled images we need a discrete transform. The discretized version of the QFT will be called *discrete quaternionic Fourier transform* (DQFT). It is related to the QFT in the same way as the discrete Fourier transform is related to the continuous Fourier transform.

Definition 2.10 (DQFT) *Let* f *be a discrete two-dimensional signal of the size* $M \times N$ *with components* $f_{mn} \in \mathbb{H}$*. The DQFT of* f *is then given by*

$$F^q_{uv} = \sum_{m=0}^{M-1}\sum_{n=0}^{N-1} \exp\left(-\frac{i2\pi um}{M}\right) f_{mn} \exp\left(-\frac{j2\pi vn}{N}\right).$$

The inverse DQFT reads

$$f_{mn} = \frac{1}{MN}\sum_{u=0}^{M-1}\sum_{v=0}^{N-1} \exp\left(\frac{i2\pi um}{M}\right) F^q_{uv} \exp\left(\frac{j2\pi vn}{N}\right).$$

In the case of the Fourier transform there exist algorithms which allow an efficient implementation. The most famous of these so called fast Fourier transform algorithms is the *Cooley-Tukey algorithm* (see i.e. [83]). The main idea of this algorithm in the 1D case is to divide the input vector of length N into two parts of length $N/2$, and to perform a DFT on each half. We assume N to be some integer power of 2, i.e. $N = 2^l$. The splitting of the transform domain is based on the relation

$$\begin{aligned}
F_u &= \sum_{n=0}^{N-1} \exp\left(-\frac{2\pi iun}{N}\right) f_n \\
&= \sum_{k=0}^{N/2-1} \exp\left(-\frac{2\pi iu(2k)}{N}\right) f_{2k} + \sum_{k=0}^{N/2-1} \exp\left(-\frac{2\pi iu(2k+1)}{N}\right) f_{2k+1} \\
&= \sum_{k=0}^{N/2-1} \exp\left(-\frac{2\pi iuk}{N/2}\right) f_{2k} + \exp\left(-\frac{2\pi iu}{N}\right) \sum_{k=0}^{N/2-1} \exp\left(-\frac{2\pi iuk}{N/2}\right) f_{2k+1}.
\end{aligned}$$

This process can be iterated until the domain is split into $N/2$ parts of length 2. Using this procedure the multiplicative complexity is reduced from $O(N^2)$ to $O(N\log(N))$.

There are other FFT-algorithms which split the domain at each iterative step into n parts, depending on the value of N. These algorithms are called *radix-*n *algorithms*. In this terminology the Cooley-Tukey algorithm is a *radix-2 algorithm*. Additional speed-up can be reached when the input data is known to be real-valued. In this case the real input vector of length N can be transformed into a complex vector of length $N/2$ following the scheme

$$\begin{pmatrix} f_0 \\ f_1 \\ \vdots \\ f_{N-1} \end{pmatrix} \rightarrow \begin{pmatrix} f_0 + if_1 \\ f_2 + if_3 \\ \vdots \\ f_{N-2} + if_{N-1} \end{pmatrix}.$$

This method is called *overlapping* [24].

The simplest implementation of the DQFT is a cascaded 1D FFT algorithm, which we will call *row-column algorithm*. It starts by computing the one-dimensional DFT of f_{mn} row-wise.

$$\tilde{f}_{un} = \sum_{m=0}^{M-1} \exp\left(-\frac{i2\pi um}{M}\right) f_{mn}$$

The intermediate spectrum $\tilde{f}$ is split into real and imaginary part on each of which a column-wise one-dimensional DFT is performed.

$$F^{\mathcal{R}}_{uv} = \sum_{n=0}^{N-1} \mathcal{R}(\tilde{f}_{un}) \exp\left(-\frac{i2\pi vn}{N}\right) \quad (2.111)$$

$$F^{\mathcal{I}}_{uv} = \sum_{n=0}^{N-1} \mathcal{I}(\tilde{f}_{un}) \exp\left(-\frac{i2\pi vn}{N}\right) \quad (2.112)$$

From (2.111) and (2.112) the DQFT can be evaluated by

$$F^q_{uv} = \mathcal{R}(F^{\mathcal{R}}_{uv}) + i\mathcal{R}(F^{\mathcal{I}}_{uv}) + j\mathcal{I}(F^{\mathcal{R}}_{uv}) + k\mathcal{I}(F^{\mathcal{I}}_{uv}).$$

The one-dimensional DFTs are performed as FFTs such that the multiplicative complexity of the *row-column algorithm* is $O(MN\log(MN))$. Thus, the complexity is of the same order as the complexity of the two-dimensional FFT (FFT2). However, the number of multiplications required for the row-column algorithm is higher than the number of multiplications in an FFT2 algorithm by a constant factor.

In [39] a fast quaternionic Fourier transform (FQFT) algorithm has been developed. For this algorithm the lengths M of the image rows and N of the columns are assumed to be powers of two. Further we assume the image to be square ($M = N$). The algorithm uses a *decimation in space* method, which is similar to the Cooley-Tukey two-dimensional FFT. In each recursion step the domain is split into four smaller domains of half the side-length.

Additionally an overlapping algorithm can be used if the input data is known to be real valued. Overlapping in this case reduces the domain size from $N \times N$ to $N/2 \times N/2$ by combining four real numbers to one quaternion:

$$\begin{pmatrix} f_{11} & f_{12} & \cdots & f_{1N} \\ \vdots & \vdots & & \vdots \\ f_{N1} & f_{N2} & \cdots & f_{NN} \end{pmatrix} \to \begin{pmatrix} q_{11} & q_{12} & \cdots & q_{1\,N/2} \\ \vdots & \vdots & & \vdots \\ q_{N/2\,1} & q_{N/2\,2} & \cdots & q_{N/2\,N/2} \end{pmatrix},$$

where $q_{kl} = f_{(2k-1)(2l-1)} + i f_{(2k-1)(2l)} + j f_{(2k)(2l-1)} + k f_{(2k)(2l)}$. Chernov et al. [24, 25] use the same overlapping procedure in order to speed up the two-dimensional FFT for real input data: The real $N \times N$ input image is shrunk to a quaternionic $N/2 \times N/2$ image. On this image a DQFT is performed from which the DFT of the original image is reconstructed.

2.2.4 Literature on the QFT

Sangwine has used the QFT for color image processing [85]. An RGB color image with the three components $r(\mathbf{x})$, $g(\mathbf{x})$ and $b(\mathbf{x})$ is written as a pure quaternion-valued image:

$$f(\mathbf{x}) = i\, r(\mathbf{x}) + j\, g(\mathbf{x}) + k\, b(\mathbf{x})$$

which can be transformed into the frequency domain by the QFT. This allows to transform color images holistically instead of transforming each color component separately using a complex Fourier transform. The same author developed an edge detector for color images based on the quaternion representation of color images [86].

Regrettably, no results of the application of the QFT to color images have been presented so far. We see the following fundamental problem. The QFT couples the imaginary units i and j to the orientations in the image plane, which gives them a meaning and interpretation. The color image approach adds a second, different interpretation to the imaginary units: Each unit is coupled to one of the channels of an RGB image. Thus, two conflicting interpretations are combined which leads to a coupling of orientation in the image plane to color.

A second problem lies in the restriction to 2D signals: apparently the three channels of a color image fit exactly the three imaginary units of the quaternions. However, the use of quaternions in harmonic transforms is restricted to two-dimensional images; in general, in order to extend the QFT to n-dimensional signals, 2^n-dimensional algebras have to be used. We develop this later in this thesis. In 3D, for example, there are seven imaginary units, and the correspondence to the color channels gets lost.

According to this discussion we see the value of the QFT for color image processing in the compact and complete representation, but not in its interpretative power. The value of the representation lies in the fact that it allows to reconstruct the Fourier transforms of the three channel images from the QFT of one color image.

Ell [34, 35] introduced the QFT and used it for the analysis of partial differential systems with a special interest in the stability of 2D linear, time-invariant systems. In contrast to our work, where the extension of the phase concept to the three-component phase plays an important role, Ell uses the polar representation (2.23) and interprets the angle ψ as the phase of a quaternion-valued system response. This single phase angle is used as a measure of stability of a system.

2.3 The Hartley Transform

In this section we consider another spectral transform closely related to the Fourier transform, namely the Hartley transform. The reason for doing so is that the relation between the Hartley transform and the Fourier transform is similar to the relation between the Fourier transform and the quaternionic Fourier transform which we have introduced in section 2.2. Thereby, it will be easier to see in the sequel which place is occupied by the QFT among the other transforms.

The Hartley transform was introduced by RALPH VINTON LYON HARTLEY in 1942 [54] and did not gain much attention during the first years of its existence. It seems that only in 1983 an article by RONALD N. BRACEWELL [13, 15] revived the interest in the Hartley transform. Since that time more than 100 articles on this subject have followed (see references in [79]).

Definition 2.11 (Hartley transform) *Let f be a real n-dimensional signal. The Hartley transform of f is defined as*

$$H(\mathbf{u}) = \int_{\mathbb{R}^n} f(\mathbf{x})(\cos(2\pi\mathbf{u}\mathbf{x}) + \sin(2\pi\mathbf{u}\mathbf{x}))d^n\mathbf{x}.$$

The Hartley transform differs from the Fourier transform only in the integral kernel which is $\text{cas}(2\pi\mathbf{u}\mathbf{x}) = \cos(2\pi\mathbf{u}\mathbf{x}) + \sin(2\pi\mathbf{u}\mathbf{x})$ (cas stands for "cosine-and-sine") for the Hartley transform and $\cos(2\pi\mathbf{u}\mathbf{x}) - i\,\sin(2\pi\mathbf{u}\mathbf{x})$ for the Fourier transform.

Later, in section 2.4 we will analyze the relations between the Hartley transform, the Fourier transform and the QFT. For the moment we start by comparing the Hartley and the Fourier transforms of a one-dimensional real-valued signal f. Both the Hartley transform and the Fourier transform of f can obviously be split into an even and an odd part. Let H be the Hartley transform of f:

$$\begin{aligned} H(u) &= \int_{\mathbb{R}} f(x)\mathrm{cas}(2\pi ux)dx & (2.113)\\ &= \int_{\mathbb{R}} f(x)\cos(2\pi ux)dx + \int_{\mathbb{R}} f(x)\sin(2\pi ux)dx \\ &= H_e(u) + H_o(u) \\ H_e(u) &= \int_{\mathbb{R}} f(x)\cos(2\pi ux)dx, \quad H_o(u) = \int_{\mathbb{R}} f(x)\sin(2\pi ux)dx & (2.114)\end{aligned}$$

where H_e and H_o denote the even and the odd part of H, respectively.

For the Fourier transform F of f we have:

$$\begin{aligned} F(u) &= \int_{\mathbb{R}} f(x)\exp(-i2\pi ux)dx & (2.115)\\ &= \int_{\mathbb{R}} f(x)\cos(2\pi ux)dx - i\int_{\mathbb{R}} f(x)\sin(2\pi ux)dx \\ &= F_e(u) + F_o(u) \\ F_e(u) &= \int_{\mathbb{R}} f(x)\cos(2\pi ux)dx, \quad F_o(u) = -i\int_{\mathbb{R}} f(x)\sin(2\pi ux)dx & (2.116)\end{aligned}$$

We introduce the following transforms which are derived from the cosine- and the sine-transform [12] by dividing by two:

$$\begin{aligned} C(u) &= \int_{\mathbb{R}} f(x)\cos(2\pi ux)dx & (2.117)\\ S(u) &= \int_{\mathbb{R}} f(x)\sin(2\pi ux)dx & (2.118)\end{aligned}$$

We can see easily, how both the Hartley transform and the Fourier transform can be derived from combinations of these two transforms. Note that neither C nor S contains the whole information of the input signal, i.e. none of them is invertible [94]. In order to derive an invertible harmonic transform, C and S must be combined in one way or the other. The Hartley transform and the Fourier transform are composed from C and S by $H = C + S$ and $F = C - iS$, respectively. Thus, it is easy to see that the Hartley transform and the Fourier transform are related to one another by $F = H_e - iH_o$ and $H = \mathcal{R}(F) - \mathcal{I}(F)$, where we again make use of the fact that the input signal is supposed to be real, such that the real part of the Fourier transform is even while the imaginary part is odd.

Both, the Hartley transform and the Fourier transform are invertible (the inverse of the Fourier transform has already been shown in section 2.2.1) and it is a remarkable fact that the inverse of the Hartley transform is identical with the transform itself. Consequently, both H and F carry the whole information about the original signal but in a different way.

As shown earlier, F contains redundant information in one half of the range of frequencies. This fact is known as the Hermite symmetry of the Fourier transform of a real signal: $F(u) = F^*(-u)$. However, the information in F is encoded in terms of amplitude and phase as well. On the other hand, the Hartley transform is a real-valued transform and carries no redundant information. The information is encoded only in terms of amplitude in this case.

When BRACEWELL first turned his attention towards the Hartley transform, it was thought to be valuable as a numerical tool in the first place. For example it has the advantages of being real for real input data and of being its own inverse transform. Furthermore, there exist very good fast algorithms for the evaluation of the discrete Hartley transform. Besides that the Hartley transform seemed to have no real physical significance and to be less fundamental than the Fourier transform, though [31].

However, it turned out that the analogue Hartley transform can also be implemented optically [94], where it is advantageous that the Hartley transform is a real-valued transform: Many optical recording devices are sensitive only to the intensity but not to the phase information. This leads to a loss of information in the case of the Fourier transform whereas only sign information is lost in the case of the Hartley transform.

2.4 The Hierarchy of 2D Harmonic Transforms

In the introduction to the current chapter we announced to establish a hierarchy of harmonic transforms. This hierarchy is constructed according to the following principle: The more detailed the symmetry components of a real input signal are separated by the transform, the higher the transform stands in the hierarchy. Two symmetry components are said to be separated, if they belong to different basis elements of the underlying algebra after the transformation. **We restrict ourselves to real two-dimensional signals in this section.**

The underlying algebra of the Hartley transform is $\mathbb{R}$. Since $\mathbb{R}$ is a one-dimensional algebra, the complete transform H of f belongs to the basis element 1 of $\mathbb{R}$. Thus, no separation of symmetry components is performed by the Hartley transform. The Fourier transform with the two-dimensional underlying algebra $\mathbb{C}$ separates two

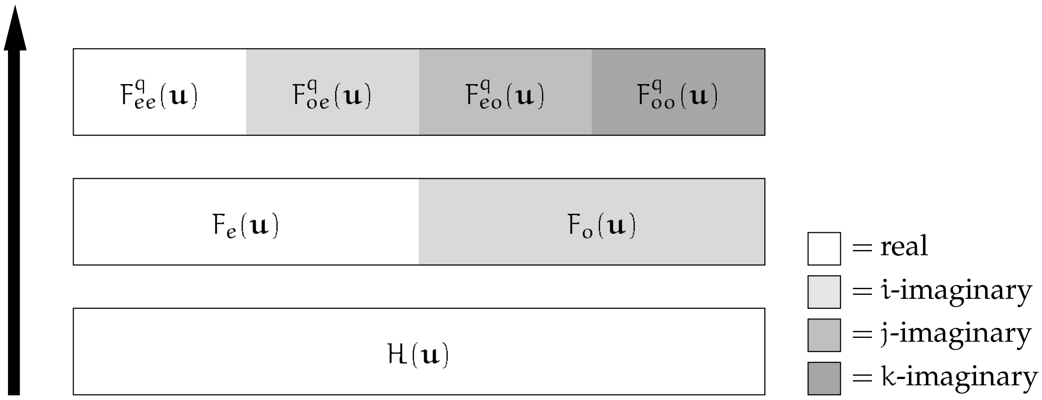

Figure 2.5: The hierarchy of 2D harmonic transforms.

components of different symmetry. This is due to the fact that the Fourier transform of a real signal is hermitian. Thus, the even part of the Fourier transform F of f belongs to the real basis element 1, while the odd part belongs to the imaginary element i, i.e. $\mathcal{R}F = F_e$ and $i\mathcal{I}F = F_o$. However, the two symmetry components F_e and F_o can be separated even finer by a separation in even and odd components with respect to both coordinate axes. This is done by the quaternionic Fourier transform. As shown earlier, for the QFT of a real signal we have $\mathcal{R}F^q = F^q_{ee}$, $i\mathcal{I}F^q = F^q_{oe}$, $j\mathcal{J}F^q = F^q_{eo}$, and $k\mathcal{K}F^q = F^q_{oo}$. The signal component f_{ee} corresponds to F^q_{ee}, f_{oe} corresponds to F^q_{oe}, and so on. Thus, the four symmetry components of f are completely separated by the QFT.

According to this discussion, it follows that in 2D the hierarchy of transforms consist of three levels with the Hartley transform on the lowest level, the Fourier transform on the next and the quaternionic Fourier transform on the highest level (see figure 2.5).

The three transforms are closely related, and since each of them contains the entire signal information, each can be transformed into the others. Let H, F, and F^q be the Hartley, Fourier, and quaternionic Fourier transforms of the same signal f, respectively. First we will show how H can be recovered from F. Since F is hermitian we have

$$F_e = \frac{F + F^*}{2}, \quad F_o = \frac{F - F^*}{2}. \tag{2.119}$$

From the definitions of the Hartley transform and the Fourier transform it follows that $H = F_e - F_o$ and thus

$$H = \frac{F + F^*}{2} - \frac{F - F^*}{2i}. \tag{2.120}$$

Further F and H can be recovered from F^q. As stated by theorem (2.11) F^q is quaternionic hermitian, such that

$$\mathcal{R}F^q = F^q_{ee} = \frac{F^q + \alpha(F^q) + \beta(F^q) + \gamma(F^q)}{4} \quad (2.121)$$

$$i\mathcal{I}F^q = F^q_{oe} = \frac{F^q + \alpha(F^q) - \beta(F^q) - \gamma(F^q)}{4} \quad (2.122)$$

$$j\mathcal{J}F^q = F^q_{eo} = \frac{F^q - \alpha(F^q) + \beta(F^q) - \gamma(F^q)}{4} \quad (2.123)$$

$$k\mathcal{K}F^q = F^q_{oo} = \frac{F^q - \alpha(F^q) - \beta(F^q) + \gamma(F^q)}{4}. \quad (2.124)$$

Using these equations and the fact that H and F can be written as

$$H = F^q_{ee} - F^q_{oe}/i - F^q_{eo}/j - F^q_{oo}/k \quad (2.125)$$

$$F = F^q_{ee} + i(F^q_{oe}/i + F^q_{eo}/j) - F^q_{oo}/k, \quad (2.126)$$

where $F^q_{ee} - F^q_{oo}/k = F_e$ and $i(F^q_{oe}/i + F^q_{eo}/j) = F_o$, we can construct the Fourier and the Hartley transform of a signal from its QFT.

These expressions show how higher-level transforms can be used in order to express lower level transforms. The other direction is possible as well, since each function $f : \mathbb{R}^2 \to \mathbb{R}$ can be decomposed into its symmetry components by

$$f_{ee}(\mathbf{x}) = \frac{1}{4}(f(\mathbf{x}) + f(-x, y) + f(x, -y) + f(-\mathbf{x})) \quad (2.127)$$

$$f_{oe}(\mathbf{x}) = \frac{1}{4}(f(\mathbf{x}) - f(-x, y) + f(x, -y) - f(-\mathbf{x})) \quad (2.128)$$

$$f_{eo}(\mathbf{x}) = \frac{1}{4}(f(\mathbf{x}) + f(-x, y) - f(x, -y) - f(-\mathbf{x})) \quad (2.129)$$

$$f_{oo}(\mathbf{x}) = \frac{1}{4}(f(\mathbf{x}) - f(-x, y) - f(x, -y) + f(-\mathbf{x})). \quad (2.130)$$

Now we can construct F and F^q from H using

$$F = H_{ee} - iH_{oe} - iH_{eo} + H_{oo} \quad (2.131)$$

$$F^q = H_{ee} - iH_{oe} - jH_{eo} - kH_{oo}. \quad (2.132)$$

We have derived the formulas for the reconstruction of F^q from H ($H \to F^q$), and of H from F ($F \to H$) which implies the formula for the reconstruction of F^q from F ($F \to F^q = F \to H \to F^q$).

So far we have analyzed the hierarchy of harmonic transforms for two-dimensional signals. An n-dimensional signal f can be separated into 2^n different symmetry components $f_{ee\dots e}$, $f_{oe\dots e}$, $\dots$, $f_{oo\dots o}$. In order to establish the full hierarchy of

n-dimensional harmonic transforms we would thus expect on the highest level a transform with a 2^n-dimensional underlying algebra. We will introduce a transform fulfilling this criterion in the next section.

2.5 Hypercomplex Fourier Transforms in nD

Up to this point in this thesis, the algebras of the complex numbers and the quaternion algebra played a special role. Complex numbers occur in the one-dimensional Fourier transform. We introduced quaternions in order to extend the two-dimensional Fourier transform concept.

In this chapter we make use of other so called hypercomplex number systems for two reasons: First, the use of quaternions is restricted to the two-dimensional transform. In order to define the n-dimensional analogue of the QFT we will need *higher-dimensional algebras*. Secondly, even in the two-dimensional case the quaternion algebra was not completely satisfactory because of the fact that the multiplication does not commute. For this reason we will introduce commutative hypercomplex algebras for the use in hypercomplex Fourier transforms in section 2.5.5.

2.5.1 The Clifford Algebra Cl_n

In the last section we showed that for an n-dimensional analogue to the QFT an 2^n-dimensional algebra is needed. As one possibility we introduce the Clifford algebra Cl_n. Before Cl_n is defined we give a general definition of a Clifford algebra (see [71]).

Definition 2.12 (Clifford algebra) *Let V be a linear space with the quadratic form*

$$\langle x, y \rangle = \sum_{l,m=1}^{n} a_{lm} x_l y_m, \quad a_{lm} = a_{ml} \in \mathbb{R}.$$

The algebra generated by the symbols $\{i_1, \ldots, i_n\}$ and the relations $i_l i_m + i_m i_l - 2a_{lm} = 0$ is called the Clifford algebra of the quadratic form $\langle \cdot, \cdot \rangle$.

The Clifford algebra Cl_n is the Clifford algebra of the Euclidean scalar product in $\mathbb{R}^n$, i.e. $a_{ij} = 1$ if $i = j$ and $a_{ij} = 0$ else. Cl_n can be generated from n elements as follows.

Let $\{i_1, \ldots, i_n\}$ be n symbols obeying the multiplication rules $i_l^2 = -1$ for all $l \in \{1, \ldots, n\}$ and $i_l i_m = -i_m i_l$ for $l \neq m$. The elements $i_l i_m$ are called elements of grade two and denoted by $i_l i_m = i_{lm}$. There are $\binom{n}{2}$ basis elements of grade two. Applying the same procedure to the elements of grade two we get elements of grade three: $i_k(i_{lm}) = (i_{kl})i_m = i_{klm}$ for pair–wise different k, l and m. We continue like this and get as element with the highest grade one basis element with grade n. Altogether we get $\sum_{k=0}^{n} \binom{n}{k} = 2^n$ basis elements. The n basis elements of grade one $\{i_1, i_2, \ldots, i_n\}$ will be called *basis vectors of* Cl_n.

These 2^n elements build a basis of the real Clifford algebra Cl_n. Addition is defined component-wise, multiplication according to the generation rules above, and multiplication by a real scalar a is performed by multiplying all 2^n components by a. Cl_n contains the n complex subfields

$$\mathbb{R}\{1, i_m\} = \{z = a + b i_m | a, b \in \mathbb{R}\}, \quad m \in \{1, \ldots, n\}. \tag{2.133}$$

For later use we define conjugation in Cl_n.

Definition 2.13 *The conjugation of the basis vectors of* Cl_n *is defined by*

$$\bar{}: i_m \mapsto \overline{i_m} = -i_m.$$

The conjugation of general elements of Cl_n *is generated by the vector conjugation as anti-involution, i.e.*

$$\bar{}: i_{ab\ldots c} \mapsto (i_{ab\ldots c})^{-} = \bar{i_c} \ldots \bar{i_b}\bar{i_a}.$$

2.5.2 Clifford Fourier Transforms

The Clifford Fourier transform, which will be introduced in this section, is the extension of the quaternionic Fourier transform to n-dimensional signals.

Definition 2.14 (Clifford Fourier transform (CFT))
The Clifford Fourier transform $F^c(\mathbf{u})$ *of an* n*–dimensional signal* $f(\mathbf{x})$ *is defined by*

$$F^c(\mathbf{u}) = \int_{\mathbb{R}^n} f(\mathbf{x}) \prod_{k=1}^{n} \exp(-i_k 2\pi u_k x_k) d^n\mathbf{x} \quad . \tag{2.134}$$

where $\mathbf{u} = (u_1, u_2, \ldots, u_n)$, $\mathbf{x} = (x_1, x_2, \ldots, x_n)$ *and* $i_1, i_2, \ldots, i_n$ *are the basis vectors of the Clifford algebra* Cl_n. *The product is meant to be performed in a fixed order:* $\prod_{j=1}^{n} a_j = a_1 a_2 \cdots a_n$. *For simplicity we introduce the notation*

$$f \;\circ\!\xrightarrow{Cl_n}\!\bullet\; F^c \quad \textit{or} \quad F^c \;\bullet\!\xrightarrow{Cl_n}\!\circ\; f$$

in order to indicate that F^c *is the Clifford Fourier transform of* f.

For $n = 1$ the Clifford Fourier transform is the one-dimensional complex Fourier transform, for $n = 2$, and for real signals, it is the quaternionic Fourier transform. We have to introduce the restriction to real signals merely because of the different order of factors under the integrals in definitions 2.9 and 2.14. However, even for quaternion-valued signals the QFT is closely related to the two-dimensional CFT.

Theorem 2.13 (Inverse Clifford Fourier transform)
The inverse Clifford Fourier transform exists and is obtained by

$$\mathcal{F}_c^{-1}\{F^c\}(\mathbf{x}) = \int_{\mathbb{R}^n} F^c(\mathbf{u})\overline{\left(\prod_{k=1}^{n} \exp(-i_k 2\pi u_k x_k)\right)} d^n\mathbf{u} \tag{2.135}$$

$$= \int_{\mathbb{R}^n} F^c(\mathbf{u})\left(\prod_{k=1}^{n} \exp(i_{n+1-k} 2\pi u_{n+1-k} x_{n+1-k})\right) d^n\mathbf{u}. \tag{2.136}$$

Proof: Inserting term (2.134) into the formula (2.135) yields

$$\begin{aligned}
&\int_{\mathbb{R}^n}\int_{\mathbb{R}^n} f(\mathbf{x}')\prod_{j=1}^{n} e^{-i_j 2\pi u_j x'_j} d^n\mathbf{x}' \prod_{k=0}^{n-1} e^{i_{n-k} 2\pi u_{n-k} x_{n-k}} d^n\mathbf{u} \\
=& \int_{\mathbb{R}^n} f(\mathbf{x}')\delta^n(\mathbf{x}-\mathbf{x}') d^n\mathbf{x}' \\
=& f(\mathbf{x}),
\end{aligned}$$

where again the orthogonality of the harmonic exponential functions is used. □

2.5.3 Hypercomplex Numbers

The algebras that occurred so far (namely $\mathbb{C}$, $\mathbb{H}$, and the Clifford algebra Cl_n) are examples of so called hypercomplex number systems. In general a hypercomplex number system is a set of expressions of the form

$$a_0 + a_1 i_1 + \ldots + a_n i_m \tag{2.137}$$

where $a_0, \ldots a_m$ are real numbers and $i_1, \ldots i_m$ are symbols for which multiplication can be defined by prescribing a multiplication table which assigns to each ordered pair $i_k i_l$ an expression of the form (2.137).

	1	i
1	1	i
i	i	−1

	1	i	j	k
1	1	i	j	k
i	i	−1	k	−j
j	j	−k	−1	i
k	k	j	−i	−1

Table 2.3: The multiplication tables of $\mathbb{C}$ (left) and $\mathbb{H}$ (right).

The addition of two hypercomplex numbers is performed component-wise, i.e.

$$\begin{aligned} & a_0 + a_1 i_1 + \dots a_m i_m \\ + \;& b_0 + b_1 i_1 + \dots b_m i_m \\ = \;& (a_0 + b_0) + (a_1 + b_1) i_1 + \dots (a_m + b_m) i_m . \end{aligned} \tag{2.138}$$

The set of expressions of the form (2.137) together with the addition and multiplication as defined above forms an algebra. Whether algebraic properties such as commutativity, associativity, and alternativity are fulfilled or not, depends only on the form of the multiplication table.

In table 2.3 the multiplication tables of the complex numbers and of the quaternions are shown, respectively. In the multiplication tables the columns on the left-hand side give the first factor while the top row indicates the second factor. This is important since hypercomplex numbers are not commutative, in general.

2.5.4 Commutative Hypercomplex Algebras

For a modification of the CFT we choose another algebra from the set of hypercomplex algebras introduced before. The most problematic property of the QFT and the CFT has been the non-commutativity of the multiplication. Therefore, we define a hypercomplex algebra with similar construction rules as the Clifford algebra Cl_n but with commutative multiplication rules. This algebra was used in [40] in order to introduce an alternative to the Clifford Fourier transform.

Definition 2.15 (HCA_n**)** *Let* $\{i_1, \dots, i_n\}$ *be* n *symbols obeying the multiplication rules* $i_l^2 = -1$ *for all* $l \in \{1, \dots, n\}$ *and* $i_l i_m = i_m i_l$ *for* $l \neq m$*. The elements* $i_l i_m$ *are called elements of grade two and are denoted by* $i_l i_m = i_{lm}$*. There are* $\binom{n}{2}$ *basis elements of grade two. Applying the same procedure to the elements of grade two we get elements of grade three:* $i_k(i_{lm}) = (i_{kl}) i_m = i_{klm}$ *for pair–wise different* k, l *and* m*. We continue like this and get as the element with the highest grade one basis element with grade* n*. Altogether we get* $\sum_{k=0}^{n} \binom{n}{k} = 2^n$ *basis elements.*

These 2^n elements build a basis of the real commutative algebra HCA_n. Addition is defined component-wise, multiplication according to the generation rules above and multiplication by a real scalar a is performed by multiplying all 2^n components by a.

In order to identify the algebra HCA_n among known algebras we state the following theorem.

Theorem 2.14 *The algebra HCA_n is isomorphic to $\mathbb{C}^m$ with $m = 2^{n-1}$.*

Proof: See [40]. □

Note: By $\mathbb{C}^m$ we denote the m-fold Cartesian product of $\mathbb{C}$. An element $Z \in \mathbb{C}^m$ has the form $Z = (z_1, z_2, \ldots, z_m)$. Let $Z, W \in \mathbb{C}^m$ and $a \in \mathbb{R}$. Then addition, multiplication and multiplication by a scalar are defined via

$$\begin{aligned} Z + W &= (z_1 + w_1, z_2 + w_2, \ldots, z_m + w_m) && (2.139)\\ ZW &= (z_1 w_1, z_2 w_2, \ldots, z_m w_m) && (2.140)\\ aZ &= (az_1, az_2, \ldots, az_m), && (2.141)\end{aligned}$$

i.e. the operations are performed component-wise. The algebra $\mathbb{C}^m$ is not a division algebra as can easily be seen from the fact, that the equation

$$(0, 1, \ldots, 1)(x_1, x_2, \ldots, x_n) = (0, 2, \ldots, 2) \qquad (2.142)$$

has infinitely many solutions, namely

$$(x_1, x_2, \ldots, x_n) = (x_1, 2, \ldots, 2), \quad \text{for all } x_1 \in \mathbb{C}.$$

More generally the above fact follows from Frobenius' theorem which states that there are only three associative division systems. We state the theorem without proof.

Theorem 2.15 (Frobenius' theorem) *Every associative division algebra is isomorphic to one of the following: the algebra of real numbers, the algebra of complex numbers, and the algebra of quaternions.*

Example ($n = 2$): We denote the basis of HCA_2 by $e_1 = 1$, $e_2 = i_1$, $e_3 = i_2$, $e_4 = i_{12}$. The multiplication table of HCA_2 in this basis is given by

	e_1	e_2	e_3	e_4
e_1	e_1	e_2	e_3	e_4
e_2	e_2	$-e_1$	e_4	$-e_3$
e_3	e_3	e_4	$-e_1$	$-e_2$
e_4	e_4	$-e_3$	$-e_2$	e_1

Table 2.4: The multiplication table of HCA_2

On the other hand we denote a basis of $\mathbb{C}^2$ by

$$\begin{aligned} f_1 &= (1,0), & f_2 &= (i,0) \\ f_3 &= (0,1), & f_4 &= (0,i). \end{aligned} \tag{2.143}$$

Let a new basis of $\mathbb{C}^2$ be given by $E_i = \sum_{j=1}^{4} A_{ij} f_j$ with the transformation matrix

$$A = \begin{pmatrix} 1 & 0 & 1 & 0 \\ 0 & 1 & 0 & 1 \\ 0 & -1 & 0 & 1 \\ 1 & 0 & -1 & 0 \end{pmatrix}.$$

The E_i follow the same multiplication table as the e_i, thus A establishes the isomorphism between HCA_2 and $\mathbb{C}^2$.

Remark: From the fact that HCA_2 is commutative it is immediately clear that it is not a Clifford algebra. However, HCA_2 can be embedded into the Clifford algebra Cl_4 by the substitutions:

$$i_1 \to i_{12} \quad i_2 \to i_{34} \quad i_{12} \to i_{1234}. \tag{2.144}$$

I.e. the set $\{1, i_{12}, i_{34}, i_{1234}\}$ generates a subalgebra of Cl_4 which is isomorphic to HCA_2.

Example ($n = 3$): We denote the basis of HCA_3 by $e_1 = 1$, $e_2 = i_1$, $e_3 = i_2$, $e_4 = i_3$, $e_5 = i_{12}$, $e_6 = i_{13}$, $e_7 = i_{23}$, $e_8 = i_{123}$. The multiplication table of HCA_3 in this basis is given by

	e_1	e_2	e_3	e_4	e_5	e_6	e_7	e_8
e_1	e_1	e_2	e_3	e_4	e_5	e_6	e_7	e_8
e_2	e_2	$-e_1$	e_5	e_6	$-e_3$	$-e_4$	e_8	$-e_7$
e_3	e_3	e_5	$-e_1$	e_7	$-e_2$	e_8	$-e_4$	$-e_6$
e_4	e_4	e_6	e_7	$-e_1$	e_8	$-e_2$	$-e_3$	$-e_5$
e_5	e_5	$-e_3$	$-e_2$	e_8	e_1	$-e_7$	$-e_6$	e_4
e_6	e_6	$-e_4$	e_8	$-e_2$	$-e_7$	e_1	$-e_5$	e_3
e_7	e_7	e_8	$-e_4$	$-e_3$	$-e_6$	$-e_5$	e_1	e_2
e_8	e_8	$-e_7$	$-e_6$	$-e_5$	e_4	e_3	e_2	$-e_1$

Table 2.5: The multiplication table of HCA_3

On the other hand we denote a basis of $\mathbb{C}^4$ by

$$\begin{aligned} f_1 &= (1,0,0,0), & f_2 &= (i,0,0,0) \\ f_3 &= (0,1,0,0), & f_4 &= (0,i,0,0) \\ f_5 &= (0,0,1,0), & f_6 &= (0,0,i,0) \\ f_7 &= (0,0,0,1), & f_8 &= (0,0,0,i) \end{aligned} \tag{2.145}$$

We introduce a new basis of $\mathbb{C}^4$ by $E_i = \sum_{j=1}^{4} A_{ij} f_j$ with the transformation matrix

$$A = \begin{pmatrix} 1 & 0 & 1 & 0 & 1 & 0 & 1 & 0 \\ 0 & 1 & 0 & 1 & 0 & 1 & 0 & 1 \\ 0 & 1 & 0 & 1 & 0 & -1 & 0 & -1 \\ 0 & 1 & 0 & -1 & 0 & 1 & 0 & -1 \\ -1 & 0 & -1 & 0 & 1 & 0 & 1 & 0 \\ -1 & 0 & 1 & 0 & -1 & 0 & 1 & 0 \\ -1 & 0 & 1 & 0 & 1 & 0 & -1 & 0 \\ 0 & -1 & 0 & 1 & 0 & 1 & 0 & -1 \end{pmatrix}.$$

It is easily shown that the E_i follow the same multiplication table as the e_i, thus A establishes the isomorphism between HCA_3 and $\mathbb{C}^4$.

2.5.5 Commutative Hypercomplex Fourier Transforms

Since the n-dimensional CFT contains n exponential functions with n different imaginary units, it is a main property of any algebra which is used in an n-dimensional hypercomplex Fourier transform to contain n complex subfields with orthogonal imaginary units. We can use this freedom of choosing a hypercomplex algebra in order to overcome the problems caused by the non-commutativity of the Clifford algebras used before. These problems became apparent when trying to establish fast algorithms for the CFT [40] and in the complicated form of the convolution theorem (Theorem 2.6) of the QFT. The stated requirement is fulfilled by HCA_n since there are n complex subfields given by $\mathbb{R}\{1, i_l\}$, $l \in \{1, \ldots, n\}$. Thus, we can introduce a hypercomplex Fourier transform with HCA_n as underlying algebra.

Definition 2.16 (Commutative Hypercomplex Fourier Transform (HCFT)) *The HCFT $F^h(\mathbf{u})$ of an n–dimensional signal $f(\mathbf{x})$ is defined by*

$$F^h(\mathbf{u}) = \int_{\mathbb{R}^n} f(\mathbf{x}) \exp(-2\pi \mathbf{u}^T I_n \mathbf{x}) d^n\mathbf{x} \quad . \tag{2.146}$$

where $\mathbf{u} = (u_1, u_2, \ldots, u_n)$, $\mathbf{x} = (x_1, x_2, \ldots, x_n)$, I_n is the matrix given by

$$I_n = \begin{pmatrix} i_1 & 0 & \ldots & 0 \\ 0 & i_2 & \ddots & \vdots \\ \vdots & \ddots & \ddots & 0 \\ 0 & \ldots & 0 & i_n \end{pmatrix} , \tag{2.147}$$

and $i_1, i_2, \ldots, i_n$ are the basis vectors of the commutative hypercomplex algebra HCA_n.

Note, that the HCFT can be written in a more compact way than the CFT. This is due to the fact that the commutativity of HCA_n allows us to use the addition formula of the exponential function ($\exp(x)\exp(y) = \exp(x+y)$). As noted above this is not possible in non-commutative algebras.

In order to compare the results of the CFT and HCFT we introduce a simple mapping between Cl_n and HCA_n in the following.

Definition 2.17 (Switching) *Let S_n be a one-to-one linear mapping from Cl_n to HCA_n generated by $S_n(1) = 1$, $S_n(i_k) = i_k$ and $S_n(i_{kl\ldots m}) = i_{kl\ldots m}$.* **The indices of $i_{kl\ldots m}$ are assumed to be in ascending order.**

Since S_n is one-to-one, it is an invertible mapping. The process of applying S_n and S_n^{-1} will be called *switching between Cl_n and HCA_n* in the following. Switching between Cl_n and HCA_n is used to establish the following relation between the CFT and the HCFT.

Theorem 2.16 *Let F^c and F^h be the CFT and the HCFT of the real n-dimensional signal f. Then we have*

$$S_n(F^c(\mathbf{u})) = F^h(\mathbf{u}).$$

Proof: The proof follows directly from the following facts:

1. The exponential functions $\exp(2\pi i_m u_m x_m)$ in the CFT-kernel are ordered by ascending m.

2. The switching mapping S is linear.

□

As an example we compare the QFT to the two-dimensional HCFT. The 2D commutative hypercomplex Fourier transform (HCFT) of a two-dimensional signal f is given by

$$F^h(\mathbf{u}) = \int_{\mathbb{R}^2} f(\mathbf{x}) \exp(-2\pi \mathbf{x}^\top I_2 \mathbf{u}) d\mathbf{x}.$$

with I_2 containing the imaginary units

$$I_2 = \begin{pmatrix} i_1 & 0 \\ 0 & i_2 \end{pmatrix}.$$

Using the switching function S_2 it is possible to compare the QFT and the HCFT of a two-dimensional signal f according to theorem 2.16: For the QFT and the HCFT of a real two-dimensional signal we have $S_2(F^q(\mathbf{u})) = F^h(\mathbf{u})$.

In section 2.2.2 we proved the convolution theorem for the QFT and found an expression which is more complicated than the analogue of the Fourier transform. We recall the QFT convolution theorem (see equation (2.6)):

$$g(\mathbf{x}) * h(\mathbf{x}) \quad \circ\!\!\overset{\mathbb{H}}{\longrightarrow}\!\!\bullet \quad G^q_{\cdot e}(\mathbf{u}) H^q(\mathbf{u}) + G^q_{\cdot o}(\mathbf{u}) \beta(H^q)(\mathbf{u}).$$

This apparent drawback of the QFT is due to the non-commutativity of the quaternion algebra, since in the proof of the convolution theorem two exponential functions containing two different imaginary units as arguments have to be commuted. This can only be accomplished by splitting up one exponential by applying Euler's rule. Thus, the result cannot be expressed as a simple product but only as the sum of two products. The number of products would increase in higher dimensional Clifford algebras and soon reach a form which could be hard to overlook. Theorem 2.17 shows how switching to a commutative algebra simplifies the situation.

Theorem 2.17 *Let f and g be two real two-dimensional functions, and F^h and G^h their HCFT's. Then the convolution of f and g corresponds to a multiplication in the HCFT-domain:*

$$f * g \quad \circ\!\!\overset{\mathbb{C}^2}{\longrightarrow}\!\!\bullet \quad F^h G^h. \tag{2.148}$$

Proof: The proof follows the proof of theorem 2.6 with the simplification that because of the commutativity it is not necessary to split the exponential function into sine and cosine.

Corollary 2.1 *Let* f *and* g *be two two-dimensional functions, and* F^q *and* G^q *their QFT's. Then the following relation is valid:*

$$f * g \quad \circ\!\!\xrightarrow{\;\mathbb{H}\;}\!\!\bullet \quad S_2^{-1}(S_2(G^q)S_2(H^q)). \tag{2.149}$$

Proof: From Theorem 2.17 we know that

$$f * g \quad \circ\!\!\xrightarrow{\;\mathbb{C}^2\;}\!\!\bullet \quad F^h G^h.$$

Applying the switching function S_2 this can be rewritten as

$$f * g \quad \circ\!\!\xrightarrow{\;\mathbb{C}^2\;}\!\!\bullet \quad S_2(F^q)S_2(G^q) \tag{2.150}$$

According to theorem 2.16 equation (2.150) can be expressed in terms of the QFT:

$$f * g \quad \circ\!\!\xrightarrow{\;\mathbb{H}\;}\!\!\bullet \quad S_2^{-1}(S_2(F^q)S_2(G^q)) \tag{2.151}$$

which completes the proof. □

2.6 Summary

In this chapter we introduced the 2D quaternionic Fourier transform (QFT) and its n-dimensional extension, the Clifford Fourier transform (CFT). These transforms are built by using n different imaginary units in the arguments of the n exponential functions of the nD Fourier transform. The imaginary units are elements of 2^n-dimensional, non-commutative Clifford algebras.

An important feature of the QFT and of the CFT are their symmetry properties. The construction of the transforms was actually motivated by the aim to gain these properties. The symmetry properties of the 1D Fourier transform have been analyzed in detail e.g. in [12]. The Fourier transform of a real signal is hermitian, i.e. even and odd part of the signal are separated by the complex algebra: the even part of the transform is real, the odd part is imaginary. In contrast, the Hartley transform is a real transform and thus it is not selective with respect to symmetry. We have shown that the QFT extends the symmetry selectivity of the 1D complex Fourier transform to 2D. In 2D there are four components of different symmetry which are transformed by the QFT into real, i-imaginary, j-imaginary, and k-imaginary parts, respectively. Thus, we were able to establish a hierarchy of transforms with respect to the symmetry selectivity. In 1D this hierarchy contains only the Hartley transform and the Fourier transform, while in 2D it is extended by the QFT. In nD the 2^n components of different symmetry are separated by the CFT.

Concentrating on the QFT, we established corresponding theorems to the main theorems of the complex Fourier transform, such as the shift theorem and the modulation theorem, the affine theorem, Rayleigh's theorem, the convolution theorem, and the existence of the inverse transform. The convolution theorem of the QFT is slightly more complicated than the convolution theorem of the complex Fourier transform. This is a result of the non-commutativity of the quaternion algebra. For this reason another transform has been introduced, similar to the QFT, but using a *commutative* four-dimensional hypercomplex number system. Also in nD it is possible to define a transform using a (2^n-dimensional) commutative algebra. We have shown that for real signals there exists a simple mapping between the results of a non-commutative CFT and the commutative hypercomplex transform.

Chapter 3

The Phase Concept

On the bases laid in the former chapter we will turn our attention to the *phase of a signal*. We will distinguish three different types of signal phase: *Global* or *Fourier* phase, *instantaneous* phase, and *local* phase. Sometimes the last two terms are used interchangeably. However, we will make a distinction as explained below. Global phase denotes the angular phase of the complex Fourier transform of a signal. Thus, it gives a real number $\phi \in [-\pi, \pi[$ at each position in the complex frequency domain. The Fourier phase indicates the relative position of the frequency components. It has been shown by Oppenheim and Lim [80] that the phase information is more important for the perceptual impression of an image than the energy of the frequency components. Figure 3.1 demonstrates this effect[1]. Two images of Fourier and Hilbert are Fourier transformed and represented in amplitude/phase representation in the frequency domain. We first reconstruct Fourier's image from its amplitude spectrum alone. Therefore, we set the phase to zero in all frequency channels. The second reconstruction uses merely phase information. The amplitude is set to a constant value. This choice is very unnatural since the power spectra of natural images are known to be of $1/f^2$ characteristic [41]. However, in this case the original image can be recognized shadowy, while in the first case nothing can be seen. The third reconstruction uses the amplitude of the Fourier transform of Hilbert's image combined with the phase of the Fourier transform of Fourier's image. In this case Fourier's image can well be recognized. This shows the importance of phase information in images.

In image analysis we sometimes need another kind of phase information. Instead of asking for the phase of a certain frequency component, which is given by the

[1] The images of Fourier and Hilbert have been taken from a web site on the history of Mathematics: http://www-groups.dcs.st-and.ac.uk/~history

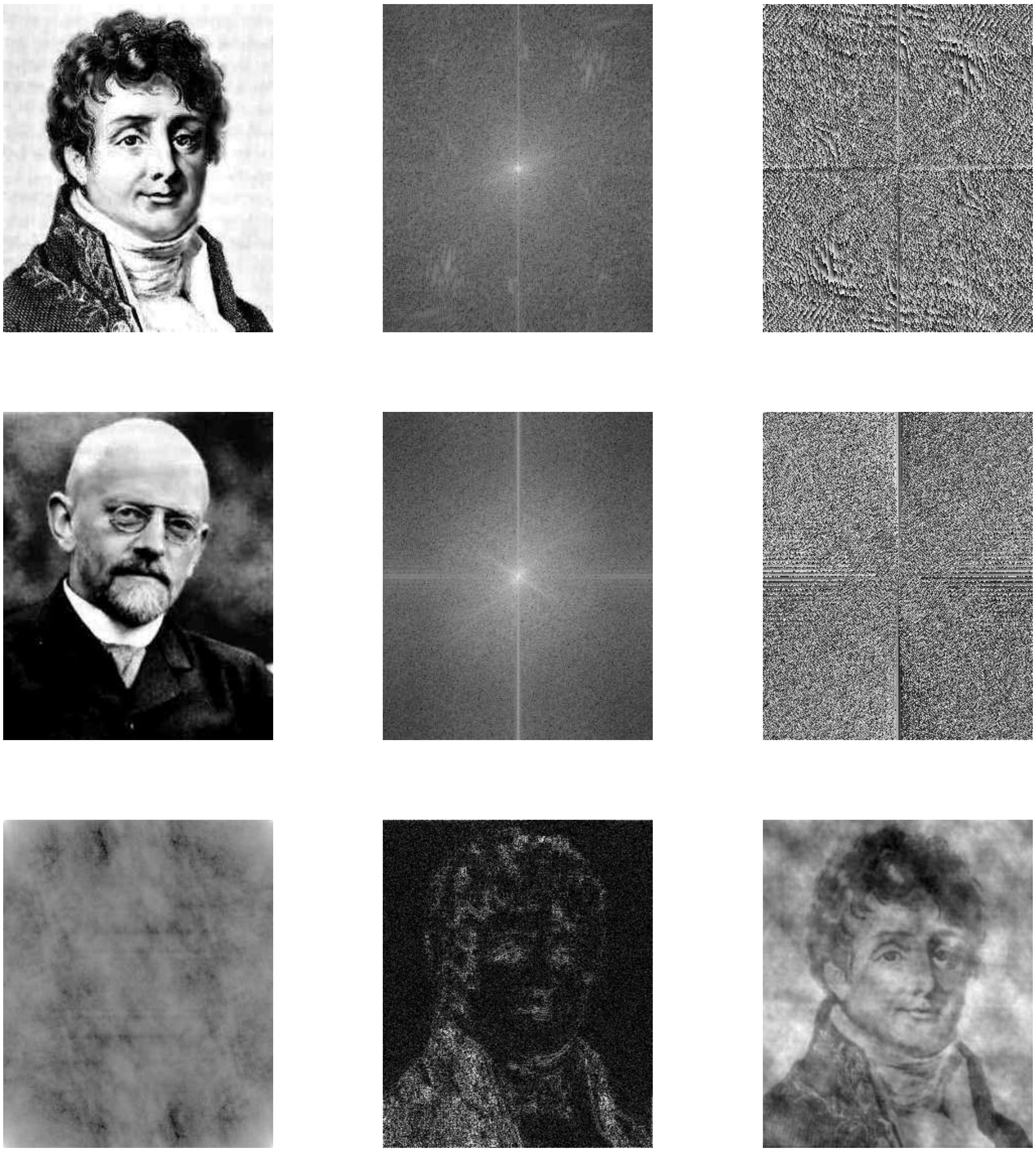

Figure 3.1: First row: an image of Fourier (left), and its Fourier transform: amplitude (middle) and phase (right). Second row: an image of Hilbert (left), and its Fourier transform: amplitude (middle) and phase (right). Third row: the reconstruction of Fourier's image from amplitude information only (left), from phase information only (middle), and from the combination of Hilbert's amplitude with Fourier's phase. For a more detailed description see text. A similar experiment is shown in [23].

Fourier phase, we might ask for the phase at a certain position in a real signal. The answer to this question is given by the instantaneous and the local phase in two different ways. In order to evaluate the instantaneous phase we first construct the analytic signal which is a combination of the original signal and its Hilbert transform. From the analytic signal the instantaneous phase can be read of as the angular phase of the complex value at each position of the signal. Although, the instantaneous phase seems to yield local information, it depends on the whole signal, since constructing the analytic signal involves the Hilbert transform which is a global transform. Thus, the instantaneous phase at any point changes with signal parts however far away from the point of interest. In order to overcome this, we use local filters the impulse responses of which are analytic signals themselves. These filters are called quadrature filters. The filter responses of these filters to a real signal are complex valued. The local phase is defined as the angular phase of the complex filter response at a certain position of the signal.

All these concepts are well defined for one-dimensional signals. However, the extension to higher dimensions is only trivial for the Fourier phase. The extension of the instantaneous and local phase concept to higher dimensions has been treated in the literature mostly in a way which is restricted to intrinsically one-dimensional signals.

We will show how the analytic signal can be defined in 2D using the quaternionic Fourier transform. We compare the quaternionic analytic signal to earlier approaches to the 2D analytic signal. The quaternionic analytic signal allows to generalize the instantaneous phase which is defined as the triple of phase angles of the quaternionic value of the quaternionic analytic signal at each position. In the line indicated above it follows immediately that in addition to the instantaneous quaternionic phase there should be the possibility to define a local quaternionic phase. This is accomplished by introducing quaternionic quadrature filters. Actually, we will deal with quaternionic Gabor filters which are no exact quaternionic quadrature filters but provide a good approximation to such filters.

3.1 The Analytic Signal

The notion of the analytic signal of a real one-dimensional signal was introduced in 1946 by Gabor [44]. Before going into technical details we will give a vivid explanation of the meaning of the analytic signal. If we regard a real one-dimensional signal f as varying with time, it can be represented by the oscillating vector from the origin to $f(t)$ on the real line. Taking a snapshot of the vector at time t_0 as shown in figure 3.1 reveals no information about the amplitude or the instantaneous phase of the oscillation. I.e. it is invisible whether f is still growing to the right or already on the returning way and what is the amplitude of the oscillation. The analytic signal of f is a complex-valued signal, denoted by f_A. Thus, f_A can be visualized as a rotating vector in the complex plane. This vector has the property that its projection to the real axis is identical to the vector given by f. Moreover, if a snapshot is taken, the length of the vector, and its angle against the real axis give the instantaneous amplitude and the instantaneous phase of f, respectively. The analytic signal is constructed by adding to the real signal f a signal which is shifted by $-\pi/2$ in phase against f.

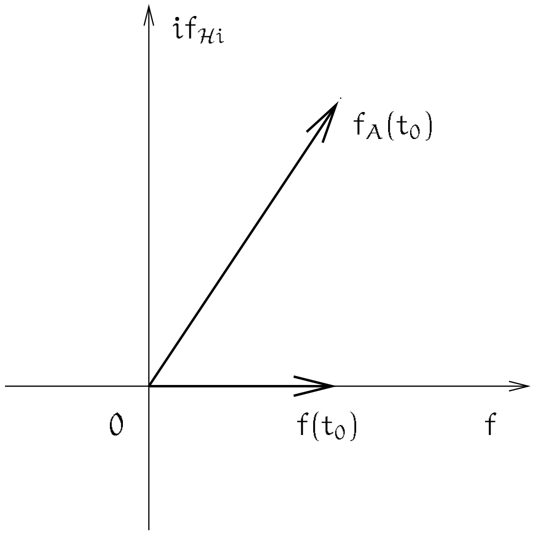

Figure 3.2: Snapshot of the oscillating vector to f and the rotating vector to f_A at time t_0.

In this chapter we will shortly review the analytic signal in 1D and four approaches to the analytic signal in 2D which have occurred in the literature [48, 49, 45, 90]. We investigate the different principles which lie at the basis of the definitions and conclude with a set of desirable properties of the 2D analytic signal. Based on the QFT it is possible to introduce a novel definition of the analytic signal which fulfills most of the desired properties.

3.1.1 The 1D Analytic Signal

As mentioned above, the analytic signal f_A of a real one-dimensional signal f is defined as the sum of f and a version of f which is shifted in phase by $(-\pi/2)$ multiplied by i. The shifted version of f is the Hilbert transform $f_{\mathcal{H}i}$ of f. Thus, the analytic signal can be written as $f_A = f + if_{\mathcal{H}i}$. This is the generalization of the complex notation of harmonic signals given by Euler's equation $\exp(i2\pi ux) = \cos(2\pi ux) + i\sin(2\pi ux)$.

A phase shift by $(-\pi/2)$ – which is expected to be done by the Hilbert transform – can be realized by taking the negative derivative of a function. E.g. we have

$$-\frac{\partial}{\partial x}\cos(2\pi ux) = 2\pi u \sin(2\pi ux),$$

which shifts the cosine-function and additionally scales the amplitude with the angular frequency $\omega = 2\pi u$. In order to avoid this extra scaling we divide each frequency component by the absolute value of the angular frequency. This procedure can easily be described in the Fourier domain: Taking the negative derivative results in multiplication by $-i2\pi u$. Dividing by $|2\pi u|$ results in the following procedure in the frequency domain:

$$F(u) \mapsto -i\frac{u}{|u|}F(u) = -i\,\mathrm{sign}(u)F(u),$$

which makes plausible the definition of the Hilbert transform.

The formal definitions of the Hilbert transform and of the analytic signal are as follows:

Definition 3.1 (Hilbert Transform) *Let f be a real 1D signal and F its Fourier transform. The Hilbert transform of f is then defined in the frequency domain by*

$$F_{\mathcal{H}i}(u) = -i\,sign(u)F(u) \quad \textit{with} \quad \mathrm{sign}(u) = \begin{cases} 1 & \textit{if}\; u > 0 \\ 0 & \textit{if}\; u = 0 \\ -1 & \textit{if}\; u < 0 \end{cases}. \tag{3.1}$$

In spatial domain this reads

$$f_{\mathcal{H}i}(x) = f(x) * \frac{1}{\pi x}, \tag{3.2}$$

where $*$ denotes the convolution operation.

The convolution integral in (3.2), namely

$$f_{\mathcal{H}i}(x) = \frac{1}{\pi} \int_{\mathbb{R}} \frac{f(\xi)}{x-\xi} d\xi$$

contains a singularity at $x = \xi$. This is handled by evaluating Cauchy's principle value, i.e.

$$\begin{aligned} f_{\mathcal{H}i}(x) &= \frac{1}{\pi} P \int_{\mathbb{R}} \frac{f(\xi)}{x-\xi} d\xi & (3.3) \\ &= \frac{1}{\pi} \lim_{\epsilon \to 0} \left(\int_{-\infty}^{x-\epsilon} \frac{f(\xi)}{x-\xi} d\xi + \int_{x+\epsilon}^{\infty} \frac{f(\xi)}{x-\xi} d\xi \right) & (3.4) \end{aligned}$$

Definition 3.2 (Analytic Signal) *Let f be a real 1D signal and F its Fourier transform. Its analytic signal in the Fourier domain is then given by*

$$\begin{aligned} F_A(u) &= F(u) + iF_{\mathcal{H}i}(u) & (3.5) \\ &= F(u)(1 + \text{sign}(u)). \end{aligned}$$

In the spatial domain this definition reads:

$$f_A(x) = f(x) + if_{\mathcal{H}i}(x) = f(x) * \left(\delta(x) + \frac{i}{\pi x} \right). \quad (3.6)$$

Thus, the analytic signal of f is constructed by taking the Fourier transform F of f, suppressing the negative frequencies and multiplying the positive frequencies by two. Note that, applying this procedure, we do not lose any information about f because of the Hermite symmetry of the spectrum of a real function.

The analytic signal enables us to define the notions of the instantaneous amplitude and the instantaneous phase of a signal [45].

Definition 3.3 (Instantaneous Amplitude and Phase) *Let f be a real 1D signal and f_A its analytic signal. The instantaneous amplitude and and phase of f are then defined by*

$$\begin{aligned} \textit{instantaneous amplitude of } f(x) &= |f_A(x)| & (3.7) \\ \textit{instantaneous phase of } f(x) &= \text{atan2}(\mathcal{I}f_A(x), \mathcal{R}f_A(x)). & (3.8) \end{aligned}$$

For later use we introduce the notion of a Hilbert pair.

Definition 3.4 (Hilbert Pair) *Two real one-dimensional functions f and g are called a Hilbert pair if one is the Hilbert transform of the other, i.e.*

$$f_{\mathcal{H}i} = g \quad \textit{or} \quad g_{\mathcal{H}i} = f.$$

If $f_{\mathcal{H}i} = g$ it follows that $g_{\mathcal{H}i} = -f$.

We illustrate the above definitions by a simple example: The analytic signal of $f(x) = a\cos(\omega x)$ is given by $a\cos_A(\omega x) = a\cos(\omega x) + ia\sin(\omega x) = a\exp(i\omega x)$. The instantaneous amplitude of f is given by $|f_A(x)| = a$ while the instantaneous phase is $\mathrm{atan2}(\mathcal{I}f_A(x), \mathcal{R}f_A(x)) = \omega x$. Thus, the instantaneous amplitude and phase of the cosine-function are exactly equal to the expected values a and ωx, respectively. Furthermore, cos and sin constitute a *Hilbert pair*. Figure 3.3 shows another example of an oscillating signal together with its instantaneous amplitude and its instantaneous phase.

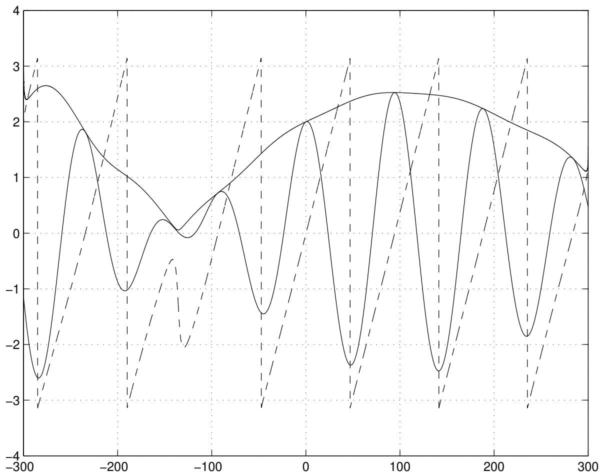

Figure 3.3: An oscillating signal, its instantaneous amplitude (signal envelope) and its instantaneous phase (dashed).

However, the close relation of the instantaneous amplitude and phase to the local structure of the signal gets lost if the signal has no well defined angular frequency. Most of the time it is sufficient to require the signal to be of narrow bandwidth ([45], p. 171).

For this reason later (see the introduction to this chapter) Gabor filters will be introduced which establish a relation between the local structure and the local phase of a broader class of signals.

Comment on the Notion "Analytic Signal"

When Gabor introduced the *analytic signal*, he did not use this term. Instead, he called it the *complex signal*. The reason why the attribute changed from *complex* to *analytic* may lie in the following fact: The Laplace transform of a right-sided, complex, one-dimensional signal f is an analytic function in the open right half-plane [87]. By *right-sided* we mean that f vanishes for negative arguments[2]: $f(x) = 0$ if $x < 0$. Since the analytic signal is the Fourier-dual to a right-sided signal ($F(u) = 0$ if $u < 0$), this may be the reason for the notion "analytic signal".

Since this notion sometimes causes confusion, we stress the fact that **the analytic signal is not an analytic function**. The analytic signal $f_A : \mathbb{R} \to \mathbb{C}$ maps the real numbers to the complex numbers, while the notion of an analytic function f is defined only for functions $f : \mathbb{C} \to \mathbb{C}$. Even if we extend the domain of f_A to the complex numbers by embedding $\mathbb{R}$ into $\mathbb{C}$

$$f_A : \mathbb{C} \to \mathbb{C}, \quad f_A(x + iy) := f_A(x),$$

f_A is not an analytic function. However, the analytic signal can be derived from a function, analytic in one half-plane, namely the Laplace transform of $F_A(\mathbf{u})$ as

$$f_A(x) = \mathcal{L}\{F_A\}(x + i0).$$

In the following we will use the term *analytic signal* as a notion on its own right, without stressing the relation to analytic functions.

3.1.2 Approaches to an Analytic Signal in 2D

In order to extend the definition of the analytic signal to 2D we need some guidelines. As such a guideline we give a list of the main properties of the analytic signal in 1D. Any new definition will be measured according to the degree to which it extends these properties to higher dimensions.

1.	The spectrum of an analytic signal is right-sided ($F_A(u) = 0$ for $u < 0$).
2.	Hilbert pairs are orthogonal.
3.	The real part of the analytic signal f_A is equal to the original signal f.
4.	The analytic signal is compatible (in a way explained below) with the associated harmonic transform (in case of the 1D analytic signal with the complex Fourier transform.)

Table 3.1: Four properties of the analytic signal.

[2]Sometimes the notion *causal* signal is used instead of right-sided signal. The reason for this notion is that the impulse response of a causal system is right-sided.

We will explain the forth point. The analytic signal is called compatible with the associated harmonic transform with transformation kernel K if $\mathcal{R}K$ and $\mathcal{I}K$ are a Hilbert pair. In case of the one-dimensional Fourier transform this property is fulfilled, since the real part of the Fourier kernel, i.e. $\mathcal{R}(\exp(-i2\pi ux)) = \cos(-2\pi ux)$ is the Hilbert transform of $\sin(-2\pi ux)$, as was shown above.

As mentioned before there is no unique straightforward extension of the analytic signal to higher dimensions. The above properties will serve as a quality measure for any extension of the analytic signal to 2D.

All of the extensions of the analytic signal to 2D which will be made in this chapter have a straightforward extension to n-dimensional signals. Again, we will use the notation $\mathbf{x} = (x, y)$ and $\mathbf{u} = (u, v)$.

The first definition is based on the 2D Hilbert transform [90]:

Definition 3.5 (Total 2D Hilbert Transform) *Let f be a real two-dimensional signal. Its Hilbert transform is given by*

$$f_{\mathcal{H}i}(\mathbf{x}) = f(\mathbf{x}) * \left(\frac{1}{\pi^2 xy}\right), \tag{3.9}$$

where $*$ denotes the 2D convolution. In the frequency domain this reads

$$F_{\mathcal{H}i}(\mathbf{u}) = -F(\mathbf{u})\text{sign}(u)\text{sign}(v).$$

Sometimes $f_{\mathcal{H}i}$ is called the total Hilbert transform of f [49].

For later use, we define also the partial Hilbert transforms of a 2D signal.

Definition 3.6 (Partial Hilbert Transform) *Let f be a real two-dimensional signal. Its partial Hilbert transforms in x- and y-direction are given by*

$$f_{\mathcal{H}i_1}(\mathbf{x}) = f(\mathbf{x}) * \left(\frac{\delta(y)}{\pi x}\right), \quad \textit{and} \tag{3.10}$$

$$f_{\mathcal{H}i_2}(\mathbf{x}) = f(\mathbf{x}) * \left(\frac{\delta(x)}{\pi y}\right), \tag{3.11}$$

respectively. In the frequency domain this reads

$$F_{\mathcal{H}i_1}(\mathbf{u}) = -iF(\mathbf{u})\text{sign}(u) \quad \textit{and} \quad F_{\mathcal{H}i_2}(\mathbf{u}) = -iF(\mathbf{u})\text{sign}(v).$$

The partial Hilbert transform of a 2D signal can of course be defined with respect to any orientation.

In analogy to 1D an extension of the analytic signal can be defined as follows:

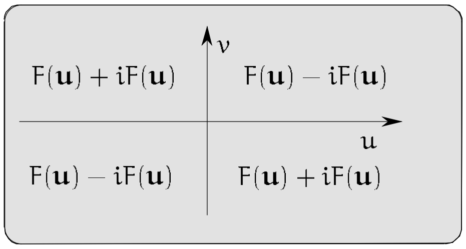

Figure 3.4: The spectrum of the analytic signal according to definition 3.7.

Definition 3.7 (Total Analytic Signal) *The analytic signal of a real 2D signal* f *is defined as*

$$\begin{aligned} f_A(\mathbf{x}) &= f(\mathbf{x}) * (\delta^2(\mathbf{x}) + \frac{i}{\pi^2 xy}) & (3.12) \\ &= f(\mathbf{x}) + i f_{\mathcal{H}i}(\mathbf{x}), & (3.13) \end{aligned}$$

where $f_{\mathcal{H}i}$ *is given by (3.9). In the frequency domain this definition reads*

$$F_A(\mathbf{u}) = F(\mathbf{u})(1 - i\,\mathrm{sign}(u)\mathrm{sign}(v)).$$

The spectrum of f_A according to definition 3.7 is shown in figure 3.4. It does not vanish anywhere in the frequency domain. Hence, there is no analogy to the causality property of an analytic signal's spectrum in 1D. Secondly, Hilbert pairs according to this definition are only orthogonal if the functions are separable [49]. Furthermore, the above definition of the analytic signal is not compatible with the two-dimensional Fourier transform, since $\sin(2\pi\mathbf{u}\mathbf{x})$ is not the total Hilbert transform of $\cos(2\pi\mathbf{u}\mathbf{x})$. Thus, the properties 1, 2 and 4 from table 3.1 are not satisfied by this definition. A common approach to overcome this fact can be found e.g. in Granlund [45]. This definition starts with the construction in the frequency domain. While in 1D the analytic signal is achieved by suppressing the negative frequency components, in 2D one half-plane of the frequency domain is set to zero in order to fulfill property no. 1 in table 3.1. It is not immediately clear how negative frequencies can be defined in 2D. However, it is possible to introduce a direction of reference defined by the unit vector $\hat{\mathbf{e}} = (\cos(\theta), \sin(\theta))$. A frequency $\mathbf{u}$ with $\hat{\mathbf{e}} \cdot \mathbf{u} > 0$ is called positive while a frequency with $\hat{\mathbf{e}} \cdot \mathbf{u} < 0$ is called negative. The 2D analytic signal can then be defined in the frequency domain.

Definition 3.8 (Partial Analytic Signal) *Let f be a real 2D signal and F its Fourier transform. The Fourier transform of the analytic signal is defined by:*

$$F_A(\mathbf{u}) = \left\{ \begin{array}{ccc} 2F(\mathbf{u}) & \textit{if} & \mathbf{u} \cdot \hat{\mathbf{e}} > 0 \\ F(\mathbf{u}) & \textit{if} & \mathbf{u} \cdot \hat{\mathbf{e}} = 0 \\ 0 & \textit{if} & \mathbf{u} \cdot \hat{\mathbf{e}} < 0 \end{array} \right\} = F(\mathbf{u})(1 + \operatorname{sign}(\mathbf{u} \cdot \hat{\mathbf{e}})). \tag{3.14}$$

In the spatial domain (3.14) reads

$$f_A(\mathbf{x}) = f(\mathbf{x}) * \left(\delta(\mathbf{x} \cdot \hat{\mathbf{e}}) + \frac{i}{\pi \mathbf{x} \cdot \hat{\mathbf{e}}} \right) \delta(\mathbf{x} \cdot \hat{\mathbf{e}}_\perp). \tag{3.15}$$

The vector $\hat{\mathbf{e}}_\perp$ is a unit vector which is orthogonal to $\hat{\mathbf{e}}$: $\hat{\mathbf{e}} \cdot \hat{\mathbf{e}}_\perp = 0$.

Please note the similarity of this definition with the one-dimensional definition (Def. 3.2). For $\hat{\mathbf{e}}^\top = (1, 0)$ equation (3.15) takes the form

$$\begin{aligned} f_A(\mathbf{x}) &= f(\mathbf{x}) * \left(\delta(x) + \frac{i}{\pi x} \right) \delta(y) && (3.16) \\ &= f(\mathbf{x}) + i f_{\mathcal{H}i_1}. && (3.17) \end{aligned}$$

Thus, the reason for the name *partial analytic signal* lies in the fact that it is the sum of the original signal and the *partial Hilbert transform* as imaginary part. The partial analytic signal with respect to the two coordinate axes has been used by Venkatesh et al. [93, 92] for the detection of image features. They define the energy maxima of the partial analytic signal as image features.

According to this definition the analytic signal is calculated line-wise along the direction of reference. The lines are processed independently. Hence, definition 3.8 is intrinsically 1D, such that it is no satisfactory extension of the analytic signal to 2D. Its application is reasonable only for simple signals, i.e. signals which vary only along one orientation [45]. The orientation $\hat{\mathbf{e}}$ can then be chosen according to the direction of variation of the image.

If negative frequencies are defined in the way indicated above, we can say that property 1 of table 3.1 is fulfilled. Properties 2 and 3 are valid as well. This follows from the fact that merely the 1D analytic signal is evaluated line-wise, which leads to a trivial extension of these properties. Even property 4 is "almost" valid: $\sin(ux+vy)$ is the partial Hermite transform (i.e. with respect to the x direction) of $\cos(ux+vy)$ for all frequencies $\mathbf{u}$ with $u \neq 0$. However, the main drawback of definition 3.8 is the intrinsic one-dimensionality of the definition and the non-uniqueness with regard to the orientation of reference $\hat{\mathbf{e}}$.

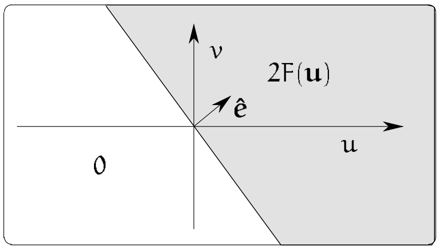

Figure 3.5: The spectrum of the analytic signal according to definition 3.8.

Both definitions presented so far seem to establish the following dilemma: Either an intrinsically two-dimensional definition of the analytic signal based on the total Hilbert transform can be introduced, which does not extend the main properties of the 1D analytic signal, or these properties are extended by an intrinsically one-dimensional definition based on the partial Hilbert transform.

An alternative to these approaches was recently introduced by Hahn [48, 49]. Hahn avoids the term "analytic signal" and uses Gabor's original term "complex signal" instead.

Definition 3.9 *Let f be a real, two-dimensional function and F its Fourier transform. The 2D complex signal (according to Hahn [49]) is defined in the frequency domain by*

$$F_A(\mathbf{u}) = (1 + \mathrm{sign}(u))(1 + \mathrm{sign}(v))F(\mathbf{u}).$$

In the spatial domain this reads

$$\begin{aligned} f_A(\mathbf{x}) &= f(\mathbf{x}) * \left(\delta(x) + \frac{i}{\pi x}\right)\left(\delta(y) + \frac{i}{\pi y}\right) && (3.18)\\ &= f(\mathbf{x}) - f_{\mathcal{H}i}(\mathbf{x}) + i(f_{\mathcal{H}i_1}(\mathbf{x}) + f_{\mathcal{H}i_2}(\mathbf{x})), && (3.19)\end{aligned}$$

where $f_{\mathcal{H}i}$ is the total Hilbert transform $f_{\mathcal{H}i_1}$ and $f_{\mathcal{H}i_2}$ are the partial Hilbert transforms.

The meaning of definition 3.9 becomes clear in the frequency domain: Only the frequency components with $u > 0$ and $v > 0$ are kept, while the components in the three other quadrants are suppressed (see figure 3.6):

$$F_A(\mathbf{u}) = (1 + \mathrm{sign}(u))(1 + \mathrm{sign}(v))F(\mathbf{u}).$$

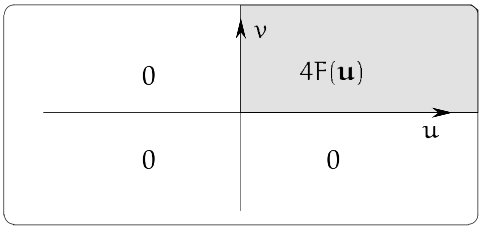

Figure 3.6: The spectrum of the analytic signal according to Hahn [48] (definition 3.9).

Thus, the problem of defining positive frequencies is solved in another way then in definition 3.8.

A main problem of definition 3.9 is the fact that the original signal cannot be reconstructed from the analytic signal, since due to the Hermite symmetry only one half-plane of the frequency domain of a real signal is redundant. For this reason Hahn proposes to calculate not only the analytic signal with the spectrum in the upper right quadrant but also another analytic signal with its spectrum in the upper left quadrant. It can be shown that these two analytic signals together contain all the information of the original signal [49]. When necessary we distinguish the two analytic or complex signals by referring to them as definition 3.9 and 3.9a, respectively.

Thus, the complete analytic signal according to definition 3.9 consists of two complex signals, i.e. two real parts and two imaginary parts or, in polar representation, of two amplitude- and two phase-components which makes the interpretation, especially of the amplitude, difficult. Furthermore, it would be more elegant to express the analytic signal with only one function instead of two. Definition 3.9 fulfills properties 1 and 2 from table 3.1. The very important property that it should be possible to reconstruct the signal from its analytic signal is only fulfilled if two different complex signals are calculated using two neighbored quadrants of the frequency domain. Hahn [49] mentions that his definition of the 2D analytic signal is compatible with the 2D Fourier transform for the following reason: The 2D Fourier kernel can be written in the form

$$
\begin{aligned}
\exp(i2\pi \mathbf{u}\mathbf{x}) &= \cos(2\pi u x)\cos(2\pi v y) - \sin(2\pi u x)\sin(2\pi v y) && (3.20)\\
&+ i(\cos(2\pi u x)\sin(2\pi v y) + \sin(2\pi u x)\cos(2\pi v y)) && (3.21)
\end{aligned}
$$

where for convenience we omitted the minus sign in the exponential. According to definition 3.9 this is exactly the complex signal of $f(\mathbf{x}) = \cos(2\pi u x)\cos(2\pi v y)$. However, this fulfills only a weak kind of compatibility and not the one defined by us above. This would require that the analytic signal of $\mathcal{R}\exp(i2\pi\mathbf{u}\mathbf{x})$ would equal $\exp(i2\pi\mathbf{u}\mathbf{x})$.

The remaining problems can be summarized as follows. The original signal cannot be recovered from Hahn's analytic signal. This restriction can only be overcome by introducing two complex signals for each real signal, which is not a satisfactory solution. Furthermore, Hahn's analytic signal is not compatible with the 2D Fourier transform in the strong sense.

Apart from these disadvantages, it is clear from the above analysis, that, among the definitions introduced so far, Hahn's definition is closest to a satisfactory 2D extension of the analytic signal. In the following section we will show how Hahn's frequency domain construction can be applied to the construction of a quaternionic analytic signal, which overcomes the remaining problems.

3.1.3 The Quaternionic Analytic Signal

Hahn's approach to the analytic signal faces the problem that a two-dimensional complex hermitian function cannot be recovered if it is known in only one quadrant of its domain. For this reason Hahn introduced two complex signals to each real two-dimensional signal. We will show how this problem is solved using the QFT.

Since the QFT of a real signal is quaternionic hermitian (see theorem 2.11), we do not lose any information about the signal in this case (see figure 3.7).

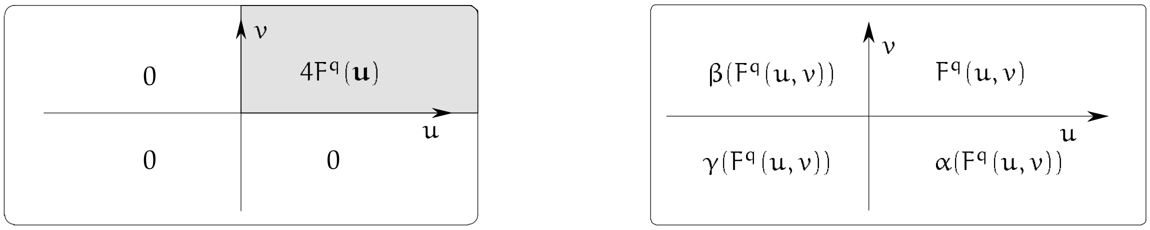

Figure 3.7: The quaternionic spectrum of a quaternionic analytic signal (left). The quaternionic analytic signal contains the whole information of the original real signal, since the QFT of a real signal is quaternionic hermitian. Thus, the quaternionic spectrum of a real signal can be reconstructed from only one quadrant (right).

Thus, we define the quaternionic analytic signal in the frequency domain as in definition 3.9, with the only difference that we use the quaternionic frequency domain defined by the QFT instead of the complex frequency domain.

Definition 3.10 (Quaternionic Analytic Signal) *Let* f *be a real two-dimensional signal and* F^q *its QFT. In the quaternionic frequency domain we define the quaternionic analytic signal of a real signal as*

$$F^q_A(\mathbf{u}) = (1 + \mathrm{sign}(u))(1 + \mathrm{sign}(v))F^q(\mathbf{u}),$$

where $\mathbf{x} = (x, y)$ *and* $\mathbf{u} = (u, v)$. *Definition 3.10 can be expressed in the spatial domain as follows:*

$$f^q_A(\mathbf{x}) = f(\mathbf{x}) + \mathbf{n}^\top \mathbf{f}_{\mathcal{H}i}(\mathbf{x}), \tag{3.22}$$

where $\mathbf{n} = (i, j, k)^\top$ *and* $\mathbf{f}_{\mathcal{H}i}$ *is a vector which consists of the total and the partial Hilbert transforms of* f *according to definitions 3.5 and 3.6:*

$$\mathbf{f}_{\mathcal{H}i}(\mathbf{x}) = \begin{pmatrix} f_{\mathcal{H}i_1}(\mathbf{x}) \\ f_{\mathcal{H}i_2}(\mathbf{x}) \\ f_{\mathcal{H}i}(\mathbf{x}) \end{pmatrix}. \tag{3.23}$$

Note that, formally, (3.22) resembles the definition of the one-dimensional analytic signal (3.6). Since the quaternionic analytic signal consists of four components we replace the notion of a Hilbert pair (definition 3.4) by the notion of a *Hilbert quadruple*.

Definition 3.11 (Hilbert Quadruple)
Four real two-dimensional functions f_η, $\eta \in \{1, \ldots 4\}$ *are called a Hilbert quadruple if*

$$\mathcal{I}(f_\kappa)^q_A = f_\lambda \tag{3.24}$$
$$\mathcal{J}(f_\kappa)^q_A = f_\mu \tag{3.25}$$
$$\mathcal{K}(f_\kappa)^q_A = f_\nu \tag{3.26}$$

for some permutation of pairwise different $\kappa, \lambda, \mu, \nu \in \{1, \ldots 4\}$.

Theorem 3.1 *The four components of the QFT-kernel build a Hilbert quadruple.*

Proof: Since the quaternionic analytic signal of $f(\mathbf{x}) = \cos(\omega_x x)\cos(\omega_y y)$ is given by $f^q_A(\mathbf{x}) = \exp(i\omega_x x)\exp(j\omega_y y)$, which is the QFT-kernel, we have

$$\mathcal{I}(\mathcal{R}\exp(i\omega_x x)\exp(j\omega_y y))^q_A = \mathcal{I}\exp(i\omega_x x)\exp(j\omega_y y) \tag{3.27}$$
$$\mathcal{J}(\mathcal{R}\exp(i\omega_x x)\exp(j\omega_y y))^q_A = \mathcal{J}\exp(i\omega_x x)\exp(j\omega_y y) \tag{3.28}$$
$$\mathcal{K}(\mathcal{R}\exp(i\omega_x x)\exp(j\omega_y y))^q_A = \mathcal{K}\exp(i\omega_x x)\exp(j\omega_y y). \tag{3.29}$$

which concludes the proof. □

analytic signal	instantaneous amplitude
Def. 3.7	$\sqrt{f^2(\mathbf{x}) + f_{\mathcal{H}i}^2(\mathbf{x})}$
Def. 3.8	$\sqrt{f^2(\mathbf{x}) + f_{\mathcal{H}i_1}^2(\mathbf{x})}$
Def. 3.9	$\sqrt{[f(\mathbf{x}) - f_{\mathcal{H}i}(\mathbf{x})]^2 + [f_{\mathcal{H}i_1}(\mathbf{x}) + f_{\mathcal{H}i_2}(\mathbf{x})]^2}$
Def. 3.9a	$\sqrt{[f(\mathbf{x}) + f_{\mathcal{H}i}(\mathbf{x})]^2 + [f_{\mathcal{H}i_1}(\mathbf{x}) - f_{\mathcal{H}i_2}(\mathbf{x})]^2}$
Def. 3.10	$\sqrt{f^2(\mathbf{x}) + f_{\mathcal{H}i_1}^2(\mathbf{x}) + f_{\mathcal{H}i_2}^2(\mathbf{x}) + f_{\mathcal{H}i}^2(\mathbf{x})}$

Table 3.2: The tabular shows the different possible definitions of the instantaneous magnitude in 2D. On the right hand side the instantaneous amplitude of the 2D signal f is given according to the definition of the analytic signal indicated on the left hand side.

3.1.4 Comparison of the Different Approaches to the 2D Analytic Signal

One major advantage of the analytic signal over the original real signal is the possibility to easily define the instantaneous amplitude and phase of a signal. Of course in 2D the different definitions given above lead to different definitions of the instantaneous amplitude and phase in 2D. We will give these definitions explicitly in the following.

As shown in section 3.1.1 the instantaneous amplitude of a real 1D signal can be defined as the absolute value of the associated analytic signal. We will use the same definition in 2D. Depending on the chosen form of the 2D analytic signal the definition of the instantaneous amplitude varies. In order to give a clear overview we list the possible definitions in table 3.2. The instantaneous phase of a real one-dimensional signal f is defined as the angular phase of the analytic signal f_A. We will use the same definition in 2D. In order to define the instantaneous phase via the quaternionic analytic signal (definition 3.10) we make use of the notion of the angular phase of a quaternion as defined in section 2.1.2 (definition 2.7). The different definitions of the instantaneous phase corresponding to the different definitions of the two-dimensional analytic signal are given in table 3.3

analytic signal	instantaneous phase
Def. 3.7	$\mathrm{atan2}(f_{\mathcal{H}i}(\mathbf{x}), f(\mathbf{x}))$
Def. 3.8	$\mathrm{atan2}(f_{\mathcal{H}i_1}(\mathbf{x}), f(\mathbf{x}))$
Def. 3.9	$\mathrm{atan2}([f_{\mathcal{H}i_1}(\mathbf{x}) + f_{\mathcal{H}i_2}(\mathbf{x})], [f(\mathbf{x}) - f_{\mathcal{H}i}(\mathbf{x})])$
Def. 3.9a	$\mathrm{atan2}([f_{\mathcal{H}i_1}(\mathbf{x}) - f_{\mathcal{H}i_2}(\mathbf{x})], [f(\mathbf{x}) + f_{\mathcal{H}i}(\mathbf{x})])$
Def. 3.10	$\arg(f(\mathbf{x}) + \mathbf{n}f_{\mathcal{H}i}(\mathbf{x}))$

Table 3.3: The tabular shows the different possible definitions of the instantaneous phase in 2D. On the right hand side the instantaneous phase of the 2D signal f is given according to the definition of the analytic signal indicated on the left hand side.

In order to compare the different approaches to the 2D analytic signal we test them on the four properties of the 1D analytic signal given in table 3.1.

The first property (”The spectrum of the analytic signal is right-sided.”) cannot be tested uniquely, since positive frequencies are not well defined in 2D. If we take the viewpoint of Hahn [48] that positive frequencies in 2D are those frequencies which are positive with respect to each component, only the definitions 3.9 and 3.10 fulfill the first property. However, in table 3.4, where the results of this comparison are listed, we claim that property no. 1 in table 3.1 is fulfilled if the spectrum of the analytic signal vanishes either in one half or in three quadrants of the frequency domain.

Property 3 is concerned with the reconstructibility of the original signal as the real part of its analytic signal. This property is fulfilled for all definitions except for definition 3.9. However, we have to mention that in definition 3.9 it is possible to retain the original image by evaluating both analytic signals (3.9 and 3.9a). This is not necessary in definition 3.10, since the QFT of a real signal is quaternionic hermitian. For definitions 3.7, 3.8 and 3.9 the real part of the analytic signal is identical with the original signal.

As we will show in the next section, the last property is fulfilled optimally by the new definition (def. 3.10). We demonstrate the effects of the different definitions of the analytic signal in 2D by applying them to two test-images (see figure 3.8). The first of these test-images is the product of a horizontal and a vertical cosine-function

Definition	Property 1	2	3	4	5
Def. 3.7	−	−	+	−	+
Def. 3.8	+	+	+	−	−
Def. 3.9	+	+	−	−	+
Def. 3.9a	+	+	−	−	+
Def. 3.10	+	−	+	+	+

Table 3.4: Behavior of the different definitions of the two-dimensional analytic signal according to the properties listed in table 3.1. As a fifth point we added the property of a definition of being intrinsically two-dimensional .

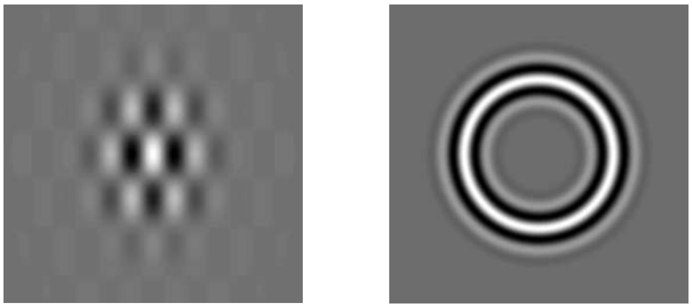

Figure 3.8: The test-images. Left: product of a horizontal and a vertical cosine-wave, multiplied by a Gaussian window. Right: modulated Gaussian circle.

together with a Gaussian window, the second is a modulated Gaussian weighted circle (see figure 3.8). In figure 3.9 we show the magnitudes of the different analytic signals of the test-images. Note, that Hahn's definition yields two different analytic signals, denoted here by def. 3.9 and def. 3.9a, respectively. Definition 3.8 is applied with $\hat{\mathbf{e}} = (1, 0)$. Obviously definitions 3.7 and 3.8 are not successful in providing the envelope of the first test-image.

In this case, the two amplitudes given by definition 3.9 are identical and coincide with the result of definition 3.10. It is easy to show that this is always the case for x_1-x_2-separable signals. As another interesting property of the quaternionic analytic signal of a separable signal f we find that the first two quaternionic phase-components $\phi(\mathbf{x})$ and $\theta(\mathbf{x})$ equal the complex phase of the separable components

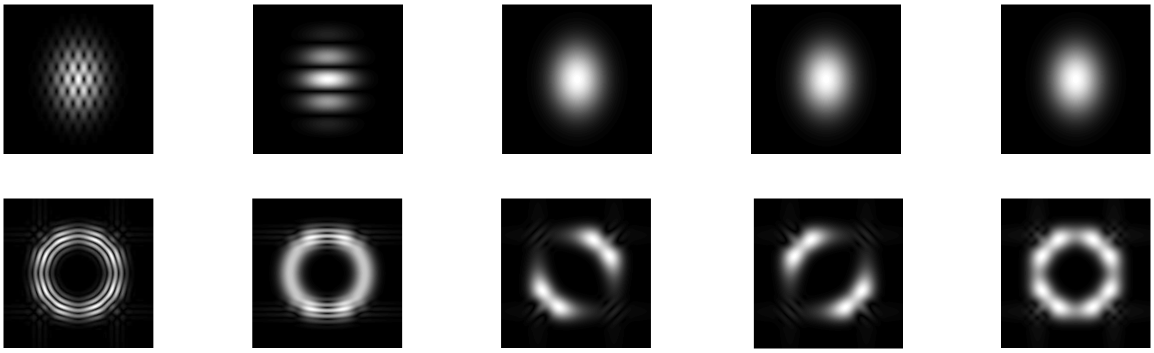

Figure 3.9: The magnitudes of the different analytic signals of the test-images. From left to right: def. 3.7, def. 3.8, def. 3.9, def. 3.9a, def. 3.10.

of f, $\phi_1(x_1)$ and $\phi_2(x_2)$, respectively[3]:

$$\phi(x_1, x_2) = \phi_1(x_1) \tag{3.30}$$
$$\theta(x_1, x_2) = \phi_2(x_2). \tag{3.31}$$

The envelope of the second test-image is provided most satisfactorily by definition 3.10. Only definition 3.10 handles both cases satisfactorily. Of course, one should keep in mind that a definition cannot ever be true or false. However, the value of a definition can be estimated.

Here we are dealing with the extension of an existing definition (the 1D analytic signal) to a higher-dimensional case. Thus, we can compare the features of the original and the extended definition and take the compatibility of both as a measure of the value of the new definition. In this sense, we can say that the new definition of the analytic signal in 2D is superior to the older approaches. Furthermore, the quaternionic analytic signal comprises in its components the partial analytic signals with respect to the coordinate axes and the total analytic signal.

The quaternionic analytic signal combines in itself the earlier approaches in a natural way: The vector $f_{\mathcal{H}i}$ in (3.23) is not constructed artificially. The quaternionic analytic signal is rather defined in a very simple way in the frequency domain.

3.2 Gabor Filters and the Local Phase

We have shown how the instantaneous phase can be evaluated using the analytic signal. However, the instantaneous phase loses its direct relation to the local signal

[3] I am grateful to Prof. S. Hahn for pointing out this fact during a personal communication.

structure, when the signal is not of narrow bandwidth [45]. In order to overcome this restriction, local linear shift-invariant bandpass filters with a one-sided transfer function can be applied to a signal. According to the definition of the 1D analytic signal the impulse responses of these filters, and the filter responses to any real signal as well, are analytic signals. Filters of this kind are called *quadrature filters*. The angular phase of the quadrature filter response to a real signal is called the *local phase*. In this section we will review 1D and 2D complex Gabor filters which are an approximation of a quadrature filter. Further, we regard the relation between the local structure of a signal and the local phase estimated by a Gabor filter.

Gabor filters correspond to the Fourier kernel in a way clarified below. Thus, it is possible to define quaternionic Gabor filters based on the quaternionic Fourier transform and to introduce the local quaternionic phase. Quaternionic Gabor filters are introduced in section 3.2.3. We will show how some interesting properties of 1D complex Gabor filters are extended to 2D by quaternionic Gabor filters in sections 3.2.5.4 and 3.2.5.5.

3.2.1 Complex Gabor Filters

Gabor filters have been shown to be a useful tool in different image processing and analysis tasks such as texture segmentation and classification, edge detection, and local phase and frequency estimation for image matching. Gabor filters are appropriate wherever one is interested in local spectral properties of a signal. They have the main advantage of being optimally localized with respect to the uncertainty principle in the spatial and the frequency domain simultaneously [44]. In other words, they fulfill the uncertainty relation as an equality.

Complex Gabor filters are defined as linear shift-invariant filters with the Gaussian windowed basis functions of the Fourier transform as their basis functions.

Definition 3.12 (1D Complex Gabor Filter) *A one-dimensional complex Gabor filter is a linear shift-invariant filter with the impulse response*

$$h(x; N, u_0, \sigma) = g(x; N, \sigma) \exp(i 2\pi u_0 x), \tag{3.32}$$

where $g(x; N, \sigma)$ *is the Gauss function*

$$g(x; N, \sigma) = N \exp\left(-\frac{x^2}{2\sigma^2}\right).$$

The Gabor filters have as parameters the normalization constant N*, the* center frequency u_0 *and the variance* σ *of the Gauss function. However, most of the time we will not write* *down these arguments explicitly. Where no confusion is possible we use the notation* $h(x)$ *and* $g(x)$ *for the Gabor filter and the Gaussian function at position* x*, respectively.*

Except where specifically indicated we use the normalization $N = (\sqrt{2\pi\sigma^2})^{-1}$ such that $\int_{\mathbb{R}} g(x)\,dx = 1$. Sometimes other parameterizations of the Gabor filter than the one given in definition 3.12 are used:

$$\begin{aligned} h(x) &= g(x)\exp(i\omega_0 x) && (3.33)\\ &= g(x)\exp\left(\frac{icx}{\sigma}\right). && (3.34)\end{aligned}$$

In (3.33) we simply replaced the center frequency u_0 by the angular frequency $\omega_0 = 2\pi u_0$. This can be converted into (3.34) by defining

$$c = \omega_0\sigma \tag{3.35}$$

and substituting ω_0 by c/σ. The latter parameterization is especially useful when the emphasis lies on *Gabor wavelets*. The reason is that the Gabor filter does not change its shape when σ is varied while we keep c fixed. Thus, all Gabor filters with the same value c can be derived from one filter by scaling. This is the main property of wavelets. However, when the attention lies on spatial frequencies directly, it may be preferable to parameterize the Gabor filters through σ and u_0. The meaning of the different parameterizations is visualized in figure 3.10. Analogously the definition of 2D complex Gabor filters is based on the 2D Fourier transform:

Definition 3.13 (2D Complex Gabor Filter) *A two-dimensional complex Gabor filter is a linear shift-invariant filter with the impulse response*

$$h(\mathbf{x}; \mathbf{u}_0, \sigma, \epsilon, \phi) = g(x', y')\exp(2\pi i(u_0 x + v_0 y)) \tag{3.36}$$

with

$$g(x, y) = N\exp\left(-\frac{x^2 + (\epsilon y)^2}{\sigma^2}\right)$$

where ϵ *is the aspect ratio. The coordinates* (x', y') *are derived from* (x, y) *by a rotation about the origin through the angle* ϕ*:*

$$\begin{pmatrix} x' \\ y' \end{pmatrix} = \begin{pmatrix} \cos\phi & \sin\phi \\ -\sin\phi & \cos\phi \end{pmatrix}\begin{pmatrix} x \\ y \end{pmatrix}. \tag{3.37}$$

Again, we will choose the normalization such that $\int_{\mathbb{R}} g(x, y)\,dx\,dy = 1$, i.e. $N = \frac{\epsilon}{2\pi\sigma^2}$.

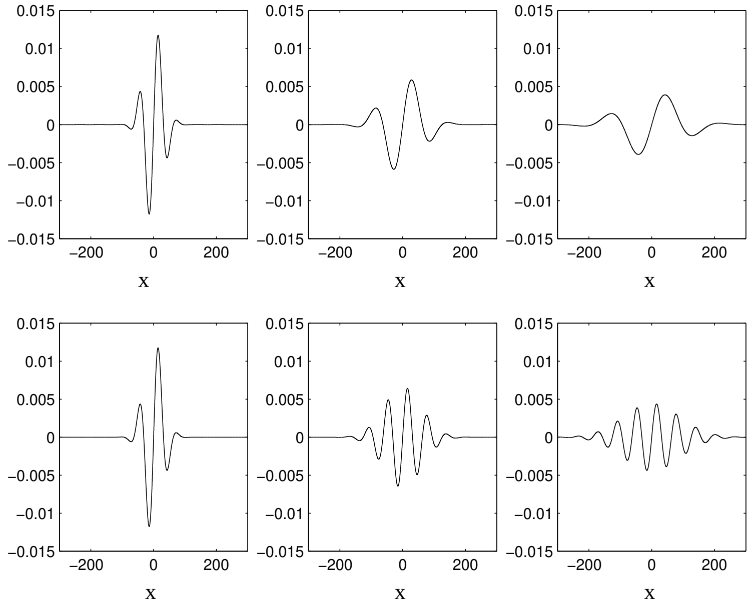

Figure 3.10: Upper row: the imaginary part of three Gabor filters with $c = 3$ and variance $\sigma = 30$ (left), $\sigma = 60$ (middle), and $\sigma = 90$ (right). Lower row: the imaginary part of three Gabor filters with $\omega = 1/10$ and variance $\sigma = 30$ (left), $\sigma = 60$ (middle), and $\sigma = 90$ (right).

In frequency domain the 1D Gabor filters take the following form:

$$h(x; u_0, \sigma) \circ\!\!-\!\!\bullet\; H(u; u_0, \sigma) = \exp(-2\pi^2\sigma^2(u - u_0)^2).$$

The transfer function of a 2D Gabor filter is given by

$$h(\mathbf{x}; \mathbf{u}_0, \sigma, \epsilon, \phi) \circ\!\!-\!\!\bullet\; H(\mathbf{u}; \mathbf{u}_0, \sigma, \epsilon, \phi) = \exp(-2\pi^2\sigma^2[(u' - u_0') + (v' - v_0')^2/\epsilon]).$$

Thus, Gabor filters are bandpass filters. The radial center frequency of the 2D Gabor filter is given by $F = \sqrt{u_0^2 + v_0^2}$ and its orientation is $\theta = \operatorname{atan}(v_0/u_0)$. In most cases it is convenient to choose $\theta = \phi$ such that the orientation of the complex sine gratings is identical with the orientation of one of the principle axes of the Gauss function. Figure 3.11 shows the transfer function of a one-dimensional complex Gabor filter.

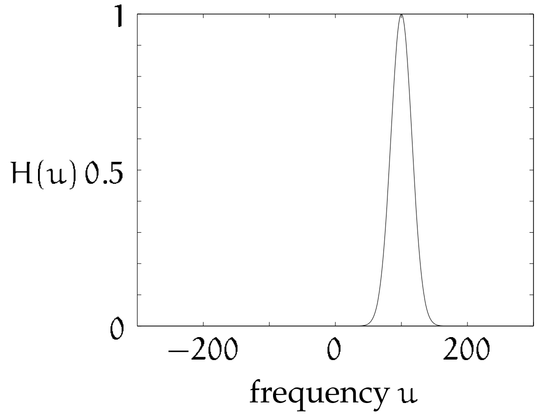

Figure 3.11: The transfer function of a one-dimensional Gabor filter with $u_0 = 100$ and $\sigma = 0.01$.

It can be seen that the main amount of energy of the Gabor filter is centered around the frequency u_0 in the positive half of the frequency domain. However, the energy in the negative half is not equal to zero. Because of this property, the filter response of the Gabor filter to a real signal is only an approximation to an analytic signal (which is only one-sided in the frequency domain). The error of this approximation decreases with increasing u and with increasing σ.

3.2.2 Local Phase in 1D

The local phase of a signal is defined as the angular phase of its complex Gabor filter response. The relation to the local structure of the signal becomes clear in the following way. At a signal position with locally even symmetry only the even part of the Gabor filter which is real-valued matches. The angular phase of a real number is either 0 for a positive number or π for a negative one. Thus, if the even filter component matches the signal positive, the local phase is 0, if it matches negative, the local phase is π. A similar reflection clarifies the case of a locally odd structure. In this case only the odd, and thus imaginary, filter component matches the signal. Since the angular phase of a pure imaginary number is $\pi/2$ for a positive imaginary part and $-\pi/2$ otherwise, these values represent odd local structures. Figure 3.12 shows the variation of the local phase around the four fundamental structures.

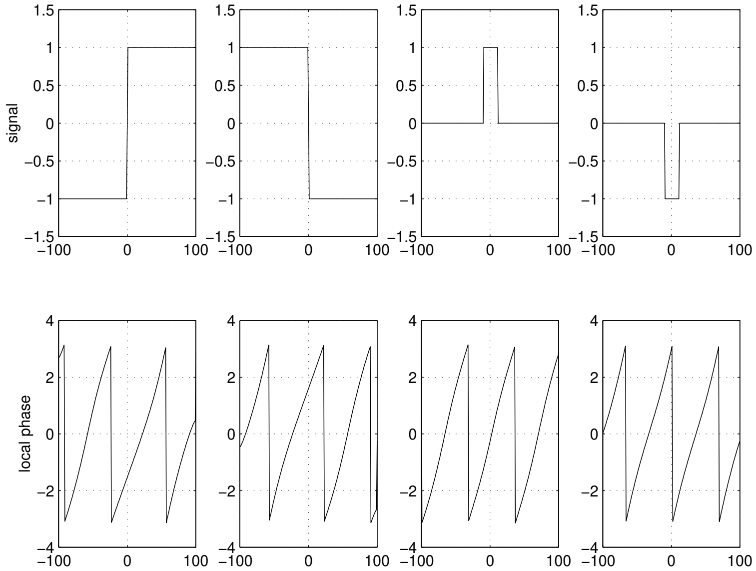

Figure 3.12: Top row: the four fundamental local structures (rising and falling step edge, and positive and negative peak) and the variations of the local phase around these structures (bottom).

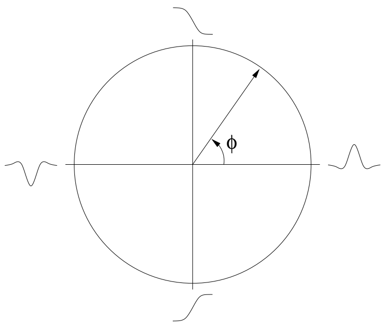

Figure 3.13: The relation between local signal structure and local phase. (See [45].)

Figure 3.13 sketches the relation between structure and phase in another way: the orientation in the circle indicates the value of the local phase. At the values 0, $\pi/2$, π and $-\pi/2$ the related structure is shown. An important feature of the local phase is that it is **independent of the signal energy**. This makes the local phase very robust against changing lighting conditions.

Note, that the value of the local phase at a certain signal position depends on the chosen filter parameters. I.e. Gabor wavelets will only detect features at the scale to which they are tuned.

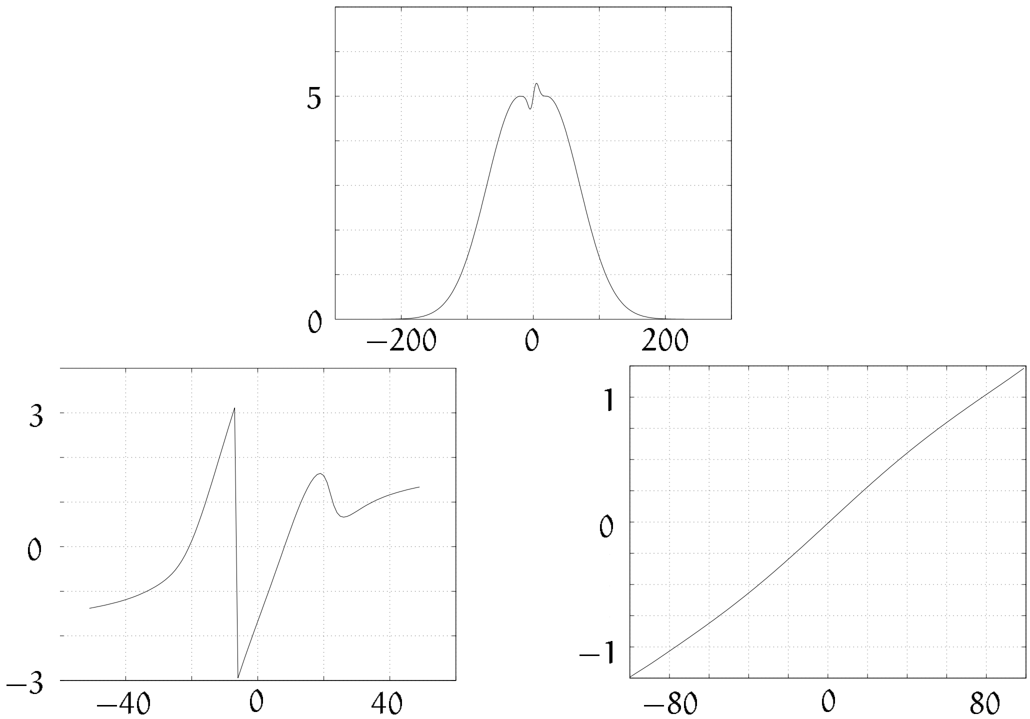

Figure 3.14: Top: a signal with features on two different scales. Bottom left: the local phase of the signal around the origin on a fine scale ($\sigma = 10$, $c = 2$). Bottom right: the local phase of the signal around the origin on a coarse scale ($\sigma = 100$, $c = 2$). At the origin the local phase equals $-\pi/2$ (rising edge) on a fine scale and 0 (peak) on a coarse scale.

3.2.3 Quaternionic Gabor Filters

Definition 3.14 (Quaternionic Gabor Filter) *In analogy to the complex Gabor filters we introduce quaternionic Gabor filters. The impulse response of a quaternionic Gabor filter is a Gaussian-windowed basis functions of the QFT:*

$$\begin{aligned} h^q(\mathbf{x}; \mathbf{u}_0, \sigma, \epsilon) &= g(\mathbf{x}; \sigma, \epsilon) \exp(i2\pi u_0 x) \exp(j2\pi v_0 y) && (3.38)\\ &= g(\mathbf{x}; \sigma, \epsilon) \exp(i\omega_1 x) \exp(j\omega_2 y) && (3.39)\\ &= g(\mathbf{x}; \sigma, \epsilon) \exp\left(i\frac{c_1 \omega_1 x}{\sigma}\right) \exp\left(j\frac{c_2 \epsilon \omega_2 y}{\sigma}\right). && (3.40) \end{aligned}$$

The different possible parameterizations can be explained in analogy to complex one-dimensional Gabor filters. We do not use rotated Gaussian windows here.

It follows from the modulation theorem of the Fourier transform that complex Gabor filters are shifted Gaussians in the frequency domain. In section 2.2.2 we

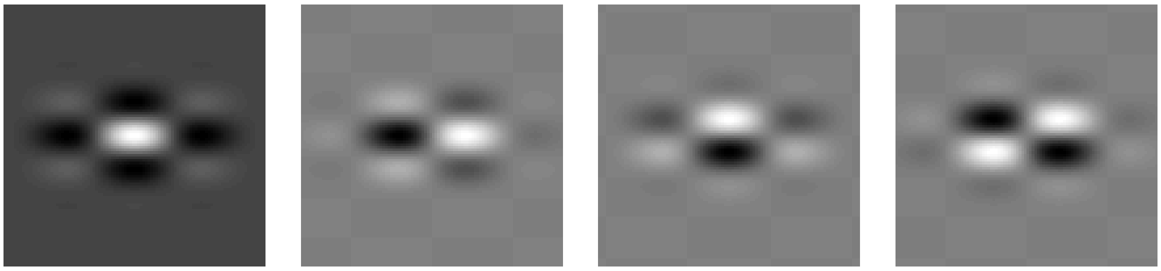

Figure 3.15: A quaternionic Gabor filter with parameters $\sigma_1 = 20$, $\sigma_2 = 10$, $c_1 = c_2 = 2$. The size of the filter mask is 100×100.

showed that there exists a modulation theorem for the QFT as well. Consequently, quaternionic Gabor filters are shifted Gaussian functions in the quaternionic frequency domain. Quaternionic Gabor filters thus belong to the "world" of the QFT rather than to the "complex Fourier world". The QFT of a quaternionic Gabor filter is given by

$$h^q(\mathbf{x}; \mathbf{u}_0, \sigma, \epsilon) \overset{\mathbb{H}}{\circ\!\!-\!\!-\!\!\bullet} H^q(\mathbf{u}; \mathbf{u}_0, \sigma, \epsilon) = \exp(-2\pi^2\sigma^2[(u-u_0)^2 + (v-v_0)^2/\epsilon^2])$$

Thus, for positive frequencies u_0 and v_0 the main amount of the Gabor filter's energy lies in the upper right quadrant. Therefore, convolving a real signal with a quaternionic Gabor filter yields an approximation to a quaternionic analytic signal.

A typical quaternionic Gabor filter is shown in figure 3.15.

3.2.4 Local Phase in 2D

The extension of the phase concept to two or more dimensions is an important, though nontrivial subject. One approach which has been made by Granlund [45] shall be reported here. It is based on the orientation tensor which was first introduced by Knutsson [65].

3.2.4.1 Intermezzo: The Orientation Tensor

Local orientation analysis requires a mathematically valid representation of orientation. One main requirement is that the representation takes account of the fact that orientation of a grey value structure can only be defined modulo 180°. Thus, a unit vector pointing into the direction of the gradient is not an appropriate representation.

Knutsson [65] proposed the tensor

$$\mathbf{T} = c\hat{x}\hat{x}^\top = c \begin{pmatrix} \hat{x}_1^2 & \hat{x}_1\hat{x}_2 \\ \hat{x}_1\hat{x}_2 & \hat{x}_2^2 \end{pmatrix} \tag{3.41}$$

as representation of the orientation of the vector x. Here c is some real number and $\hat{x} = x/|x| = (\hat{x}_1, \hat{x}_2)^\top$. The tensor representation is valid in the above sense since a change of sign of x does not influence the corresponding tensor $\mathbf{T}$.

This abstract conception can be understood using the following interpretation. The projection operator onto the line defined by x is a valid representation of the orientation of x since it is invariant with respect to rotations through $180°$ since x and $-x$ define the same line. The projection of a vector a onto the line given by x is

$$P_x(a) = (a \cdot \hat{x})\hat{x} \tag{3.42}$$

$$= \begin{pmatrix} (a_1\hat{x}_1 + a_2\hat{x}_2)\hat{x}_1 \\ (a_1\hat{x}_1 + a_2\hat{x}_2)\hat{x}_2 \end{pmatrix} \tag{3.43}$$

$$= \begin{pmatrix} \hat{x}_1^2 & \hat{x}_1\hat{x}_2 \\ \hat{x}_1\hat{x}_2 & \hat{x}_2^2 \end{pmatrix} \begin{pmatrix} a_1 \\ a_2 \end{pmatrix}. \tag{3.44}$$

Thus, the projection operator P_x is nothing else but the orientation tensor $\mathbf{T}$ with $c = 1$.

A filter method for measuring the local orientation tensor using polar separable quadrature filters is described in [45]. Jähne [59] proposes a simple filter method based on separable partial derivative operators and smoothing filters.

The orientation tensor concept is based on the idealized assumption that the image varies only along one orientation. Such signals are sometimes called *simple signals* and can be written as $f(x) = g(x \cdot \hat{e})$, where g depends only on one real variable. The unit vector $\hat{e}$ indicates the direction of variation. Natural images are not generally simple and consequently the measured local tensors are not necessarily of the form (3.41)[4]. For this reason sometimes the name *structure tensor* is preferred instead of *orientation tensor*. The 2D structure tensor is always a linear combination of the identity operator and the projection operator to a line in $\mathbb{R}^2$.

3.2.4.2 Local Complex Phase

Using the structure tensor $\mathbf{T}$ the image can be adaptively filtered with an orientation selective quadrature filter or Gabor filter. The orientation of this filter is chosen according to the eigenvector $\hat{e}$ corresponding to the largest eigenvalue of $\mathbf{T}$.

[4]However, the tensors obtained by the filter methods cited above are always symmetric.

This eigenvector represents the dominant local orientation of the image. Thus, the intrinsically one-dimensional local phase across the dominant orientation is measured as the angular phase of the complex response of a filter with orientation $\hat{\mathbf{e}}$. This makes sense where the signal is locally simple. Granlund et al. [45] propose to represent the 2D local phase by a three component vector $\mathbf{x}$ with

$$x_1 = \lambda_1 \cos(\varphi) \sin(\theta) \tag{3.45}$$

$$x_2 = \lambda_1 \sin(\varphi) \sin(\theta) \tag{3.46}$$

$$x_3 = \lambda_1 \cos(\theta), \tag{3.47}$$

where λ_1 is the largest eigenvalue of the orientation tensor $\mathbf{T}$, φ is the angle of the corresponding eigenvector against the x-axis and θ is the local phase measured by the Gabor or quadrature filter.

3.2.4.3 Local Quaternionic Phase

We now define the local quaternionic phase of a real two-dimensional signal as the angular phase of the filter response to a quaternionic Gabor filter. The angular phase is evaluated according to the rules given in table 2.2.

In 1D we can make the statement: **The local phase estimates and spatial position are equivariant** [45]. I.e. generally the local phase of a signal varies monotonically up to 2π-wrap-arounds. There are only singular points with low or zero signal energy where this equivariance cannot be found anymore. A simple example is the cosine function $\cos(x)$. If we apply a well-tuned Gabor filter for estimating the local phase ϕ of this function, we find that it is almost equal to the spatial position: $\phi(x) \approx x$ for $x \in [0, 2\pi[$. This leads us to an interpretation of the local quaternionic phase.

We make a similar example as in the one-dimensional case by replacing $\cos(x)$ by $\cos(x)\cos(y)$. The first two components of the local phase ϕ and θ turn out to approximate the spatial position: $\phi(\mathbf{x}) \approx x$ and $\theta(\mathbf{x}) \approx y$ for $(x, y) \in [0, 2\pi[\times[0, \pi[$. In general it turns out that these two components of the local phase are equivariant with spatial position. The reason for the interval $[0, 2\pi[\times[0, \pi[$, which follows mathematically from the definition of the angular phase of unit quaternions, can be understood from figure 3.16.

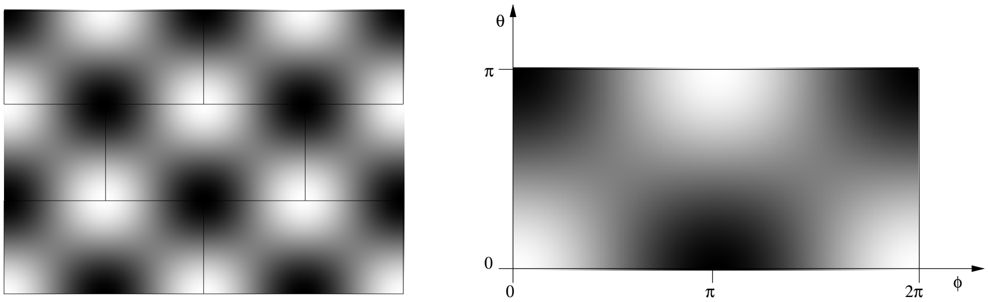

Figure 3.16: The function $f(x, y) = \cos(x)\cos(y)$ with $(x, y) \in [0, 4\pi[\times[0, 3\pi[$ (left) and $(x, y) \in [0, 2\pi[\times[0, \pi[$ (right).

While the spatial position can be recovered uniquely from the local signal structure within the interval $[0, 2\pi[\times[0, \pi[$, there will occur ambiguities if the interval is extended. The whole function $\cos(x)\cos(y)$ can be build from patches of the size $2\pi \times \pi$. Considering this example the third component of the local phase is always zero: $\psi = 0$. The meaning of this phase component becomes obvious if we vary the structure of the test signal in the following way:

The function $\cos(\omega_1 x_1)\cos(\omega_2 x_2)$ can be written as the sum

$$\cos(\omega_1 x_1)\cos(\omega_2 x_2) = \frac{1}{2}(\cos(\omega_1 x_1 + \omega_2 x_2) + \cos(\omega_1 x_1 - \omega_2 x_2)).$$

If we consider linear combinations of the form

$$f(\mathbf{x}; \lambda) = (1 - \lambda)\cos(\omega_1 x_1 + \omega_2 x_2) + \lambda\cos(\omega_1 x_1 - \omega_2 x_2) \tag{3.48}$$

we find that ψ is constant within each pattern with fixed λ, and varies monotonically with the value of $\lambda \in [0, 1]$. This behavior is shown in figure 3.17. The graph in figure 3.17 results from convolving sampled versions of $f(\mathbf{x}; \lambda)$ for different values of λ with a discrete quaternionic Gabor filter and evaluating the ψ-phase of the filter response according to table 2.2.

Another method[5] of evaluating the ψ-phase of $f(\mathbf{x}; \lambda)$ is calculating its quaternionic analytic signal $f_A^q(\mathbf{x}; \lambda)$ and its ψ-phase analytically. This leads to

$$\psi(\mathbf{x}; \lambda) = -0.5 \arcsin\left[\frac{2(1 - 2\lambda)}{1 + (2\lambda - 1)^2}\right].$$

[5]This was proposed by Prof. Hahn.

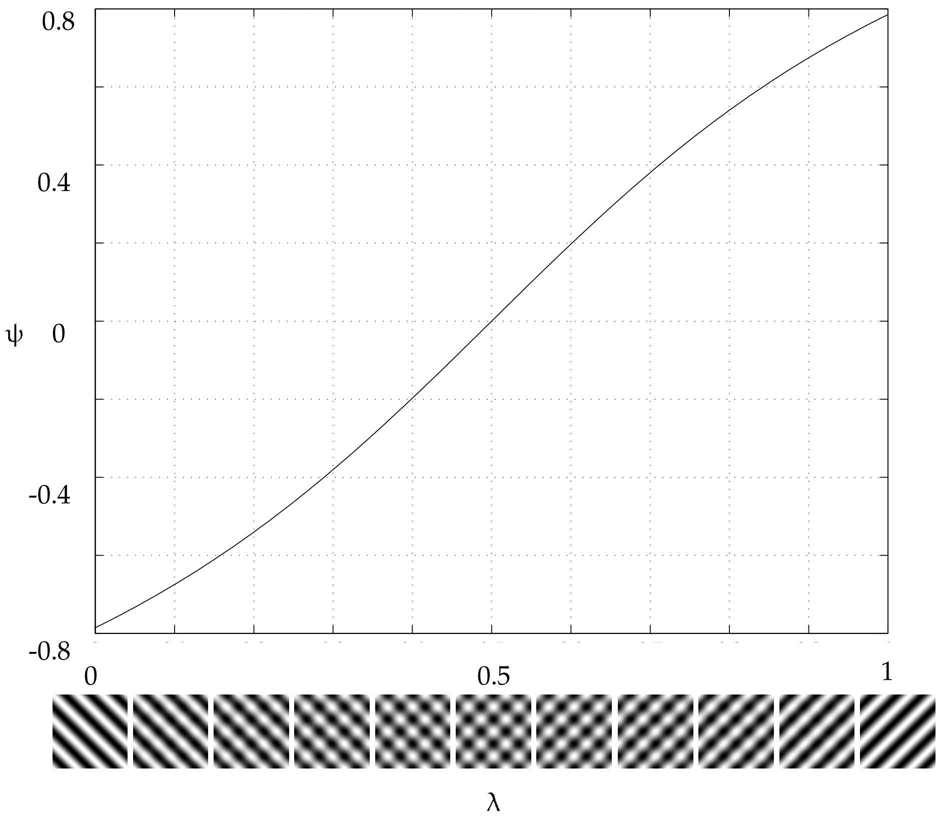

Figure 3.17: Dependence of the third phase component ψ on the local image structure.

The first two phase components, namely ϕ and θ do not change their meaning, while λ varies. Only for the values $\lambda = 0$ and $\lambda = 1$, i.e. $\psi = \mp\frac{\pi}{4}$, the structure degenerates into an intrinsically one-dimensional structure. Hence, the spatial position cannot any longer be recovered from the local structure. This corresponds to the singularity occurring in the evaluation of the angular phase of a quaternion for $\psi = \pm\frac{\pi}{4}$. In this case only $\phi \mp \theta$ can be evaluated. The remaining degree of freedom can i.e. be eliminated by setting $\theta = 0$.

In 1D there were four fundamental local structures which could be distinguished from the local phase. In 2D we find sixteen such structures as shown in figure 3.18. The structures in the first and second column respond solely to one component of the quaternionic Gabor filter.[6] The filter responses of the other three components vanish at the center of the patterns. Consequently the ψ-component of the quaternionic phase is 0 for these structures. The patterns in column three and four respond to superpositions of two components of the quaternionic Gabor

[6] We consider only the filter response at the center of the image.

filter (compare figure 3.21). For these patterns ψ takes the values $\pm\pi/4$. In this case we have the freedom to set θ to zero. The ϕ-phase component in this case takes the same values as the 1D phase for the corresponding 1D structures (compare figure 3.13).

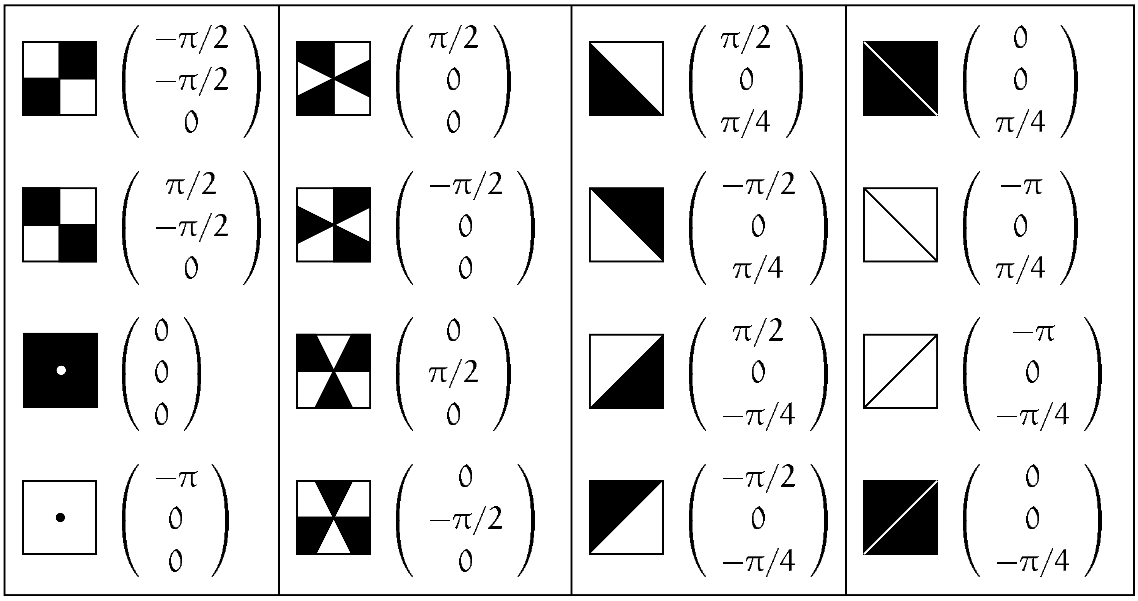

Figure 3.18: Sixteen 2D structures and the corresponding phase values $(\phi, \theta, \psi)^\top$ evaluated for the central pixel.

3.2.5 Some Properties of Quaternionic Gabor Filters

3.2.5.1 Gabor Filter Expansions of Images

In 1980 Bastiaans [6] proved that any signal can be decomposed into a discrete set of Gabor functions. However, since the Gabor functions do not build an orthogonal basis, the coefficients of the expansion cannot be obtained by projecting the signal onto the Gabor function set. Bastiaans showed that a function set biorthogonal to the Gabor functions exists which has to be used in order to obtain the expansion coefficients.

Jain [60] points out that a Gabor filter decomposition can be regarded as nearly orthogonal since the overlap between the filters in the frequency domain is small, if the parameters are well chosen. He shows results of images which were analyzed and synthesized using the same set of Gabor filters. The results show that there occurs nearly no visible error in the reconstruction. The fact that only the channel amplitudes of the reconstruction but not the phases contain a small error contributes to the good reconstruction, since as mentioned earlier (see introduction to this chapter) the phase carries the main part of the signal information.

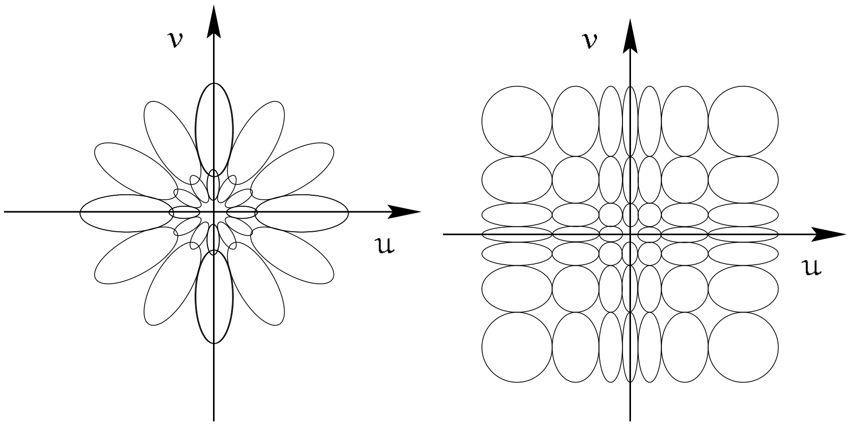

Figure 3.19: Left: the complex frequency domain covered by the transfer functions of differently tuned Gabor wavelets. Right: the quaternionic frequency domain covered by the transfer functions of differently tuned quaternionic Gabor wavelets.

3.2.5.2 Relations Between Complex and Quaternionic Gabor Filters

There is a simple relation between complex and quaternionic Gabor filters. Each component of a complex Gabor filter with aspect ratio $\epsilon = 1$ may be written as the sum of two quaternionic Gabor filter components:

$$\begin{aligned} h_e(x,y) &= g(x,y)\cos(\omega_1 x + \omega_2 y) \\ &= g(x,y)(\cos(\omega_1 x)\cos(\omega_2 y) - \sin(\omega_1 x)\sin(\omega_2 y)) \\ &= h^q_{ee}(x,y) - h^q_{oo}(x,y) \qquad (3.49) \\ h_o(x,y) &= g(x,y)\sin(\omega_1 x + \omega_2 y) \\ &= g(x,y)(\cos(\omega_1 x)\sin(\omega_2 y) + \sin(\omega_1 x)\cos(\omega_2 y)) \\ &= h^q_{oe}(x,y) + h^q_{eo}(x,y). \qquad (3.50) \end{aligned}$$

From the same quaternionic Gabor filter a second complex Gabor filter can be generated by

$$\begin{aligned} h_e(x,y) &= g(x,y)\cos(\omega_1 x - \omega_2 y)h^q_{ee}(x,y) + h^q_{oo}(x,y) \\ &= h^q_{ee}(x,y) + h^q_{oo}(x,y) \qquad (3.51) \\ h_o(x,y) &= g(x,y)\sin(\omega_1 x - \omega_2 y) \\ &= h^q_{eo}(x,y) - h^q_{oe}(x,y). \qquad (3.52) \end{aligned}$$

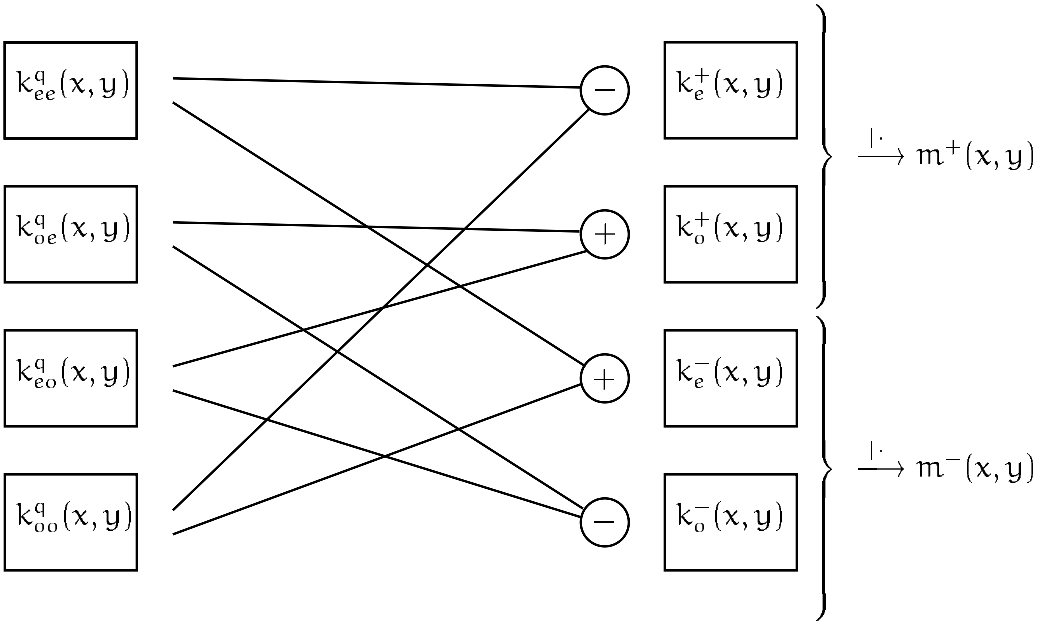

Figure 3.20: Relation between quaternionic and complex Gabor filter responses.

Thus, each quaternionic Gabor filter corresponds to *two* complex Gabor filters. Sometimes these two filters are denoted by h^+ ((3.49)+i (3.50)) and h^- ((3.51)+i(3.52)), respectively. Analogously, we denote the filter responses to h^+ and h^- by k^+ and k^-, and the local amplitudes $|k^+|$ and $|k^-|$ by m^+ and m^-, respectively. The response of a signal $f(x,y)$ to a Gabor filter will be denoted by $k(x,y)$ for a complex Gabor filter and $k^q(x,y)$ for a quaternionic Gabor filter:

$$\begin{aligned} k(x,y) &= h(x,y) * f(x,y) \\ &= (h_e(x,y) + ih_o(x,y))f(x,y) \\ &= k_e(x,y) + ik_o(x,y) \end{aligned} \tag{3.53}$$

$$\begin{aligned} k^q(x,y) &= h^q(x,y) * f(x,y) \\ &= (h^q_{ee}(x,y) + ih^q_{oe}(x,y) + jh^q_{eo}(x,y) + kh^q_{oo}(x,y))f(x,y) \\ &= k^q_{ee}(x,y) + ik^q_{oe}(x,y) + jk^q_{eo}(x,y) + kk^q_{oo}(x,y). \end{aligned} \tag{3.54}$$

Figure 3.20 shows the relations between the responses of an image f to a quaternionic Gabor filter and to the corresponding complex Gabor filters.

Theorem 3.2 *The filter responses of the complex Gabor filters h^+ and h^- can be obtained from k^q by*

$$k^+(\mathbf{x}) = (k^q_{ee} - k^q_{oo}) + i(k^q_{oe} + k^q_{eo}) \tag{3.55}$$

$$k^-(\mathbf{x}) = (k^q_{ee} + k^q_{oo}) + i(k^q_{oe} - k^q_{eo}). \tag{3.56}$$

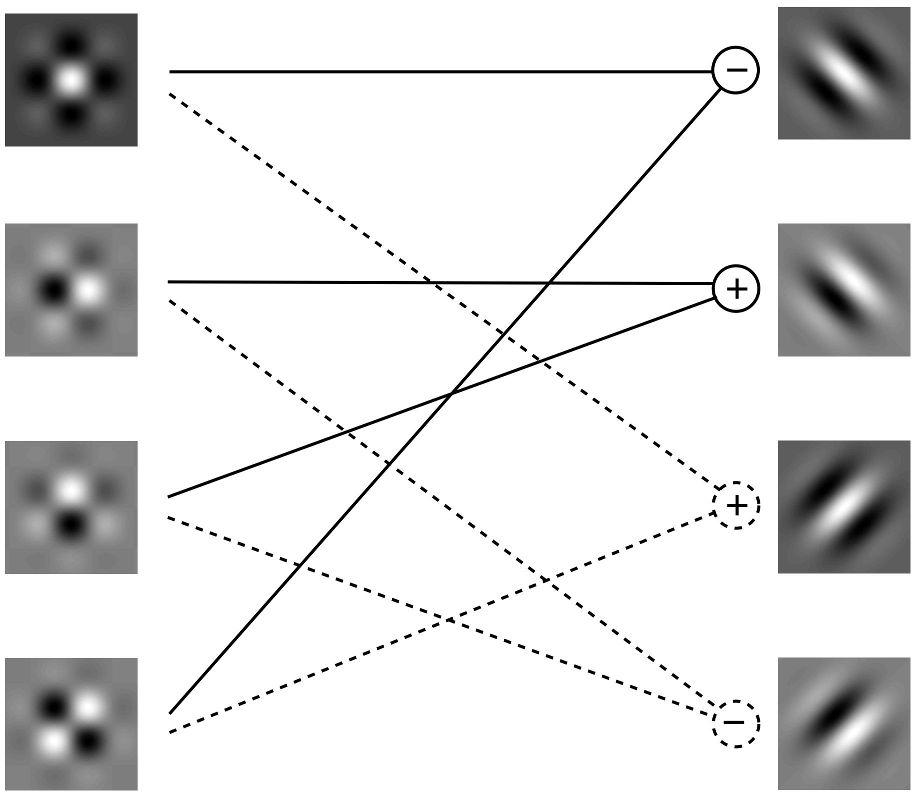

Figure 3.21: Relation between quaternionic and complex Gabor filters.

Proof: The theorem follows from the definition of h^+ and h^- and the fact that h^q is an LSI-filter. □

Algebraically, the relation between quaternionic and complex Gabor filters can be illuminated if we apply the switch operation from definition 2.17 to the quaternionic filter:

Theorem 3.3 *Let h^q be a quaternionic Gabor filter. Then*

$$\eta(S_2(h^q(\mathbf{x}))) = (h^+(\mathbf{x}), h^-(\mathbf{x})) \in \mathbb{C}^2,$$

where η establishes the isomorphism between HCA_2 and $\mathbb{C}^2$:

$$\eta : HCA_2 \;\; \rightarrow \;\; \mathbb{C}^2 \tag{3.57}$$

$$(\alpha + \beta i_1 + \gamma i_2 + \delta i_3) \;\; \mapsto \;\; ((\alpha - \delta) + i(\beta + \gamma), (\alpha + \delta) + i(\beta - \gamma)). \tag{3.58}$$

The same is true for the filter responses to real images

$$\eta(S_2(k^q(\mathbf{x}))) = (k^+(\mathbf{x}), k^-(\mathbf{x})) \in \mathbb{C}^2.$$

Proof: The theorem follows directly from applying η to $S_2(h^q(\mathbf{x}))$ and the definition of h^+ and h^-. □

3.2.5.3 Algorithmic Complexity of Gabor Filtering

When performing a Gabor filtering on the computer we have to use discrete Gabor filter masks of the form: $h = [h_{m,n}]_{m,n\in\{1,\ldots M\}}$ with

$$\begin{aligned} h_{m,n} \;\; = \;\; & \exp\left[-\left(m - \frac{M-1}{2}\right)^2 \Big/ (2\sigma_1)^2 - \left(n - \frac{M-1}{2}\right)^2 \Big/ (2\sigma_2)^2\right] \times \\ & \left[\cos\left\{\frac{2\pi}{M}\left(u\left(m - \frac{M-1}{2}\right) + v\left(n - \frac{M-1}{2}\right)\right)\right\}\right. \\ & \left. + i\sin\left\{\frac{2\pi}{M}\left(u\left(m - \frac{M-1}{2}\right) + v\left(n - \frac{M-1}{2}\right)\right)\right\}\right]. \end{aligned} \tag{3.59}$$

Using this convention the Gabor filter mask is an $M \times M$ matrix. The origin is located at the center of the matrix, therefore it is advantageous to choose M odd, in order to have a center pixel in the filter mask. The frequencies u and v count how many periods fit into the filter mask in horizontal and vertical direction, respectively.

The number of multiplications required by the convolution of an $N \times N$ image with an $M \times M$ filter mask in a direct manner is $O(N^2M^2)$. When the filter mask h is separable ($h = h_c * h_r$), where h_c and h_r are a column vector and a row vector of length M, respectively, the filtering operation is much faster. Since the convolution operation is associative we can write the filtering as

$$F = f * (h_c * h_r) = (f * h_c) * h_r. \tag{3.60}$$

Thus, the number of required multiplications reduces to $O(N^2M)$. It has been shown how Gabor filter components can be constructed as the sum of components of a quaternionic Gabor filter. Since quaternionic Gabor filters are separable, **this opens the possibility of implementing the convolution with complex Gabor filters in a separable way.** Figure 3.22 clarifies this result in "image notation".

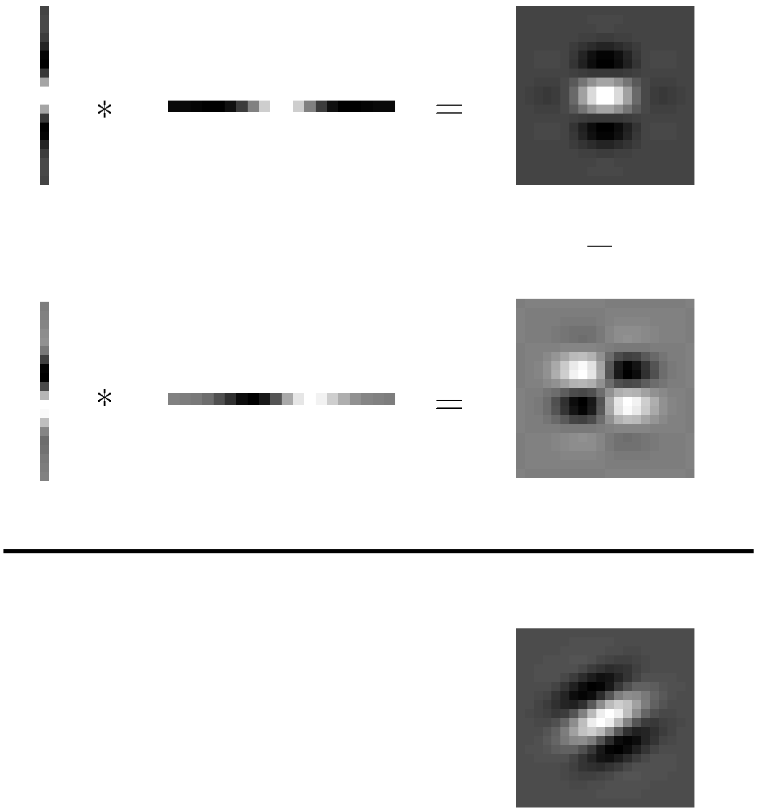

Figure 3.22: A complex Gabor filter as linear combination of separable quaternionic Gabor filter components.

The situation changes when the aspect ratio is not equal to one. The reason is that the rotated Gaussian function with $\epsilon \neq 1$ is not separable anymore, a property that was used in the above method. However, even in this case a reduction of the

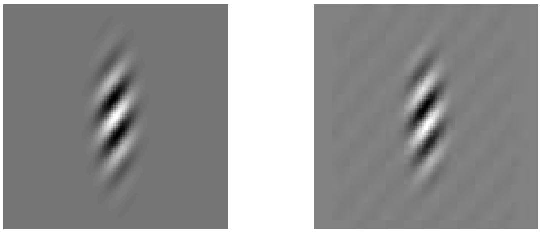

Figure 3.23: A Gabor filter with $\phi \neq \theta$.

algorithmic complexity is possible. The rotated Gaussian function with $\epsilon \neq 1$ is given by

$$\begin{aligned} g(x, y; \epsilon, \sigma, \phi) &= \exp\left(-\frac{(x\cos\phi + y\sin\phi)^2}{2\sigma^2} - \frac{(-x\sin\phi + y\cos\phi)^2}{2(\epsilon\sigma)^2}\right) && (3.61)\\ &= \exp\left(-\frac{(x^2\cos^2\phi + 2xy\sin\phi\cos\phi + y^2\sin^2\phi)}{2\sigma^2}\right. && (3.62)\\ &\quad \left. - \frac{(x^2\sin^2\phi - 2xy\sin\phi\cos\phi + y^2\cos^2\phi)}{2(\epsilon\sigma)^2}\right). && (3.63)\end{aligned}$$

Thus, a Gabor filter with orientation ϕ and aspect ratio ϵ can be written as

$$h(x, y; \phi, \sigma, \epsilon) = \exp\left(-\frac{2xy\sin\phi\cos\phi}{2\sigma^2} + \frac{2xy\sin\phi\cos\phi}{2(\epsilon\sigma)^2}\right)(A(x, y) + B(x, y)), \tag{3.64}$$

where A and B are separable functions. Regrettably it is not possible to decompose the exponential function in equation (3.64) into a sum of separable functions.

However, the method can be applied, whenever the Gaussian function is separable, even if the aspect ratio differs from 1. This is the case, when the rotation is only applied to the modulation term of the Gabor filter and not to the window function. A Gabor filter of this kind is shown in figure (3.23). This kind of Gabor filter can also be decomposed into the sum of two separable filters in the way shown above. This result is of no practical relevance though, since we know of no application which uses Gabor filters with $\phi \neq \theta$.

Often DC-corrected Gabor filters of the form

$$G(\mathbf{x}) = e^{-x^2/2\sigma_1^2} e^{-y^2/2\sigma_2^2} (e^{ic_1x/\sigma_1} e^{ic_2y/\sigma_2} - \mathit{const.})$$

are used. In this case the even component of the Gabor filter can be represented as the sum of three separable functions:

$$\begin{aligned} \mathcal{R}h(\mathbf{x}) &= e^{-x^2/2\sigma_1^2} e^{-y^2/2\sigma_2^2} \cos(c_1x/\sigma_1)\cos(c_2y/\sigma_2) \\ &\quad - e^{-x^2/2\sigma_1^2} e^{-y^2/2\sigma_2^2} \sin(c_1x/\sigma_1)\sin(c_2y/\sigma_2) \\ &\quad - e^{-x^2/2\sigma_1^2} e^{-y^2/2\sigma_2^2} \cdot \mathit{const.} && (3.65)\end{aligned}$$

Even in this case it is much faster to apply the separable convolutions and to add the results afterwards.

The above procedure of minimizing the algorithmic complexity of Gabor filtering can be applied to Gabor filters of arbitrary dimension, and with increasing dimension the effect becomes more and more important.

3.2.5.4 QGFs and the Uncertainty Principle

An often cited property of Gabor filters is their optimal simultaneous localization in the spatial and the frequency domain. This makes them suitable for local frequency analysis. For one-dimensional signals the notion "optimal localization" is formalized by the uncertainty principle of communication theory first formulated by Gabor [44]. Mathematically Gabor's formulation is equivalent to Heisenberg's uncertainty principle of quantum mechanics. For a review of the meaning of the uncertainty principle for image processing see also Wilson et al. [97]. The *effective width* or *spatial uncertainty* Δx of a complex signal f is usually defined as the square root of the variance of the energy distribution of f:

$$(\Delta x)^2 = \frac{\displaystyle\int_{\mathbb{R}} f(x) f^*(x) x^2 \, dx}{\displaystyle\int_{\mathbb{R}} f(x) f^*(x) \, dx}. \tag{3.66}$$

Analogously, the effective bandwidth is defined as

$$(\Delta u)^2 = \frac{\displaystyle\int_{\mathbb{R}} F(u) F^*(u) u^2 \, du}{\displaystyle\int_{\mathbb{R}} F(u) F^*(u) \, du}. \tag{3.67}$$

A fundamental lower bound for the joint localization of a signal in spatial and frequency domain is given by the uncertainty relation

$$\Delta x \, \Delta u \geq \frac{1}{4\pi} \tag{3.68}$$

The term "Gabor filters are optimally localized in both domains simultaneously" is justified since Gabor filters can be shown to achieve the minimum product of uncertainties [44]

$$\Delta x \, \Delta u = \frac{1}{4\pi}. \tag{3.69}$$

It could be shown by Papoulis [81] that each two-dimensional filter or signal $f(x, y)$ fulfills two uncertainty relations

$$\Delta x \, \Delta u \geq \frac{1}{4\pi} \quad \text{and} \quad \Delta y \, \Delta v \geq \frac{1}{4\pi}, \tag{3.70}$$

where Δx is defined by

$$(\Delta x)^2 = \frac{\int_{\mathbb{R}} f(x, y) f^*(x, y) x^2 \, dx \, dy}{\int_{\mathbb{R}} f(x, y) f^*(x, y) \, dx \, dy} \tag{3.71}$$

and Δy, Δu, and Δv analogously. Daugman combined these two relations to a new one which restricts the joint resolution of any two-dimensional filter in the two-dimensional spatial and frequency domains [28]:

$$\Delta x \, \Delta y \, \Delta u \, \Delta v \geq \frac{1}{16\pi^2}. \tag{3.72}$$

It can be shown that the lower limit is reached by a two-dimensional complex Gabor filter.

We extend the definition of the uncertainties in order to make it applicable to quaternion-valued functions:

$$(\Delta x)^2 = \frac{\int_{\mathbb{R}} f(x, y) \bar{f}(x, y) x^2 \, dx \, dy}{\int_{\mathbb{R}} f(x, y) \bar{f}(x, y) \, dx \, dy} \tag{3.73}$$

$$(\Delta u)^2 = \frac{\int_{\mathbb{R}} F(u, v) \bar{F}(u, v) u^2 \, du \, dv}{\int_{\mathbb{R}} F(u, v) \bar{F}(u, v) \, du \, dv}. \tag{3.74}$$

The analogous definitions apply to Δy and Δv. For complex signals the real-valued energy distribution is given by ff^*. For quaternion-valued signals this part is taken by $f\bar{f}$. Thus, the two-dimensional uncertainty relation for two-dimensional quaternionic signals is identical to Daugman's relation (3.72).

The uncertainty of a quaternionic Gabor filter h^q can be evaluated as follows. Let

h^q be given by

$$
\begin{aligned}
h^q(\mathbf{x}) &= \exp\left(-\frac{x^2}{2\sigma_x^2} - \frac{y^2}{2\sigma_y^2}\right) \exp(2\pi i\, u_0 x) \exp(2\pi j\, v_0 y) && (3.75)\\
\mathbb{H}\ \Big\updownarrow \\
H^q(\mathbf{u}) &= \exp(-2\pi^2\sigma_x^2(u-u_0)^2 - 2\pi^2\sigma_y^2(v-v_0)^2). && (3.76)
\end{aligned}
$$

Evaluating (3.73) and (3.74) we find

$$\Delta x = \frac{\sigma_x}{\sqrt{2}}, \quad \Delta y = \frac{\sigma_y}{\sqrt{2}}, \quad \Delta u = \frac{1}{8\sigma_x^2\pi^2}, \quad \Delta v = \frac{1}{8\sigma_y^2\pi^2}, \tag{3.77}$$

which leads to

$$\Delta x\, \Delta y\, \Delta u\, \Delta v = \frac{1}{16\pi^2}. \tag{3.78}$$

Thus, quaternionic Gabor filters share with their complex counterparts the property of being jointly optimally localized in the spatial and in the frequency domain.

3.2.5.5 Comparison of Quaternionic Gabor Filters and Derivatives of Gaussians

As shown in [78] 1D derivatives of Gaussians can well be approximated by Gabor filters for an appropriately chosen set of parameters. It could be verified that in the limit $n \to \infty$ where n is the order of the derivative the two filters are identically. For small n the remaining error becomes bigger with increasing c (see (3.35) for the definition of c), where the error is measured according to the L^2-norm.

This resemblance can be lifted to 2D using 2D complex Gabor filters only for derivatives of the form $\frac{\partial^n}{\partial x^n} G(x,y)$ and $\frac{\partial^n}{\partial y^n} G(x,y)$ or in general $\frac{\partial^n}{\partial x'^n} G(x,y)$ where $x' = x\cos\phi - y\sin\phi$, i.e. for directional derivatives.

Derivatives of Gaussians are frequently used in image analysis, when differential geometric methods play an essential role [68, 66, 69, 67] and [4, 5]. However, all mixed derivatives which contain derivatives with respect to the x- and the y-coordinate cannot be approximated by complex Gabor filters. In this chapter we extend the investigation of Michaelis [78] to 2D using quaternionic Gabor filters instead of complex Gabor filters and show that we can find a corresponding QGF component for each derivative of a Gaussian of the form $\frac{\partial^n}{\partial x^r \partial y^s} G(x,y), r+s=n$.

Normalization of the Filters

Before fitting the quaternionic Gabor filters to derivatives of Gaussians we normalize both filters so that they have L^2-norm equal to 1. We will then fit the Gabor filters to the derivatives of the Gaussian by minimizing the L^2-norm of the difference. We denote the four parts of a quaternionic Gabor filter as

$$
\begin{aligned}
h_{ee} &= N_{ee} e^{\frac{-x^2}{2\sigma_1^2}} e^{\frac{-y^2}{2\sigma_2^2}} \cos\left(\frac{c_1 x}{\sigma_1}\right) \cos\left(\frac{c_2 y}{\sigma_2}\right) && (3.79)\\
h_{oe} &= N_{oe} e^{\frac{-x^2}{2\sigma_1^2}} e^{\frac{-y^2}{2\sigma_2^2}} \sin\left(\frac{c_1 x}{\sigma_1}\right) \cos\left(\frac{c_2 y}{\sigma_2}\right) && (3.80)\\
h_{eo} &= N_{eo} e^{\frac{-x^2}{2\sigma_1^2}} e^{\frac{-y^2}{2\sigma_2^2}} \cos\left(\frac{c_1 x}{\sigma_1}\right) \sin\left(\frac{c_2 y}{\sigma_2}\right) && (3.81)\\
h_{oo} &= N_{oo} e^{\frac{-x^2}{2\sigma_1^2}} e^{\frac{-y^2}{2\sigma_2^2}} \sin\left(\frac{c_1 x}{\sigma_1}\right) \sin\left(\frac{c_2 y}{\sigma_2}\right). && (3.82)
\end{aligned}
$$

The L^2-norm of the quaternionic Gabor filter components can be calculated using the L^2-norms of the 1D Gabor filters given in [78] and the relations $L^2(h_{ab}) = L^2(h_a)L^2(h_b)$, where $a, b \in \{e, o\}$. Thus, we obtain:

$$
\begin{aligned}
L^2(h_{ee}) &= \frac{N_{ee}}{2}\sqrt{\sigma_1\sigma_2\pi(1+e^{-c_1^2})(1+e^{-c_2^2})} && (3.83)\\
L^2(h_{oe}) &= \frac{N_{oe}}{2}\sqrt{\sigma_1\sigma_2\pi(1-e^{-c_1^2})(1+e^{-c_2^2})} && (3.84)\\
L^2(h_{eo}) &= \frac{N_{eo}}{2}\sqrt{\sigma_1\sigma_2\pi(1+e^{-c_1^2})(1-e^{-c_2^2})} && (3.85)\\
L^2(h_{oo}) &= \frac{N_{oo}}{2}\sqrt{\sigma_1\sigma_2\pi(1-e^{-c_1^2})(1-e^{-c_2^2})}. && (3.86)
\end{aligned}
$$

The components of the quaternionic Gabor filter when normalized to $L^2(h_{ab}) = 1$ consequently take the form:

$$
\begin{aligned}
h_{ee} &= \frac{2}{\sqrt{\sigma_1\sigma_2\pi(1+e^{-c_1^2})(1+e^{-c_2^2})}} e^{\frac{-x^2}{2\sigma_1^2}} e^{\frac{-y^2}{2\sigma_2^2}} \cos\left(\frac{c_1 x}{\sigma_1}\right) \cos\left(\frac{c_2 y}{\sigma_2}\right) && (3.87)\\
h_{oe} &= \frac{2}{\sqrt{\sigma_1\sigma_2\pi(1-e^{-c_1^2})(1+e^{-c_2^2})}} e^{\frac{-x^2}{2\sigma_1^2}} e^{\frac{-y^2}{2\sigma_2^2}} \sin\left(\frac{c_1 x}{\sigma_1}\right) \cos\left(\frac{c_2 y}{\sigma_2}\right) && (3.88)\\
h_{eo} &= \frac{2}{\sqrt{\sigma_1\sigma_2\pi(1+e^{-c_1^2})(1-e^{-c_2^2})}} e^{\frac{-x^2}{2\sigma_1^2}} e^{\frac{-y^2}{2\sigma_2^2}} \cos\left(\frac{c_1 x}{\sigma_1}\right) \sin\left(\frac{c_2 y}{\sigma_2}\right) && (3.89)\\
h_{oo} &= \frac{2}{\sqrt{\sigma_1\sigma_2\pi(1-e^{-c_1^2})(1-e^{-c_2^2})}} e^{\frac{-x^2}{2\sigma_1^2}} e^{\frac{-y^2}{2\sigma_2^2}} \sin\left(\frac{c_1 x}{\sigma_1}\right) \sin\left(\frac{c_2 y}{\sigma_2}\right). && (3.90)
\end{aligned}
$$

The same procedure is performed for derivatives of the Gaussian function. By D we denote the Gaussian, while the derivatives are denoted by $D_{r,s} = (\partial_x)^r(\partial_y)^s D$. We list the first derivatives and then give the general expression.

$$
\begin{aligned}
D(\mathbf{x}) &= N^2 e^{\frac{-x^2-y^2}{2\sigma^2}} && (3.91)\\
D_{1,0}(\mathbf{x}) &= -N^2\frac{x}{\sigma^2}e^{\frac{-x^2-y^2}{2\sigma^2}} && (3.92)\\
D_{0,1}(\mathbf{x}) &= -N^2\frac{y}{\sigma^2}e^{\frac{-x^2-y^2}{2\sigma^2}} && (3.93)\\
D_{1,1}(\mathbf{x}) &= N^2\frac{xy}{\sigma^4}e^{\frac{-x^2-y^2}{2\sigma^2}} && (3.94)\\
D_{2,0}(\mathbf{x}) &= N^2\frac{1}{\sigma^2}\left(\frac{x^2}{\sigma^2}-1\right)e^{\frac{-x^2-y^2}{2\sigma^2}} && (3.95)\\
D_{0,2}(\mathbf{x}) &= N^2\frac{1}{\sigma^2}\left(\frac{y^2}{\sigma^2}-1\right)e^{\frac{-x^2-y^2}{2\sigma^2}} && (3.96)\\
D_{2,1}(\mathbf{x}) &= -N^2\frac{y}{\sigma^4}\left(\frac{x^2}{\sigma^2}-1\right)e^{\frac{-x^2-y^2}{2\sigma^2}} && (3.97)\\
D_{1,2}(\mathbf{x}) &= -N^2\frac{x}{\sigma^4}\left(\frac{y^2}{\sigma^2}-1\right)e^{\frac{-x^2-y^2}{2\sigma^2}} && (3.98)\\
D_{2,2}(\mathbf{x}) &= N^2\frac{1}{\sigma^4}\left(\frac{y^2}{\sigma^2}-1\right)\left(\frac{x^2}{\sigma^2}-1\right)e^{\frac{-x^2-y^2}{2\sigma^2}} && (3.99)\\
D_{r,s}(\mathbf{x}) &= (-1)^{r+s}N^2\frac{1}{(\sqrt{2}\sigma)^{r+s}}H_r\left(\frac{x}{\sqrt{2}\sigma}\right)H_s\left(\frac{y}{\sqrt{2}\sigma}\right)e^{\frac{-x^2-y^2}{2\sigma^2}}. && (3.100)
\end{aligned}
$$

Here, the functions H_n are Hermite polynomials. If we denote by D_n the n^{th} derivative of the 1D Gaussian $D = N\exp(-x^2/2\sigma^2)$, the above expressions can be derived from

$$D_{r,s}(\mathbf{x}) = D_r(x)D_s(y).$$

The L^2-norms of $D_n(x)$ are given in [78]. The L^2-norms of the derivatives of the 2D Gaussian function are thus found to be (assuming $r \geq s$):

$$
\begin{aligned}
L^2(D_{r,s}) &= L^2(D_{s,r}) && (3.101)\\
&= L^2(D_r)L^2(D_s) && (3.102)\\
&= N^2\pi(3\cdot 5\cdots(2s-1))\sqrt{\frac{(2s+1)(2s+3)\cdots(2r-1)}{2^{r+s}\sigma^{2(r+s)-2}}} && (3.103)
\end{aligned}
$$

Before we derive the quaternionic Gabor functions which fit optimally to the low-order derivatives of the Gaussian function, we regard the asymptotic behavior of derivatives of the Gaussian function for the differential order tending to infinity. From [78] we find

$$D_{r,s} \to \begin{cases} (-)^{p+q} N(r,s,\sigma) e^{\frac{-x^2-y^2}{4\sigma^2}} \cos\left(\frac{x\sqrt{2r+1}}{\sqrt{2}\sigma}\right) \cos\left(\frac{y\sqrt{2s+1}}{\sqrt{2}\sigma}\right), & r = 2p, s = 2q \\ (-)^{p+q+1} N(r,s,\sigma) e^{\frac{-x^2-y^2}{4\sigma^2}} \sin\left(\frac{x\sqrt{2r+1}}{\sqrt{2}\sigma}\right) \cos\left(\frac{y\sqrt{2s+1}}{\sqrt{2}\sigma}\right), & r = 2p+1, s = 2q \\ (-)^{p+q+1} N(r,s,\sigma) e^{\frac{-x^2-y^2}{4\sigma^2}} \cos\left(\frac{x\sqrt{2r+1}}{\sqrt{2}\sigma}\right) \sin\left(\frac{y\sqrt{2s+1}}{\sqrt{2}\sigma}\right), & r = 2p, s = 2q+1 \\ (-)^{p+q} N(r,s,\sigma) e^{\frac{-x^2-y^2}{4\sigma^2}} \sin\left(\frac{x\sqrt{2r+1}}{\sqrt{2}\sigma}\right) \sin\left(\frac{y\sqrt{2s+1}}{\sqrt{2}\sigma}\right), & r = 2p+1, s = 2q+1 \end{cases}$$

Thus, the higher derivatives of the Gaussian function resemble the components of quaternionic Gabor filters. In the limit these functions are identical. The appropriate values of the quaternionic Gabor filter parameters are $\sigma_1 = \sigma_2 = \sqrt{2}\sigma$, $c_1 = \sqrt{2r+1}$ and $c_2 = \sqrt{2s+1}$. The only significant errors can be found for the first derivatives. The optimal quaternionic Gabor filters which fit these derivatives are derived in the following.

Optimal Fit for D_{00}

To start with the trivial case we regard the Gaussian function itself. Normalized to $L^2(D_{00}) = 1$ it reads

$$D_{00}(\mathbf{x}) = \frac{1}{\sigma\sqrt{\pi}} e^{-\frac{x^2+y^2}{2\sigma^2}},$$

while the even/even-component of the quaternionic Gabor filter (also normalized to 1) is

$$h_{ee}(\mathbf{x}) = \frac{2}{\sqrt{\sigma_1\sigma_2\pi(1+e^{-c_1^2})(1+e^{-c_2^2})}} e^{-\frac{x^2}{2\sigma_1^2}} e^{-\frac{y^2}{2\sigma_2^2}} \cos\left(\frac{c_1 x}{\sigma_1}\right) \cos\left(\frac{c_2 y}{\sigma_2}\right). \quad (3.104)$$

With the parameters $c_1 = c_2 = 0$ and $\sigma_1 = \sigma_2 = \sigma$ (3.104) becomes

$$h_{ee}(\mathbf{x}) = \frac{1}{\sqrt{\pi}\sigma} e^{-\frac{x^2+y^2}{2\sigma^2}} \quad (3.105)$$

$$= D_{00}(\mathbf{x}). \quad (3.106)$$

With the above parameters the Gabor filter is degenerated because the frequency of the cosine function is zero, i.e. the cosine term is constant in this case.

Optimal Fits for D_{01}, D_{10} and D_{11}

We investigate the optimal fit for the Gaussian derivative D_{01}. The optimally fitting quaternionic Gabor filter component for D_{10} follows from symmetry. The Gaussian derivative D_{01} and the Gabor function h_{eo} both normalized to 1 are

$$D_{01}(\mathbf{x}) = -\sqrt{\frac{2}{\pi}}\frac{y}{\sigma^2}e^{-\frac{x^2+y^2}{2\sigma^2}} \tag{3.107}$$

$$\text{and} \quad h_{eo}(\mathbf{x}) = \frac{2e^{-\frac{x^2}{2\sigma_1^2}}e^{-\frac{y^2}{2\sigma_2^2}}}{\sqrt{\sigma_1\sigma_2\pi(1+e^{-c_1^2})(1-e^{-c_2^2})}}\cos\left(\frac{c_1x}{\sigma_1}\right)\sin\left(\frac{c_2y}{\sigma_2}\right). \tag{3.108}$$

Like in the previous example we find $c_1 = 0$ and $\sigma_1 = \sigma$ as optimal parameters. Thus, h_{eo} takes the form

$$h_{eo}(\mathbf{x}) = \sqrt{\frac{2}{\sigma\sigma_2\pi(1-e^{-c_2^2})}}e^{-\frac{x^2}{2\sigma^2}}e^{-\frac{y^2}{2\sigma_2^2}}\sin\left(\frac{c_2y}{\sigma_2}\right). \tag{3.109}$$

We divide (3.107) and (3.109) by $\exp(-x^2/(2\sigma^2))\sigma^{-1/2}\pi^{-1/4}$ and end up with D_1 and h_o (the first derivative of the one-dimensional Gaussian function and the odd part of the one-dimensional Gabor function, both normalized to 1.

$$D_1(y) = -\sqrt{\frac{2\sigma}{\sqrt{\pi}}}\frac{y}{\sigma^2}e^{-\frac{y^2}{2\sigma^2}} \tag{3.110}$$

$$\text{and} \quad h_o(y) = \sqrt{\frac{2}{\sigma_2\sqrt{\pi}(1-e^{-c_2^2})}}e^{-\frac{y^2}{2\sigma_2^2}}\sin\left(\frac{c_2y}{\sigma_2}\right). \tag{3.111}$$

The remaining parameters c_2 and σ_2 have to be chosen in order to minimize the L^2-norm of the error which is given by

$$\begin{aligned} L^2(D_1(y)+h_o(y)) &= \sqrt{L^2(D_1)+L^2(h_s)+2\int_{\mathbb{R}}D_1h_s\,dx} \\ &= \sqrt{2+2\int_{\mathbb{R}}D_1h_s\,dx} \\ &=: \sqrt{2-2A_1(c_2,\sigma,\sigma_2)}. \end{aligned} \tag{3.112}$$

If σ is set to $1/\sqrt{2}$ the integral in (3.112) can be evaluated to

$$A_1(c_2,\sigma_2) = 2^{\frac{9}{4}}c\sigma_2^{\frac{3}{2}}(1-e^{-c^2})^{-\frac{1}{2}}e^{-\frac{c^2}{2+4\sigma_2^2}}(1+2\sigma_2^2)^{-\frac{3}{2}}. \tag{3.113}$$

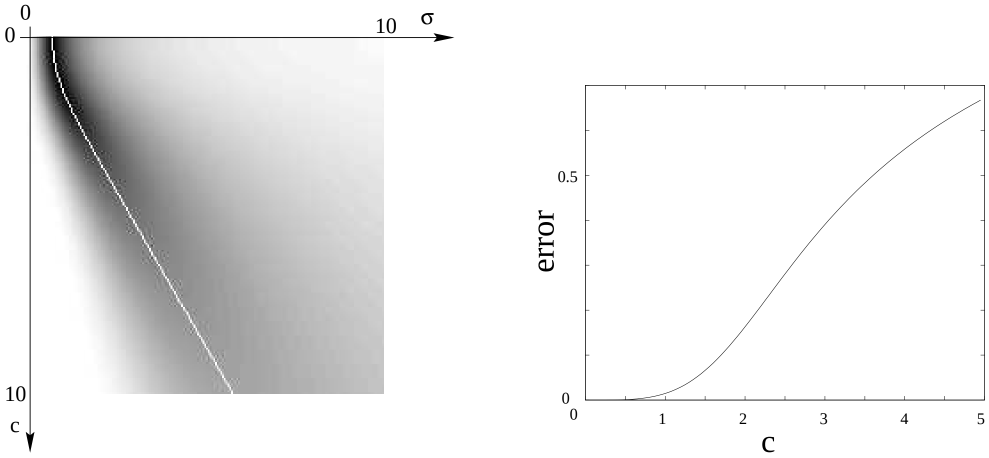

Figure 3.24: The error $L^2(D_1 - h_o)$. Left: the error as gray value image. The white line indicates the optimal value for σ depending on c. Right: the error along this line.

A grey value image of the L^2-error is shown in figure 3.24. For fixed values of c the optimal choice of σ is indicated by the white curve. From (3.112) it follows immediately that $A_1 \leq 1$ for all admissible values of c and σ_2. Thus, in order to minimize the L^2-error we have to maximize A_1. For fixed values of c it follows from the necessary condition $\partial_{\sigma_2} A_1 = 0$ that σ_2 has to be of the form

$$\sigma_2 = \frac{1}{\sqrt{6}}\sqrt{c^2 + \sqrt{c^4 + 9}} \tag{3.114}$$

which is indicated by the white curve in figure 3.24. The L^2-error turns out to be minimal in the limit $c \to 0$ where σ_2 according to (3.114) tends to $1/\sqrt{2}$. Inserting $\sigma_2 = 1/\sqrt{2}$ into (3.113) we get

$$A_1(c_2) = \frac{c_2}{\sqrt{2\sinh(\frac{c_2^2}{2})}}$$

which can be shown to tend to 1 for $c \to 0$ using de l'Hospital's rule. Consequently, setting $c_1 = c_2 = 0$ and $\sigma_1 = \sigma_2 = \sigma$ the L^2-error vanishes. For reasons of symmetry the same parameters have to be used in order to fit h_{oe} and h_{oo} optimally to D_{10} and D_{11}, respectively.

Optimal Fits for Second and Third Order Derivatives

In the preceding investigation we could simplify the two-dimensional fitting problem to a one-dimensional fitting problem using the separability of Gaussian derivatives and quaternionic Gabor filters. We will prove the general applicability of this approach. Let D_{rs} be a Gaussian derivative and h_{ab} the appropriate component of a quaternionic Gabor filter with $a, b \in \{e, o\}$. We have to minimize the L^2-norm of the error which is given by

$$L^2(D_{rs} \pm h_{ab}) = \sqrt{L^2(D_{rs}) + L^2(h_{ab}) \pm 2\int_{\mathbb{R}^2} D_{rs}(\mathbf{x})h_{ab}(\mathbf{x})d^2\mathbf{x}} \quad (3.115)$$

$$=: \sqrt{2 - 2A_{rs}}, \quad A_{rs} = \left|\int_{\mathbb{R}^2} D_{rs}(\mathbf{x})h_{ab}(\mathbf{x})d^2\mathbf{x}\right| \quad (3.116)$$

$$L^2(D_r \pm h_a) = \sqrt{2 - 2A_r}, \quad A_r = \left|\int_{\mathbb{R}} D_r(x)h_a(x)dx\right| \quad (3.117)$$

$$L^2(D_s \pm h_b) = \sqrt{2 - 2A_s}, \quad A_s = \left|\int_{\mathbb{R}} D_s(y)h_b(y)dy\right| \quad (3.118)$$

Since the above L^2-norms exist and are non-negative real numbers we can conclude that $A_r, A_s, A_{r,s} \in [0, 1]$. Further we know that $A_{r,s} = A_r A_s$. Thus, in order to maximize A_{rs} we have to maximize A_r and A_s separately, which is the same as minimizing $L^2(D_r \pm h_a)$ and $L^2(D_s \pm h_b)$, separately.

The optimal fit for $h_e(x)$ to $D_2(x)$ with $\sigma = 1/\sqrt{2}$ is $c = 2.29$ and $\sigma_{\text{Gabor}} = 1.073$ with an error of 10%. The optimal parameters for the fit of $h_o(x)$ to $D_3(x)$ with $\sigma = 1/\sqrt{(2)}$ are $c = 2.62$ and $\sigma_{\text{Gabor}} = 1.03$ with an error of about 6%. These values are taken from [78]. The optimal parameters and the remaining L^2-errors are listed in table 3.5. In order to calculate the L^2-error of the optimal fitting Gabor filter we make use of the L^2-error of the one-dimensional Gabor filters. The desired error $L^2(D_{rs} \pm h_{ab})$ can be found from $L^2(D_r \pm h_a)$ and $L^2(D_s \pm h_b)$ using the following formula:

$$\begin{aligned} L^2(D_{rs} \pm h_{ab}) &= \sqrt{\frac{-1}{2}\left(2 - [L^2(D_r \pm h_a)]^2\right)\left(2 - [L^2(D_s \pm h_b)]^2\right) + 2} \quad (3.119) \\ &= \sqrt{[L^2(D_r \pm h_a)]^2 + [L^2(D_s \pm h_b)]^2 - \frac{[L^2(D_r \pm h_a)]^2[L^2(D_s \pm h_b)]^2}{2}} \\ &\approx \sqrt{[L^2(D_r \pm h_a)]^2 + [L^2(D_s \pm h_b)]^2}. \end{aligned}$$

The last approximation is valid for small errors.

An Example

If an image f is considered as a surface in $\mathbb{R}^3$ with the Monge representation $(x, y, f(\mathbf{x}))$ we can evaluate its Gaussian curvature. For the use of Gaussian curvature in image analysis see e.g. [3]. The derivative of a discretized image can be approximated

D_{rs}	h_{ab}	σ_1	σ_2	c_1	c_2	L^2-error
D_{20}	h_{cc}	1.073	$1/\sqrt{2}$	2.29	0	10%
D_{02}	h_{cc}	$1/\sqrt{2}$	1.073	0	2.29	10%
D_{21}	h_{cs}	1.073	$1/\sqrt{2}$	2.29	$\to 0$	10%
D_{12}	h_{sc}	$1/\sqrt{2}$	1.073	$\to 0$	2.29	10%
D_{22}	h_{cc}	1.073	1.073	2.29	2.29	14%
D_{30}	h_{sc}	1.03	$1/\sqrt{2}$	2.62	0	6%
D_{03}	h_{cs}	$1/\sqrt{2}$	1.03	0	2.62	6%
D_{31}	h_{ss}	1.03	$1/\sqrt{2}$	2.62	$\to 0$	6%
D_{13}	h_{ss}	$1/\sqrt{2}$	1.03	$\to 0$	2.62	6%
D_{32}	h_{sc}	1.03	1.073	2.62	2.29	12%
D_{23}	h_{cs}	1.073	1.03	2.29	2.62	12%
D_{33}	h_{ss}	1.03	1.03	2.62	2.62	8%

Table 3.5: The optimal parameters for the approximation of derivatives of a two-dimensional Gaussian by quaternionic Gabor filters.

by convolving the image with the corresponding derivative of the Gaussian. The Gaussian curvature of the ”image surface” is defined by

$$K = \frac{f_{xx}f_{yy} - f_{xy}^2}{(1 + f_x^2 + f_y^2)^2}. \tag{3.120}$$

We are going to investigate how well the Gaussian curvature can be approximated by using quaternionic Gabor filters instead of derivatives of the Gaussian function. If we would like to use *only one* quaternionic Gabor filter we face the problem that we have to approximate the five filters D_x, D_y, D_{xx}, D_{xy} and D_{yy} by one quaternionic filter with only four components.

As an example we try to approximate the sampled Gaussian derivatives with the parameters: side-length= 20 pixel, $\sigma = 2$, and $N = 1$. We minimize the sum of the five L^2-errors of the approximation. As optimal values for the approximating QGF we find $\sigma_1 = \sigma_2 = 2.5008$, $c_1 = c_2 = 1.2031$ and $N = 0.0113$. However, the sum of the L^2-error is about 56 % of the sum of the L^2-norms of the Gaussian derivatives and the shape of the approximations to D_{xx} and D_{yy} is unacceptable (see figure 3.25).

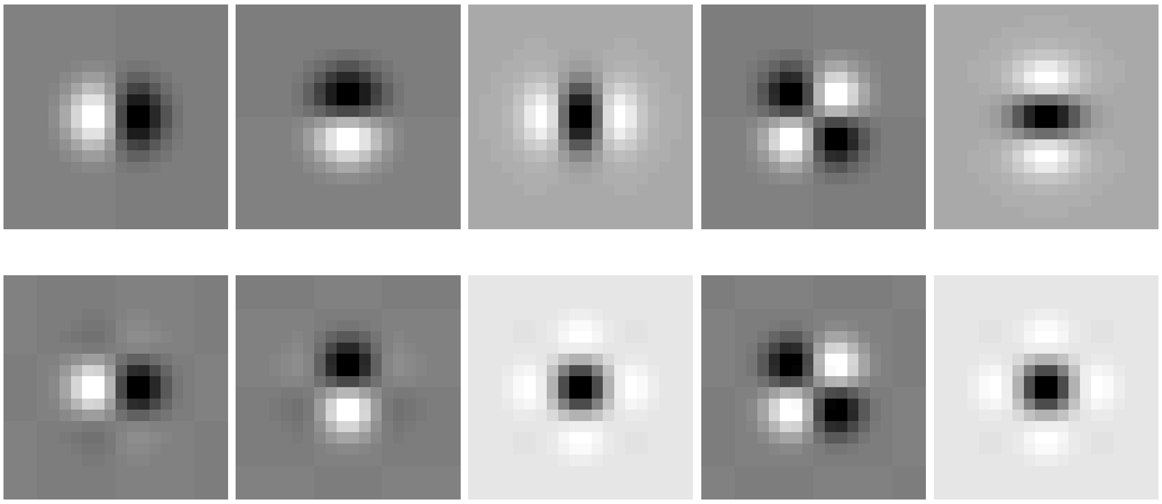

Figure 3.25: The five derivatives of the Gaussian: D_x, D_y, D_{xx}, D_{xy} and D_{yy} (top), and the approximation by *one* quaternionic Gabor filter (bottom). Where the Gabor component and the Gaussian derivative differ in sign the inverse Gabor component is shown.

A reasonable improvement can be made by approximating the derivatives by two different quaternionic Gabor filters. The first Gabor filter is tuned to approximate D_x, D_y and D_{xy} while the second Gabor filter is meant to approximate D_{xx}. D_{yy} can be taken as the transpose of D_{xx}. The optimal parameters for the first filter are $\sigma_1 = \sigma_2 = 2.1108$, $c_1 = c_2 = 0.4896$ and $N = 0.04337$ and for the second $\sigma_1 = 3.0349$, $\sigma_2 = 2$, $c_1 = 2.29$, $c_2 \to 0$ and $N = 0.04337$.

Note (for the first filter) the deviation from the results given earlier in this chapter. The reason for this is, that the filter components are tuned simultaneously and consequently the norm of the Gabor components cannot always equal the norm of the derivatives as assumed above. If we allow an additional weight for each Gabor component the optimal parameters will be $\sigma_1 = \sigma_2 = 2$ and $c_1 = c_2 \to 0$. The weight is chosen so that the L^2-norm of each component equals the L^2-norm of the corresponding Gaussian derivative. With this method the overall L^2-error is about 1.5% and there is almost no visible difference between Gaussian derivatives and the Gabor filters (see figure 3.26). Figure 3.27 shows the comparison between the Gaussian derivatives and quaternionic Gabor filters in estimating the Gaussian curvature of an image according to (3.120). The 1% of pixels with the highest curvature are marked white.

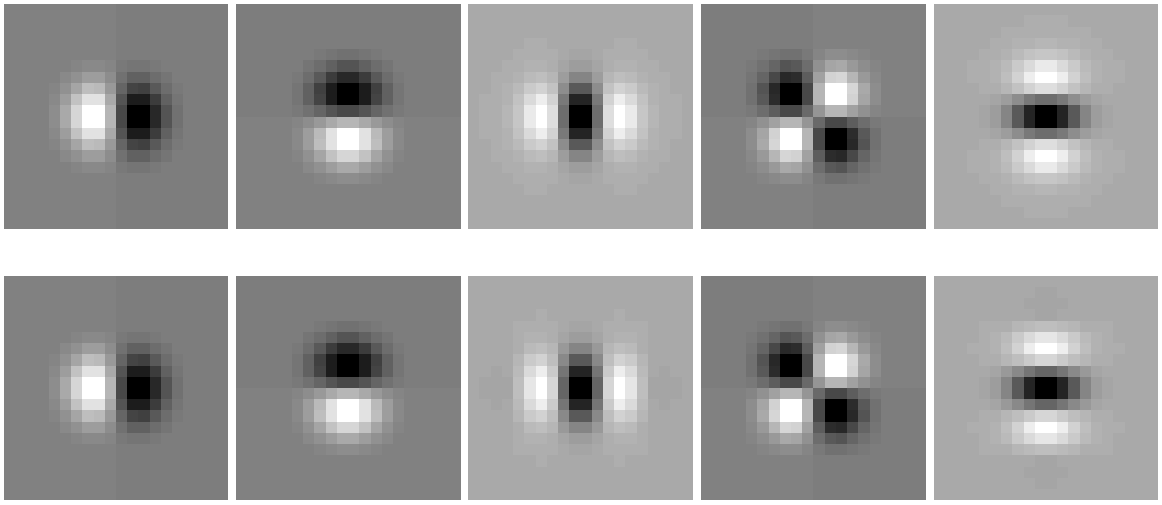

Figure 3.26: The five derivatives of the Gaussian: D_x, D_y, D_{xx}, D_{xy} and D_{yy} (top), and the approximation by *two* quaternionic Gabor filters with adjusted weights (bottom), where the Gabor component and the Gaussian derivative differ in sign the inverse Gabor component is shown.

Figure 3.27: The points with the highest Gaussian curvature estimated using derivatives of Gaussians (left) and quaternionic Gabor filters (middle). The right image shows the original image together with one component of the used filters.

Comment on the Rotational Degree of Freedom of Gabor Filters

The convolution of an image with the derivative of a Gaussian function has the same effect as first convolving the image with the original Gaussian function and afterwards differentiating the blurred image. As shown above the derivative of a Gaussian can well be approximated by Gabor functions. In this approximation quaternionic Gabor filters are related to 2D Cartesian differential operators while complex Gabor filters are in analogy to 2D directional derivatives.

In this sense for complex Gabor filters as for directional derivatives the rotation is a natural degree of freedom, while for quaternionic Gabor filters it is not.

3.3 Summary

In this chapter we were able to show that the concepts of instantaneous phase and local phase, which play an important role in signal processing and analysis, can be generalized in the case of two-dimensional signals by methods derived from the quaternionic Fourier transform.

In one-dimensional signal processing the instantaneous phase of a real signal is defined as the angular phase of its complex-valued analytic signal. There have occurred several different approaches to a definition of an analytic signal of higher-dimensional signals. We have reviewed these approaches and have proposed a new definition which is based on the quaternionic Fourier transform. Our definition is closely related to Hahn's approach [48], which is the most recent of the existing approaches. Hahn's approach is based on the idea of the analytic signal having a single quadrant spectrum. Therefore the definition suffers from the fact that the original signal cannot be extracted from its analytic signal. We have shown that this drawback can be overcome by replacing the complex Fourier transform by the quaternionic Fourier transform.

The quaternionic analytic signal allows the definition of the quaternionic instantaneous phase of a real signal. Here the definition of the angular phase of a unit quaternion, newly introduced in chapter 2, has been used. As in one-dimensional signal processing it is often desirable in image processing to evaluate the local phase instead of the instantaneous phase. In contrast to the instantaneous phase, the local phase at a certain position is evaluated merely on the basis of a local neighborhood of the location of interest. From the different filters which can be used for estimating the local phase we choose Gabor filters. Following the ideas developed in chapter 2 we were able to replace two-dimensional complex Gabor filters by quaternionic Gabor filters. The local quaternionic phase has been defined as the angular phase of the quaternionic Gabor filter response to an image.

The relation between the local phase and the local signal structure, which is well established and widely used for simple (i.e. intrinsically one-dimensional) signals and their local complex phase, has been extended to a relation between the local quaternionic phase and intrinsically 2D signal structures. Here, the newly defined quaternionic phase, consisting of a triple of real numbers instead of only one number as the complex phase, provides a new tool.

Furthermore, it has been shown that the quaternionic Gabor filters are simultaneously optimally localized in the spatial and in the frequency domain according to the two-dimensional extension of the uncertainty principle of communication theory. Finally, we have demonstrated that quaternionic Gabor filters provide a good approximation to mixed partial derivatives of the Gaussian function.

Chapter 4

Applications

In this chapter we will demonstrate how quaternionic Gabor filters and the quaternionic phase can be used in applications. The first problem we address is *phase-based disparity estimation*, the second is *texture segmentation*. For both problems many approaches using complex Gabor filters exist in the literature; the quaternionic approaches demonstrated here are mainly extensions of known methods. However, in both applications completely new features emerge from the use of quaternionic filters.

In the following we will introduce the notation used in this chapter. The next two sections are devoted to disparity estimation (section 4.2) and texture segmentation (section 4.3). The results shown in this chapter are meant to sketch the possible use and the meaning of the theory developed so far. We do not claim to have built complete systems, and so many improvements are certainly possible.

4.1 Notation

Throughout this chapter we will use the following notation. As defined in section 3.2.3 the impulse response of a quaternionic Gabor filter h^q is given as

$$\begin{aligned} h^q(\mathbf{x}; \mathbf{u}_0, \sigma, \epsilon) &= g(\mathbf{x}, \sigma, \epsilon) \exp(i 2\pi u_0 x) \exp(j 2\pi v_0 y) && (4.1) \\ &= (h^q_{ee} + i h^q_{oe} + j h^q_{eo} + k h^q_{oo})(\mathbf{x}; \mathbf{u}_0, \sigma, \epsilon), && (4.2) \end{aligned}$$

with

$$g(x, y) = \frac{\epsilon}{2\pi\sigma^2} \exp\left(-\frac{x^2 + (\epsilon y)^2}{\sigma^2}\right).$$

When talking about this impulse response, often we simply call it a quaternionic Gabor filter in the following. Note that according to this definition the filter components h^q_{ee}, h^q_{oe}, h^q_{eo}, and h^q_{oo} are defined to be *real-valued* functions. Most of the time the parameters $\mathbf{u}$, σ and ϵ will not be written explicitly, but will be given in the text when necessary. Thus, a quaternionic Gabor filter will in general be denoted by $h^q(\mathbf{x})$.

The two complex Gabor filters contained in each QGF (see section 3.2.5.2) are denoted by $h^+ = (h^q_{ee} - h^q_{oo}) + i(h^q_{oe} + h^q_{eo})$ and $h^- = (h^q_{ee} + h^q_{oo}) + i(h^q_{oe} - h^q_{eo})$. The reason for this notation is that the argument of the modulating factor is $\exp(i2\pi(ux+vy))$ for h^+ and $\exp(i2\pi(ux-vy))$ for h^-. The components of these filters are shown in figure 4.1.

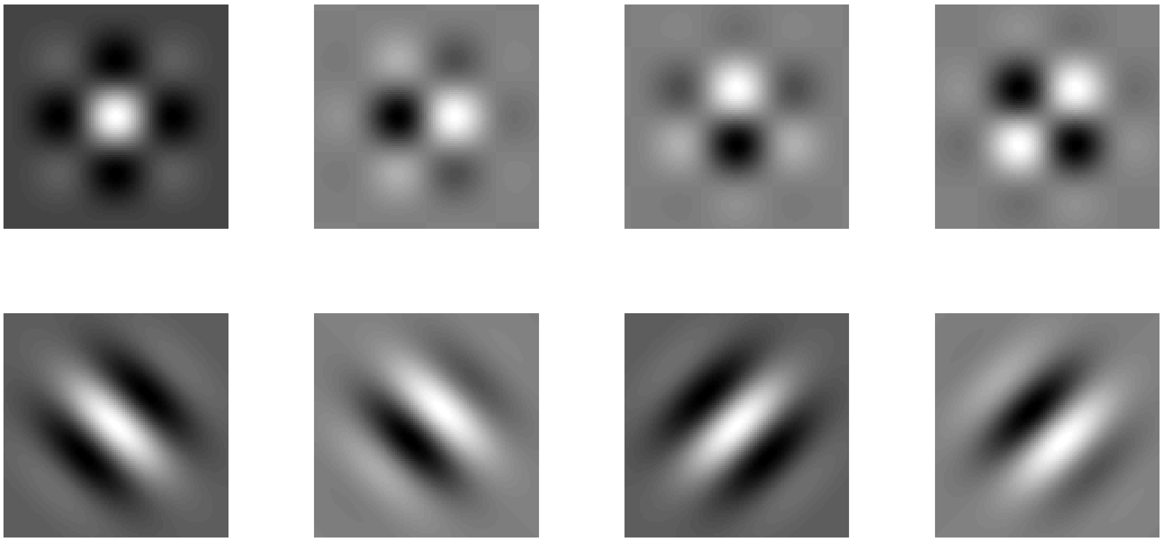

Figure 4.1: Top: The impulse response of a quaternionic Gabor filter. From left to right: h^q_{ee}, h^q_{oe}, h^q_{eo} and h^q_{oo}. Bottom: The corresponding complex Gabor filters: From left to right h^+_e, h^+_o, h^-_e and h^-_o.

Given an image f, the filter response of the quaternionic Gabor filter is denoted as $k^q(\mathbf{x}) = (f * h^q)(\mathbf{x})$. The analogous notation is used for all the components and combinations of the impulse response, i.e. $k^q_{eo}(\mathbf{x}) = (f * h^q_{eo})(\mathbf{x})$ and $k^+(\mathbf{x}) = (f * h^+)(\mathbf{x})$, and so on.

4.2 Disparity Estimation

4.2.1 The Problem

The following problem will be attacked: Given two images f_1 and f_2 differing by a local displacement (i.e. $f_1(\mathbf{x}) = f_2(\mathbf{x}+\mathbf{d}(\mathbf{x}))$) extract the vector field $\mathbf{d}$. This problem is called *disparity estimation* , and $\mathbf{d}$ is called the *displacement vector field* or *disparity field*. In components the disparity field will be written as $\mathbf{d} = (d_x, d_y)^\top$ where the indices indicate *horizontal* and *vertical* disparity.

In practice constraints have to be imposed on the input images in order for this problem to have a solution. Firstly, the range of $\mathbf{d}$ should be small compared to the domain of f_1 and f_2. Otherwise, structures visible in f_1 would lie outside the domain of f_2, i.e. f_1 and f_2 would have no visible relation to each other. In case f_1 and f_2 are images taken by a camera the constraint means that both images should represent the same scene, while $\mathbf{d}$ is due to different viewing conditions.

Another constraint on the solubility is imposed by the occurrence of intrinsically one-dimensional structures. A displacement along such a structure is locally not perceivable. In this case only the component of the displacement field perpendicular to the one-dimensional structure can locally be extracted from the images if no a priori information is available. This problem is called the *aperture problem*.

In practical applications the two images can be two consecutive frames of an image sequence, i.e. $f_1(\mathbf{x}) = f(\mathbf{x}, t_1)$ and $f_2(\mathbf{x}) = f(\mathbf{x}, t_2)$. In this case, some time interval $\Delta t = t_2 - t_1$ lies between the times when f_1 and f_2 are taken and the solution $\mathbf{d}$ can be written as $\mathbf{d} = \mathbf{v}\Delta t$ where $\mathbf{v}$ is called *image velocity* field or *optical flow* field. The image velocity is related to – but not identical with – the *motion field*. The motion field is the 2D projection of the real motion occurring in the 3D scene, while the image velocity field describes variations in the gray value structure of the images. In what ways these two fields can differ is described e.g. in [57]. The image velocity field is the input of the *structure from motion* problem, which has the aim of finding the structure of the 3D scene from an image sequence. The notion of structure can have very different meanings: In [37, 38], Faugeras introduced the stratification of 3D vision and analyzed how much information is needed in order to find the projective, affine, or the Euclidean structure of the scene.

A similar problem occurs in the diagnosis of medical images where a useful technique is to subtract two (e.g. X-ray) images taken at different times in order to reveal some changes in the tissue [46, 96]. For this application it is crucial that the images be transformed in order to match exactly, since the camera and patient position vary from image to image [75].

A problem related to the above tasks is the matching of two images taken by a stereo camera. If the epipolar geometry is known, the disparity estimation can be reduced to a one-dimensional estimation problem where only the horizontal disparity has to be found. Similar to the structure from motion task, also here further processing of the disparity field can lead to a spatial depth map of the 3D scene.

The situations referred to above deal with pairs of natural images. However, this is not generally the case, since the *disparity estimation* problem is also soluble for synthetic images like random dot stereograms. Julesz [62] showed that random dot images differing by some displacement $\mathbf{d}$ lead to spatial depth information, perceivable by human observers.

4.2.2 Methods for Solving the Disparity Estimation Problem

One class of methods used for disparity estimation is the class of *feature-based* methods. In this approach one starts with the extraction of image features like edges, corners, maxima of local curvature and so on. Generally these features are sparse, which makes it possible to find the corresponding features in the two images by searching only a small number of possible candidates. Small number means here small compared to the number of pixels in the images. One disadvantage of feature-based approaches is that they yield a sparse disparity map, where the intermediate disparity values have to be interpolated.

Another approach are *region-based* methods. These methods extract a region from the first image and look for an optimally matching region in the second image. This is either done by maximizing the cross-correlation or by minimizing the sum of squared gray-value distances. These methods are also referred to as *block-matching* methods.

Another important class of disparity estimation methods are *phase-based* methods which shall be extended to quaternionic phase in the following section. For a review on the main methods for estimating stereo disparity see e.g. [51]. We will refrain from reviewing the main idea of complex phase-based disparity estimation, since it is subsumed by the quaternionic phase-based method which will be developed here in detail. However, in the final section a comparison with aspects of phase-based approaches found in the literature is drawn.

4.2.3 Quaternionic Phase-based Disparity Estimation

In section 2.2.1 we presented the shift theorem for the QFT:

$$f(x,y) \quad \circ\!\!\stackrel{\mathbb{H}}{-\!\!-\!\!-}\!\!\bullet \quad F^q(u,v) \tag{4.3}$$

$$\Longrightarrow \quad f(x+d_1, y+d_2) \quad \circ\!\!\stackrel{\mathbb{H}}{-\!\!-\!\!-}\!\!\bullet \quad \exp(i2\pi u d_1) F^q(u,v)\exp(j2\pi v d_2). \tag{4.4}$$

Knowing the phase of the original spectrum $(\phi_1, \theta_1, \psi_1)$ and that of the translated spectrum $(\phi_2, \theta_2, \psi_2)$ the global image shift can be evaluated as $d_x = \frac{\phi_1-\phi_2}{2\pi u}$ and $d_y = \frac{\theta_1-\theta_2}{2\pi v}$ [18]. From the range of the quaternionic phase it follows that d_x and d_y can be identified within an interval of length $\frac{1}{u}$ and $\frac{1}{2v}$ respectively. We always set d_x and d_y to the smallest possible translation, i.e. $d_x \in [-\frac{1}{2u}, \frac{1}{2u}[$ and $d_y \in [-\frac{1}{4v}, \frac{1}{4v}[$.

Using the QFT approach only global translations can be estimated. However, in general the disparity will vary from point to point. Therefore, we modify the quaternionic phase approach by replacing the QFT-phase by the local quaternionic phase as defined in section 3.2.4.3. The local phase approach to disparity estimation starts with the assumption that two given images f_1 and f_2 are related by

$$f_1(\mathbf{x}) = f_2(\mathbf{x} + \mathbf{d}(\mathbf{x})),$$

where $\mathbf{d}(\mathbf{x})$ is the desired displacement field. Assuming that the phase is varying linearly, the displacement $\mathbf{d}(\mathbf{x})$ is given by

$$d_x(\mathbf{x}) = \frac{\phi_2(\mathbf{x}) - \phi_1(\mathbf{x}) + n(2\pi + k)}{2\pi u_{ref}}, \qquad d_y(\mathbf{x}) = \frac{\theta_2(\mathbf{x}) - \theta_1(\mathbf{x}) + m\pi}{2\pi v_{ref}}, \tag{4.5}$$

with some reference frequencies (u_{ref}, v_{ref}) which are not known a priori. Here $\phi(\mathbf{x})$ and $\theta(\mathbf{x})$ are the first two local quaternionic phase components measured by a quaternionic Gabor filter. Furthermore, $n, m \in \mathbb{Z}$ are chosen such that d_x and d_y take values in the admitted range. Depending on m, k is defined as

$$k = \begin{cases} 0, & \text{if } m \text{ is even.} \\ 1, & \text{if } m \text{ is odd.} \end{cases}$$

Some choice has to be made on the values of the reference frequencies (u_{ref}, v_{ref}) in order to estimate the disparity. The goodness of the approximation of $\mathbf{d}$ depends strongly on the choice of the reference frequencies u_{ref} and v_{ref}. There are two main approaches for choosing the frequencies. The first is the so-called *constant model* where u_{ref} and v_{ref} are chosen to be the center frequencies of the applied QGF. For the complex case the constant model has been used e.g. by Maki et al. [77] and Sanger [84]. The second is the *local model*. Based on the main assumption that the local phase at corresponding points of the two images will take the same value $\boldsymbol{\phi}_1(\mathbf{x}) = \boldsymbol{\phi}_2(\mathbf{x} + \mathbf{d})$, an estimate for $\mathbf{d}$ is obtained by approximating $\boldsymbol{\phi}_2$ by a first-order Taylor development about $\mathbf{x}$:

$$\boldsymbol{\phi}_2(\mathbf{x} + \mathbf{d}) \approx \boldsymbol{\phi}_2(\mathbf{x}) + (\mathbf{d} \cdot \nabla)\boldsymbol{\phi}_2(\mathbf{x}). \tag{4.6}$$

Here we used the notation $\boldsymbol{\phi} = (\phi, \theta)$. Solving (4.6) for $\mathbf{d}$ yields the disparity estimate in the local model. In our experiments we use the additional assumption that ϕ merely varies along the x-direction and θ only along the y-direction. Using this assumption we estimate the disparity by (4.5) with the reference frequencies:

$$u_{\mathrm{ref}} = \frac{1}{2\pi}\frac{\partial \phi_1}{\partial x}(\mathbf{x}), \qquad v_{\mathrm{ref}} = \frac{1}{2\pi}\frac{\partial \theta_1}{\partial y}(\mathbf{x}).$$

At locations where u_{ref} or v_{ref} equals zero (4.5) is not defined. These locations will be excluded from the evaluation by a confidence mask that we introduce later in this chapter.

In the complex case the local model has been used by Fleet et al. [42] and Langley et al. [74]. The complex phase methods using the local model can be refined by taking the mean between the derivatives of the phases in the first and the second image [61], or the weighted mean of the derivatives where the weight is the energy of the filter response in the first and the second image [74]. These refinements can also be applied in the quaternionic case. Using quaternionic Gabor filters is computationally efficient since the filter masks are separable.

4.2.4 Experiments on Synthetic Data

The first experiments were performed on synthetic images. In [52], Hansen used sinusoidal signals for testing a phase-based method for one-dimensional disparity estimation. We use the two-dimensional analogue to these, i.e. sinusoidals of the form $\cos(2\pi u x)\cos(2\pi v y)$. In figure 4.2 a pair of images is shown where the left image is the original image with the parameters $u = \frac{1}{60}$ pixels^{-1} and $v = \frac{1}{40}$ pixels^{-1}. The second image results from the first one by an affine coordinate transformation $\mathbf{x}' = A\mathbf{x} + \mathbf{b}$ with $A_1 = \begin{pmatrix} 1.03 & 0.1 \\ -0.05 & 1 \end{pmatrix}$ and $\mathbf{b}_1 = (4.15, \quad 1.38)^\top$ pixels. In the first experiment we use the constant model and choose as central frequencies of the applied quaternionic Gabor filters the same frequencies as the ones of the sinusoidal structure of the left test-image. In figure 4.3 the true disparity between the test-images is shown. For simplicity we show the horizontal and the vertical disparity in two separate plots. In the bottom row of figure 4.3 the error of the

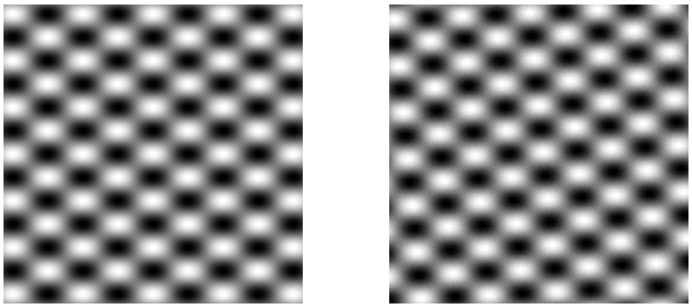

Figure 4.2: Two synthetic images. The second is a distorted version of the first one, where the distortion is the result of the affine transformation $(A_1, \mathbf{b}_1)$.

estimated disparity is shown. The error given in pixels is far below one, i.e. we achieve sub-pixel accuracy, which is a typical property of phase-based approaches to disparity estimation. As shown in figures 4.4 and 4.5 where noise up to an SNR of $0\,\mathrm{dB}$ is added the method is stable under the influence of noise.

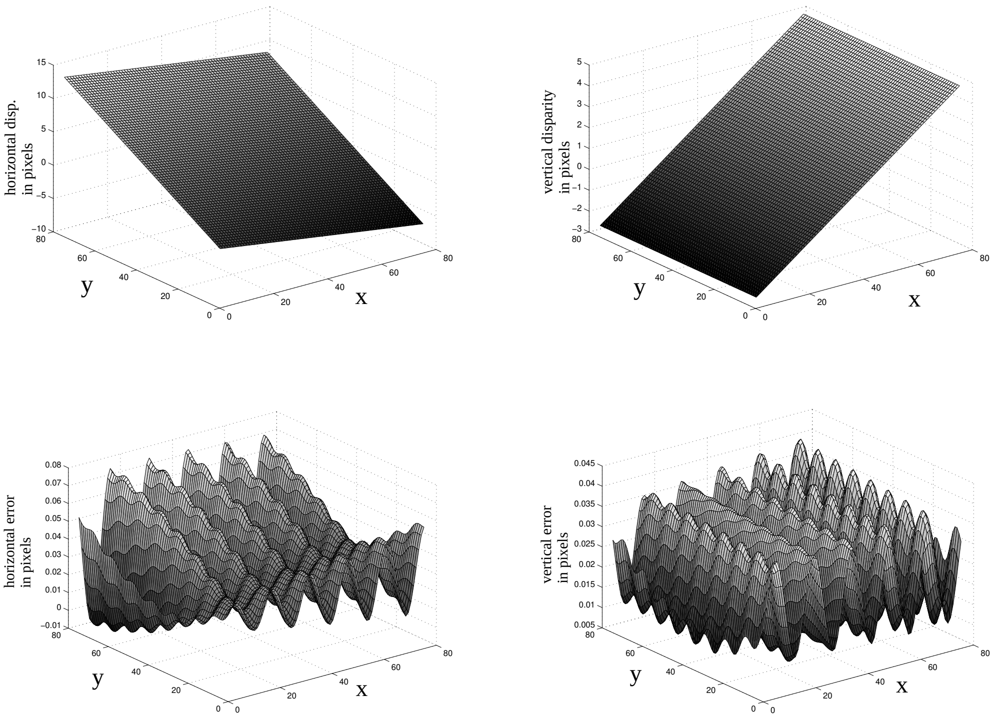

Figure 4.3: Top: The true disparity (horizontal (left) and vertical (right)) corresponding to the images in figure 4.2. Bottom: The error of the measurement in the horizontal (left) and the vertical direction (right).

However, the results of the constant model are extremely sensitive to the central frequencies of the applied filters. The reason is that, if the images contain periodic

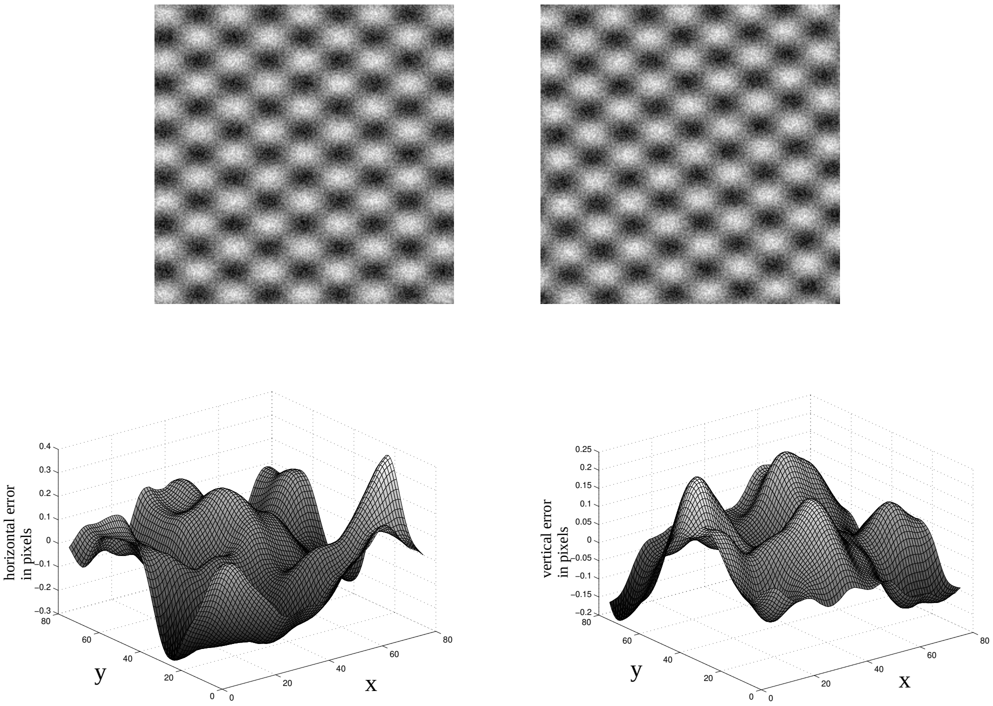

Figure 4.4: Top: The same images as in figure 4.2 but with zero-mean noise (SNR= 3). Bottom: The error of the measurement in the horizontal (left) and the vertical distortion (right).

structures, the filter responses vary with the spatial frequency of this structure and not with the central frequency of the Gabor filter. However, in the constant model the reference frequency is equal to the central frequency of the Gabor filter. Thus, the results are only reliable if the Gabor filter is exactly tuned to the frequency of the periodic image structure. An analytic investigation on the properties of the constant and the local model applied to periodic structures and the a step edge can be found in [51].

Figure 4.6 shows another pair of test-images with $u = \frac{1}{10}$ pixels^{-1}, $v = \frac{1}{10}$ pixels^{-1} $A_2 = \begin{pmatrix} 0.95 & 0.01 \\ -0.03 & 1.01 \end{pmatrix}$ and $b_2 = (0.3,\ 0.4)^\top$. In figure 4.7 the errors of the estimated disparities are shown for different central frequencies of the QGFs. Since the constant model uses as a frequency of reference the central frequencies of the QGFs, while the change of local phase depends mainly of the frequency of the investigated structure, there occur errors of up to 50% which make this model useless for application to periodic sinusoidal structures.

In order to overcome this weakness we replaced the constant model by the local model. This model uses as reference frequency the rate of change of the local phase

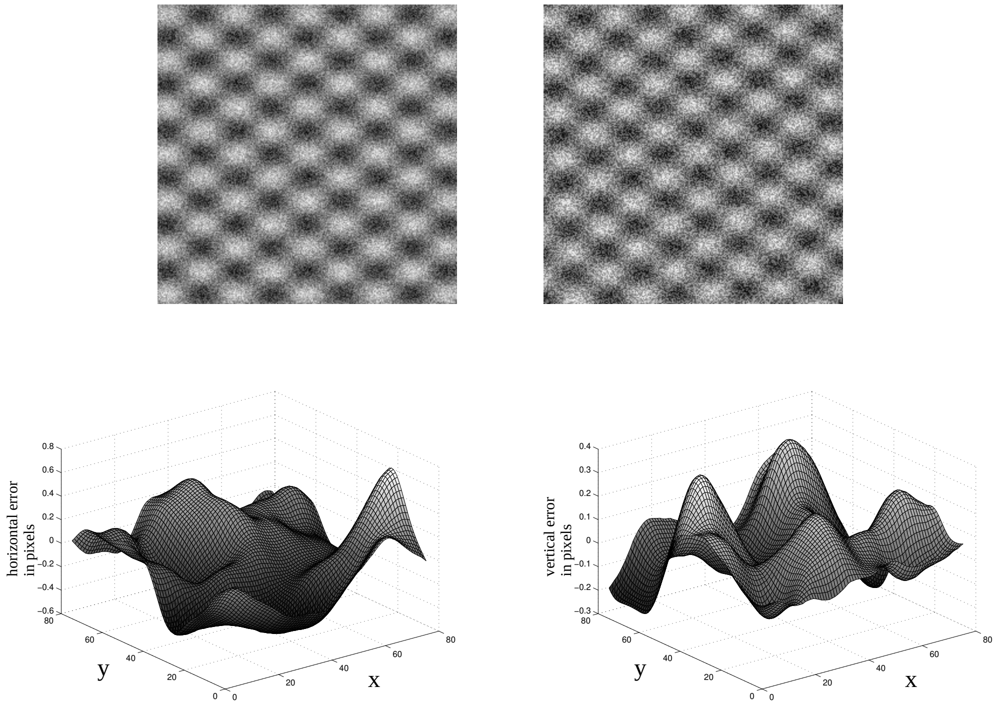

Figure 4.5: Top: The same images as in figure 4.2 but with zero-mean noise (SNR= 0). Bottom: The error of the measurement in the horizontal (left) and the vertical distortion (right).

as estimated by the QGFs. A well known problem in the calculation of the rate of change are the discontinuities of the local phase [30]. This makes it impossible to use a simple finite difference method, which estimates the derivative at a certain point as the difference of the values at two neighbored points. We use here a method that has been employed by Bovik [11] for the evaluation of the rate of change of the local phase as measured with a complex Gabor filter.

From (2.40) we know that the ϕ- and θ-components of the local quaternionic phase of an image f are given (up to a possible $\pm\pi$-correction of ϕ) almost everywhere by

$$\phi(\mathbf{x}) = \mathrm{atan2}(n_\phi(\mathbf{x}), d_\phi(\mathbf{x}))/2 \tag{4.7}$$
$$\theta(\mathbf{x}) = \mathrm{atan2}(n_\theta(\mathbf{x}), d_\theta(\mathbf{x}))/2, \tag{4.8}$$

where we introduced the functions

$$n_\phi(\mathbf{x}) = -2(k^q_{eo}(\mathbf{x})k^q_{oo}(\mathbf{x}) + k^q_{ee}(\mathbf{x})k^q_{oe}(\mathbf{x})) \tag{4.9}$$
$$d_\phi(\mathbf{x}) = (k^q_{ee}(\mathbf{x}))^2 - (k^q_{oe}(\mathbf{x}))^2 + (k^q_{eo}(\mathbf{x}))^2 - (k^q_{oo}(\mathbf{x}))^2 \tag{4.10}$$
$$n_\theta(\mathbf{x}) = -2(k^q_{oe}(\mathbf{x})k^q_{oo}(\mathbf{x}) + k^q_{ee}(\mathbf{x})k^q_{eo}(\mathbf{x})) \tag{4.11}$$
$$d_\theta(\mathbf{x}) = (k^q_{ee}(\mathbf{x}))^2 + (k^q_{oe}(\mathbf{x}))^2 - (k^q_{eo}(\mathbf{x}))^2 - (k^q_{oo}(\mathbf{x}))^2. \tag{4.12}$$

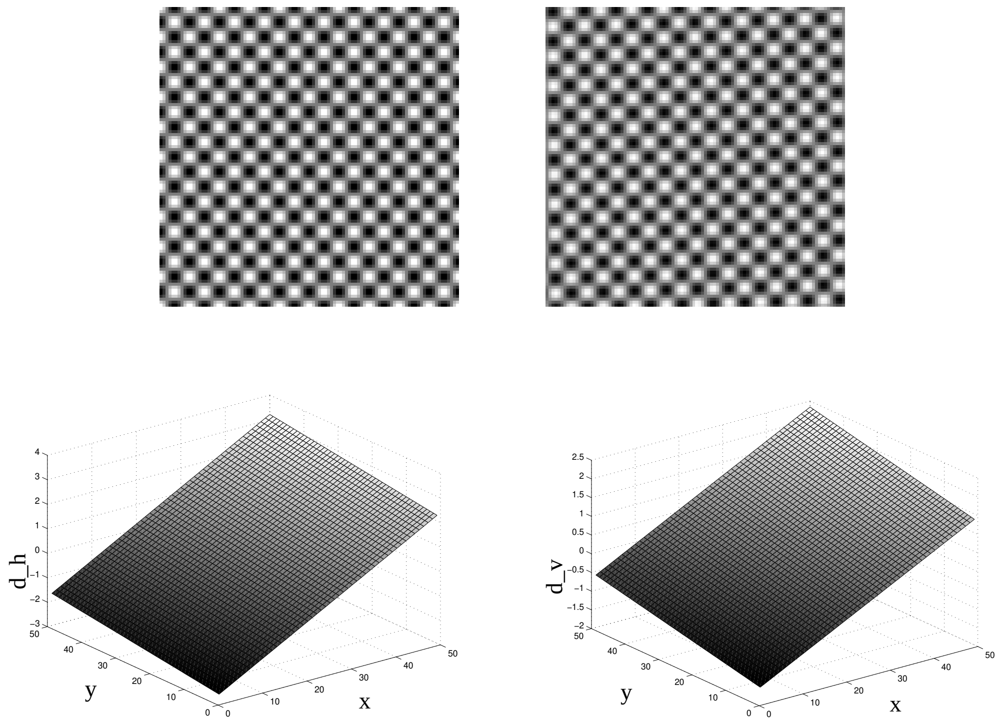

Figure 4.6: Top: Two synthetic images. The second is a distorted version of the first one, where the distortion is the result of the affine transform $(A_2, \mathbf{b}_2)$. Bottom: the true horizontal (left) and vertical (right) disparity.

The k-functions are the responses of a component of the quaternionic Gabor filter to the image, e.g. $k_{ee}(\mathbf{x}) = (h^q_{ee} * f)(\mathbf{x})$ and $k_{oe}(\mathbf{x}) = (h^q_{oe} * f)(\mathbf{x})$. From (4.7) and (4.8) the derivatives of the phase-components are found to be

$$\frac{\partial}{\partial x}\phi(\mathbf{x}) = \frac{d_\phi(\mathbf{x})\frac{\partial}{\partial x}n_\phi(\mathbf{x}) - n_\phi(\mathbf{x})\frac{\partial}{\partial x}d_\phi(\mathbf{x})}{n^2_\phi(\mathbf{x}) + d^2_\phi(\mathbf{x})} \tag{4.13}$$

$$\frac{\partial}{\partial y}\theta(\mathbf{x}) = \frac{d_\theta(\mathbf{x})\frac{\partial}{\partial y}n_\theta(\mathbf{x}) - n_\theta(\mathbf{x})\frac{\partial}{\partial y}d_\theta(\mathbf{x})}{n^2_\theta(\mathbf{x}) + d^2_\theta(\mathbf{x})}. \tag{4.14}$$

The derivatives of the functions n_ϕ, d_ϕ, n_ϕ and n_θ can be evaluated analytically. In the resulting expressions derivatives of the k-functions will occur. For differentiating these functions the following simple trick is applied: the derivation of the convolution of the image with the quaternionic Gabor filter is performed by first differentiating analytically the quaternionic Gabor filter and convolving the result with the image.

$$\frac{\partial}{\partial x}k^q(\mathbf{x}) = \frac{\partial}{\partial x}(h^q * f)(\mathbf{x}) = \left(\left(\frac{\partial}{\partial x}h^q\right) * f\right)(\mathbf{x}). \tag{4.15}$$

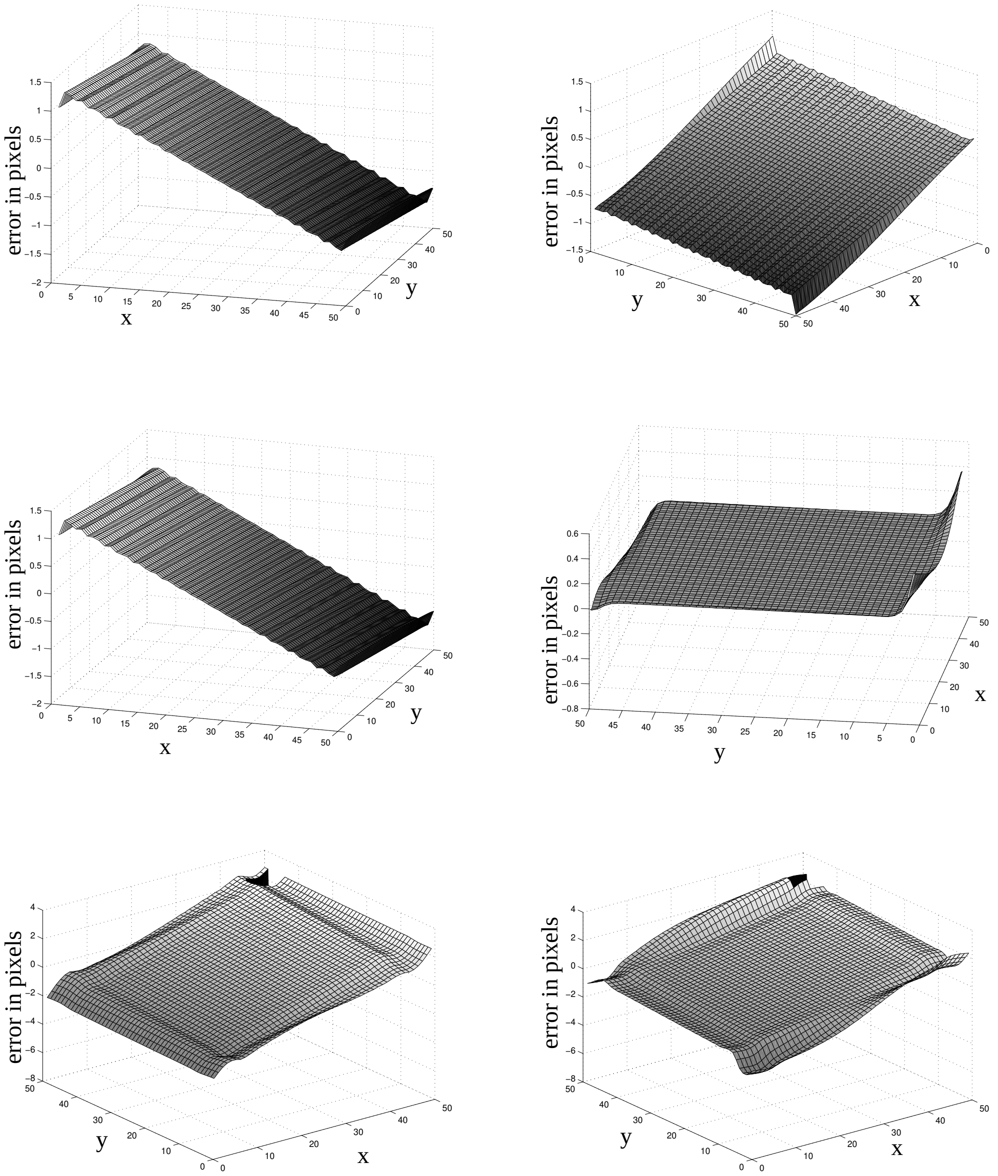

Figure 4.7: The errors of the estimated disparities (left: horizontal disparity, right: vertical disparity) between the two images in figure 4.6 using the constant model. From top to bottom the central frequencies of the applied QGFs are: $u = v = \frac{1}{5}$ (top), $u = \frac{1}{5}$, $v = \frac{1}{10}$ (middle) and $u = v = \frac{1}{20}$ (bottom).

Following this procedure we circumvent the unwrapping problem that can otherwise lead to considerable difficulties in estimating the local frequency from the local phase. The results of replacing the constant model by the local model, i.e. of setting the reference frequencies to $u_{\mathrm{ref}} = \frac{1}{2\pi}\frac{\partial}{\partial x}\phi(\mathbf{x})$ and $v_{\mathrm{ref}} = \frac{1}{2\pi}\frac{\partial}{\partial y}\theta(\mathbf{x})$ are shown in figure 4.8. Obviously the results of using the local model are much better when periodic image structures are considered. In our experiments the maximal error in the components of the disparity vectors is about 0.4 of a pixels. These results are in agreement with Hansen's results [51].

4.2.5 A Confidence Measure

In phase based disparity estimation, situations in which the phase estimate is not reliable are very probable to occur. In the case of the complex Gabor phase this is always the case when the energy of the filter response is small. In regions of the filtered image where this is the case, the local phase does not generally vary monotonically, such that in singular points the local frequency will be zero. This makes the estimation of the local disparity impossible, since the disparity equals the phase difference divided by the local frequency.

From the above considerations it becomes clear that it is desirable to have a confidence measure that indicates how reliable the estimated disparity is. By thresholding the confidence map, a binary mask is obtained that indicates in which parts of the image disparity estimation is possible or impossible. In the classic complex case such a measure will usually be based on the energy of the filter response (see Hansen [51] for a comparison of different confidence measures).

In the quaternionic case we will need two confidence measures, one for the reliability of the ϕ-component of the quaternionic phase and one for its θ-component. Interestingly, it will turn out that these two measures are identical. From (2.40) we know that the first two quaternionic phase components are defined almost everywhere via

$$\phi(\mathbf{x}) = \mathrm{arg}_i(k^q(\mathbf{x})\beta(\bar{k}^q(\mathbf{x}))), \quad \theta(\mathbf{x}) = \mathrm{arg}_j(\alpha(\bar{k}^q(\mathbf{x}))k^q(\mathbf{x})).$$

The functions arg_i and arg_j select one complex subfield from the given quaternion and return the phase-angle of the corresponding complex number. We introduce three new functions which evaluate the magnitude of these complex numbers.

Definition 4.1 *Let $q = a + bi + cj + dk$ be a quaternion. Then the partial moduli of q are defined to be*

$$\mathrm{mod}_i(q) = \sqrt{a^2 + b^2}, \quad \mathrm{mod}_j(q) = \sqrt{a^2 + c^2}, \quad \textit{and} \quad \mathrm{mod}_k(q) = \sqrt{a^2 + d^2}.$$

Thus, $\mathrm{mod}_i(q)\exp(i\,\mathrm{arg}_i(q)) = a + bi$ is the projection of q onto the first complex subfield in polar representation. Analogously the projections onto the other two complex subfield components are given.

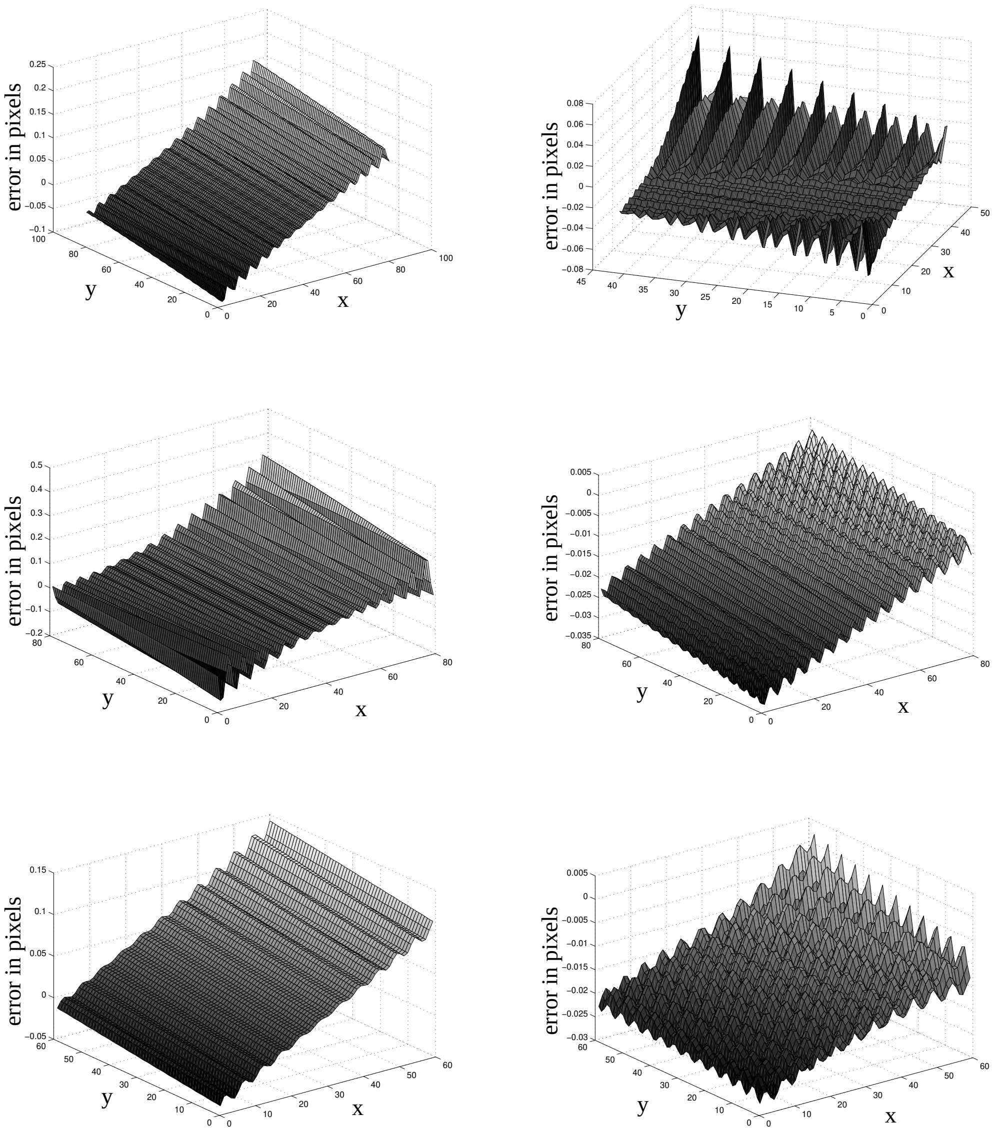

Figure 4.8: The errors of the estimated disparities (left: horizontal disparity, right: vertical disparity) between the two images in figure 4.6 using the local model. From top to bottom the central frequencies of the applied QGFs are: $u = v = \frac{1}{5}$ (top), $u = \frac{1}{5}, v = \frac{1}{10}$ (middle) and $u = v = \frac{1}{20}$ (bottom).

Given this definition it is possible to adapt the confidence measures known for complex filters. One approach is to construct a binary confidence map by thresholding the energy of the filter response [51]. Thus, the measure is given by

$$\mathrm{Conf}(\mathbf{x}) = \begin{cases} 1 & \text{if } |k(\mathbf{x})| > \tau \\ 0 & \text{else.} \end{cases}$$

The analogue of this in the quaternionic case is

$$C_h(k^q(\mathbf{x})) = \begin{cases} 1 & \text{if } \mathrm{mod}_i(k^q(\mathbf{x})\beta(\bar{k}^q(\mathbf{x}))) > \tau \\ 0 & \text{else.} \end{cases} \tag{4.16}$$

$$C_v(k^q(\mathbf{x})) = \begin{cases} 1 & \text{if } \mathrm{mod}_j(\alpha(\bar{k}^q(\mathbf{x}))k^q(\mathbf{x})) > \tau \\ 0 & \text{else.} \end{cases} \tag{4.17}$$

We will use the following confidence measure:

Definition 4.2 *Given the quaternionic Gabor filter responses k_1^q and k_2^q of two images f_1 and f_2 the binary confidence map is given by*

$$\mathrm{Conf}_h(\mathbf{x}) = C_h(k_1^q(\mathbf{x}))C_h(k_2^q(\mathbf{x})) \tag{4.18}$$

$$\mathrm{Conf}_v(\mathbf{x}) = C_v(k_1^q(\mathbf{x}))C_v(k_2^q(\mathbf{x})). \tag{4.19}$$

Here, Conf_h and Conf_v are the confidence measures for the horizontal and the vertical disparity, respectively.

However, it is not necessary to use both of these measures, since they turn out to be identical. In fact, the following general theorem holds.

Theorem 4.1 *The identity*

$$\mathrm{mod}_i(q\beta(\bar{q})) = \mathrm{mod}_j(\alpha(\bar{q})q)$$

holds for any quaternion q.

Proof: The theorem can be verified by direct computation of both sides of the equation and component-wise comparison. □

Corollary 4.1 *For the quaternionic Gabor filter responses k_1^q and k_2^q to any two images the horizontal and vertical confidence measures as defined by (4.18) and (4.19) are identical:*

$$\mathrm{Conf}_h(\mathbf{x}) = \mathrm{Conf}_v(\mathbf{x}).$$

Proof: From theorem 4.1 it follows that the two functions defined in (4.16) and (4.17) are identical. Using this fact in definition 4.2 proves the corollary. □

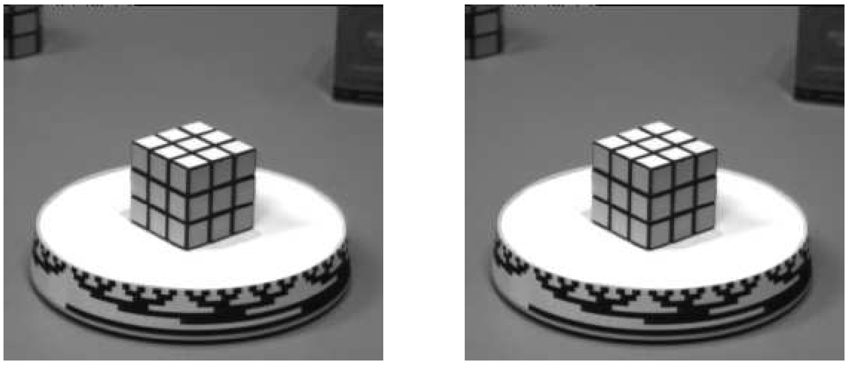

Figure 4.9: The first two frames of the Rubik cube sequence.

4.2.6 Experiments on Real Data

We apply the method developed so far to two real image sequences, namely to the *Rubik cube sequence* and to the *diverging tree sequence* [2].

First, we use the first two frames of the *Rubik cube sequence*. The sequence shows a Rubik's cube on a rotating hub where the rotation is — when viewed from above — counterclockwise. The two frames, which were used for this experiment are shown in figure 4.9. There was no ground truth available for this sequence. However, since the motion is easy and well-defined by the rotation of the hub, it is possible to a certain extent to judge the displacement estimates by eye. The QGF parameters were $u = v = \frac{1}{10}$ as center frequencies, $c = 3$, and the size of the filter mask was 40×40 pixels. Figure 4.10 shows the estimated horizontal and vertical displacements as intensity images. The brightest value in the horizontal disparity image represents a displacement of $d_x \approx 1.5$ pixels which can be confirmed by simple pixel counting over some frames of the sequence, since the rotation of the object in the scene is uniform. The displacement vectors obtained from the combination of the horizontal and vertical displacement are presented in figure 4.11. For better visibility, not the whole image, but two sub-sampled regions are shown, one containing the upper part of the cube and the other containing the lower part of the hub. These are the two regions with the highest confidence.

4.2.7 Diagonal Disparity Information

In this section we will only deal with QGFs with aspect ratio $\epsilon = 1$ and identical horizontal and vertical central frequencies $u = v$.

Given a QGF h^q with central frequencies u and v, the corresponding complex Ga-

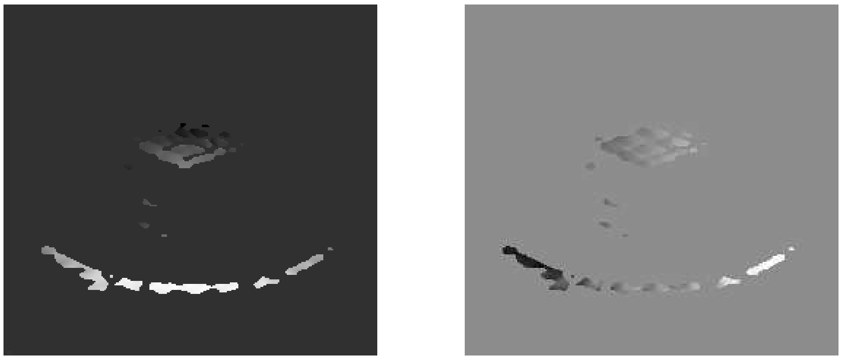

Figure 4.10: The estimates for the horizontal (right) and the vertical (left) displacement as intensity images.

bor filters h^+ and h^- as defined at the beginning of this chapter will both have the central frequency $f = \sqrt{u^2+v^2}$ and spatial orientation $\alpha = \tan^{-1}(\pm v/u)$. For $u = v$ this reduces to $f = \sqrt{2}u$ and $\alpha = \pm 45°$. Since the phase-based disparity estimation method is well known for complex Gabor phase, we can apply this method in order to estimate the local displacement along the diagonals of the image. This can lead to additional disparity estimates because at some points the reliability of the diagonal estimates may be higher, while at other points the reliability of the estimates along the axes is better than the diagonal one. The two local complex phases that can be derived from the quaternionic Gabor filter response are defined as

$$\phi^+(\mathbf{x}) = \mathrm{atan2}(\mathcal{I}(h^+(\mathbf{x})), \mathcal{R}(h^+(\mathbf{x}))) \quad (4.20)$$
$$\phi^-(\mathbf{x}) = \mathrm{atan2}(\mathcal{I}(h^-(\mathbf{x})), \mathcal{R}(h^-(\mathbf{x}))). \quad (4.21)$$

In analogy to (4.5) the disparity estimate is given by

$$d^+(\mathbf{x}) = \frac{\phi_2^+(\mathbf{x}) - \phi_1^+(\mathbf{x}) + 2\pi m}{2\pi u_{ref}^+} \quad (4.22)$$
$$d^-(\mathbf{x}) = \frac{\phi_2^-(\mathbf{x}) - \phi_1^-(\mathbf{x}) + 2\pi n}{2\pi u_{ref}^-}, \quad (4.23)$$

where m and n are chosen such that $\Delta\phi^+$ and $\Delta\phi^-$ both lie within the interval $[-\pi, \pi[$. The reference frequencies u_{ref}^+ and u_{ref}^- can again be chosen according to the constant model as $u_{ref}^+ = u_{ref}^- = \sqrt{2}u$ or according to the local model as

$$u_{ref}^+ = \frac{1}{\sqrt{2}}\begin{pmatrix} 1 \\ 1 \end{pmatrix} \cdot \nabla\phi^+(\mathbf{x}) \qquad \text{and} \qquad u_{ref}^- = \frac{1}{\sqrt{2}}\begin{pmatrix} 1 \\ 1 \end{pmatrix} \cdot \nabla\phi^-(\mathbf{x}). \quad (4.24)$$

In our experiments we restricted ourselves to the use of the local model. Again, the differentiation is performed analytically and the occurring derivatives of the

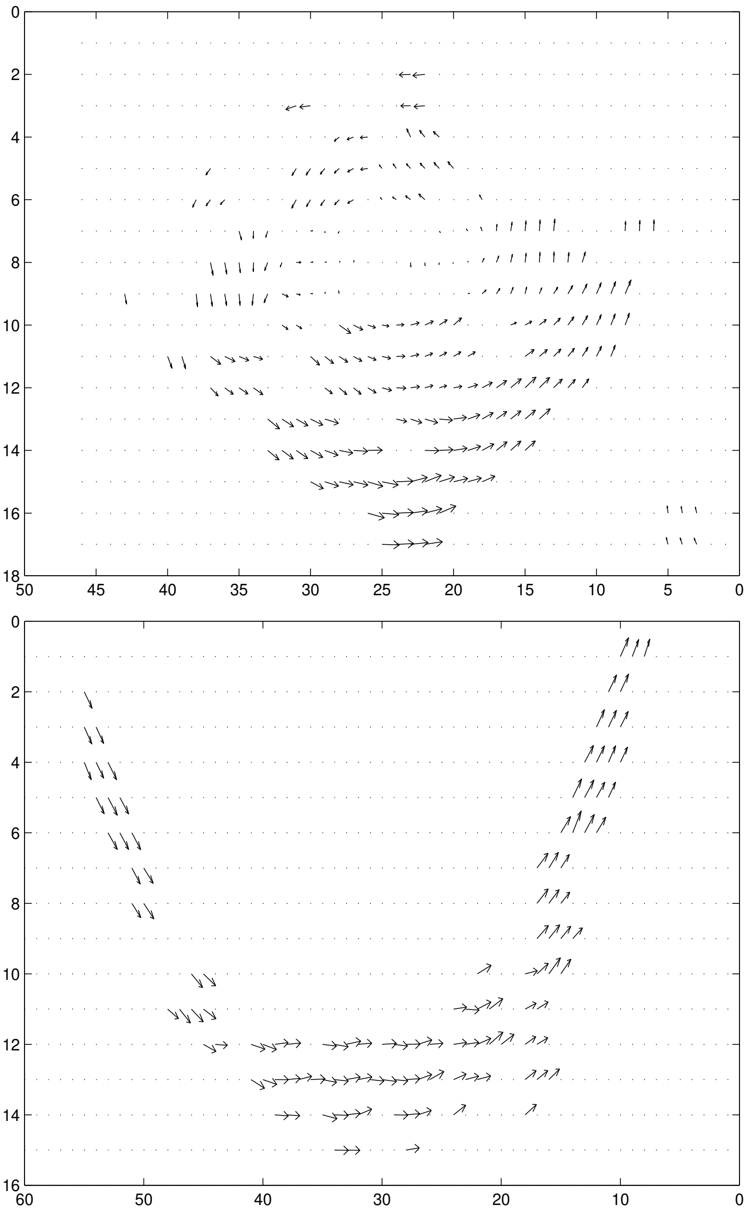

Figure 4.11: The estimates for the disparity vector field for the images in figure 4.9. For better visibility two subregions of the images are shown.

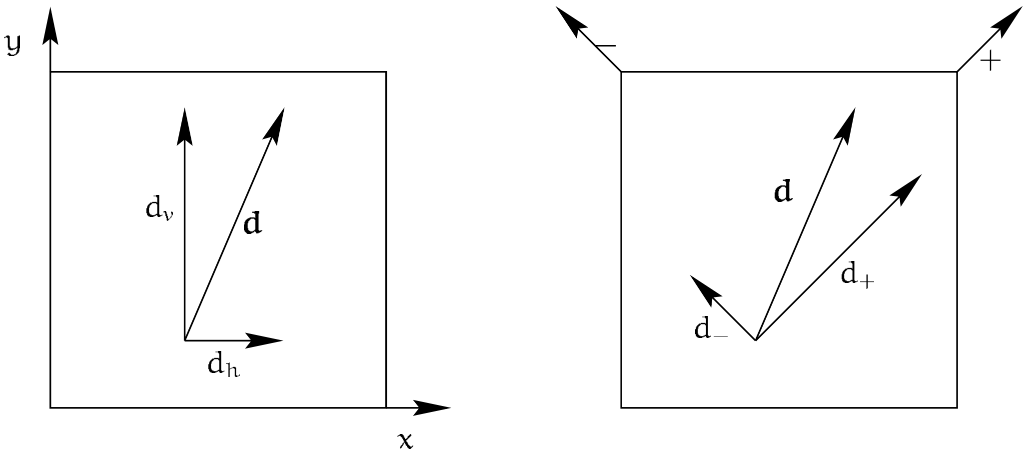

Figure 4.12: The decomposition of a displacement vector into horizontal and vertical component as measured by the quaternionic phase (left) and into the diagonal components as measured by the two complex phases ϕ^+ and ϕ^-.

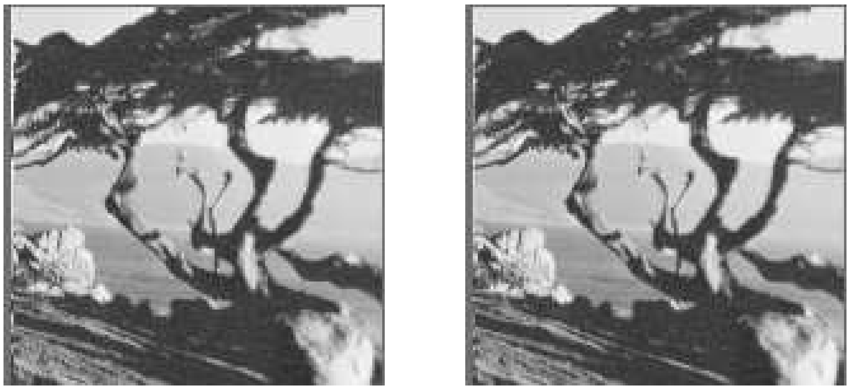

Figure 4.13: The first two frames of the tree-sequence.

filtered images are obtained as the filter response of the images to the differentiated QGFs. For clarification the decomposition of a displacement vector $\mathbf{d}$ into either horizontal and vertical or into diagonal components is sketched in figure 4.12.

It is an important fact that this additional disparity information is obtained without any additional convolution operations. The only additional operations that have to be performed are building the sums and differences of already existing filter responses and pointwise non-linear operations, actually magnitude and phase-evaluation.

As an example for the integration of local displacement information from the two methods we investigate the two frames of the tree-sequence shown in figure 4.13. The displacement field resulting only from the direct QFT-phase and the full displacement field integrating the results of both methods is shown in figure 4.14. The true displacement field of the diverging tree sequence is a radial vector field with all the vectors pointing from the center outwards. The magnitude of displacement is proportional to the distance from the center.

4.2.8 Comparison to Other Approaches and Discussion

In this section the main objective was to demonstrate how quaternionic Gabor filters and the quaternionic phase can be used for the estimation of the displacement field or image velocity field from two frames of an image sequence. It turned out that there are *two* sets of displacement information contained in the quaternionic Gabor representation of the images. The first displacement field is estimated from the ϕ- and θ-components of the local quaternionic phase which give the displacement in horizontal and vertical direction. The second way to calculate the displacement is from the two complex phases contained in the quaternionic representation. These two complex phases stem from the two complex Gabor filters which are contained in the QGF. These components evaluate the displacement in direction of the two image diagonals. From the diagonal displacement the displacement in (x, y)-coordinates is obtained by a simple coordinate change. Of course these two methods yield partly redundant information. However, there are regions where only either the one or the other of the two methods provides values with a high reliability. Integrating these two methods we obtain a denser image velocity field than can be obtained by either of the methods alone.

A main advantage of this method is that it is possible to obtain the displacement field at low computational cost. All the involved filter masks are separable, and so the convolution can be implemented very efficiently. Only six separable real convolutions are needed, including the convolutions with the differentiated QGFs for the local frequency estimation in the local model. All further computations are performed pointwise and have therefore a computational complexity of the order of the number of image pixels.

In [43], Fleet claims that phase-based disparity estimation is limited to the estimation of the component of the disparity vector normal to an oriented structure in the image. According to this view, the full 2D displacement field can only be combined from the local measurements by taking into account a larger support under the assumption of coherence of neighboring measurements. The main assumption in this claim is that the image is intrinsically one-dimensional nearly everywhere. However, even if a signal can locally well be approximated by an intrinsically one-dimensional signal there seems to be enough displacement information even along

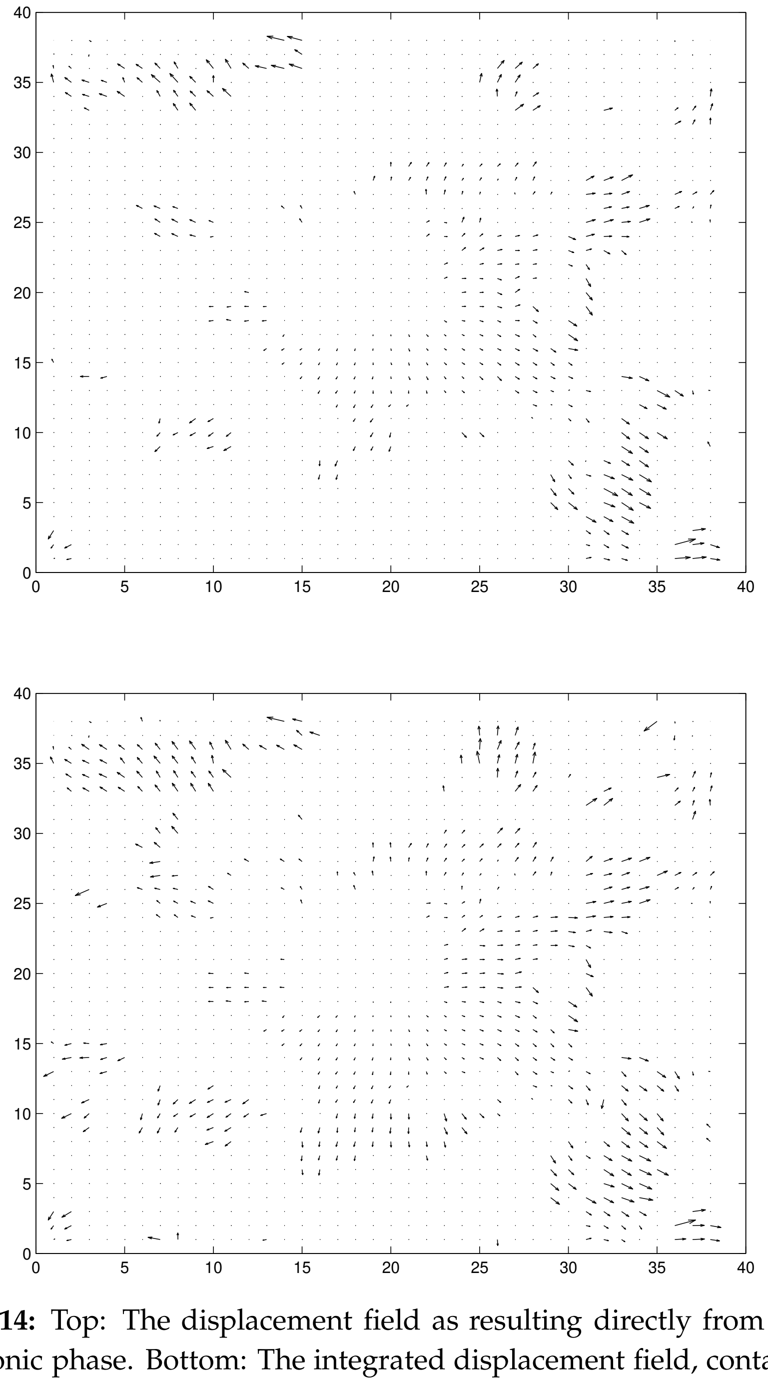

Figure 4.14: Top: The displacement field as resulting directly from the local quaternionic phase. Bottom: The integrated displacement field, containing information from direct quaternionic phase and from the diagonal phase.

the main orientation. This is especially true in natural scenes outside the block-world. The quaternionic confidence measure singles out those regions where horizontal and vertical displacement can reliably be estimated simultaneously. Using the quaternionic phase approach the full displacement vectors are evaluated locally at those points where the aperture problem can be circumvented. However, these properties have to be studied in much more detail and with more rigor, which is outside the scope of this thesis.

Of course this system is not complete and the results could be improved. Firstly, the presented method is only able to deal with small displacements. In order to overcome these restrictions one could for example implement a hierarchical multi-scale approach, which starts by estimating the displacement on a coarse scale, yielding a rough approximation of the strong displacements. Subsequently, this first estimate is projected to finer scales and a finer estimate is achieved at each level. This approach has been implemented for the complex phase in [95]. Secondly, common approaches in phase-based disparity estimation improve their result iteratively based on the following idea: In real images the local phase will not be exactly linear. Thus, there will occur some error in the estimated displacement vector $\mathbf{d}(\mathbf{x})$. With the true disparity the phase difference $\phi_2(\mathbf{x}) - \phi_1(\mathbf{x} + \mathbf{d})$ will be zero. For erroneous $\mathbf{d}$ this difference will take some non-zero value based on which a correction $\boldsymbol{\delta}$ can be derived. The estimate $\mathbf{d}$ is then replaced by $\mathbf{d} + \boldsymbol{\delta}$ and again the phase difference can be evaluated. Thus, the disparity estimate can be improved iteratively. This procedure is used by Weng [95]. An alternative iterative approach is proposed by Ahrns [1].

4.3 Texture Segmentation

The task addressed in this section is: *Segment a given image into uniformly textured regions*. This so-called *texture segmentation* problem is one branch of the general problem of *image segmentation* which is one important step in many computer vision tasks. Regarding global variations of gray values or mean gray values over some neighborhood is in most cases not sufficient for a correct segmentation. For this reason rather the global variations of local measures characterizing the texture have to be regarded.

The posed problem is rather vague since the term *texture* is not well defined and there is no unique way of characterizing mathematically the local gray-value variations perceived as texture by human observers. For this reason very different approaches to texture segmentation have been taken. As local measure for the characterization of texture local statistical properties [53, 58] and local geometric building blocks (textons) [63] have been used among others. Another whole branch in texture segmentation research is based on the local spatial frequency for characterizing texture. As mentioned earlier (see section 4.2.3) Gabor filters play a special role in the analysis of local frequency. On the one hand the Gabor filter based approaches to texture analysis are motivated by psychophysical research since 2D Gabor filters have proven to be a good model for the cortical receptive field profiles [27] while on the other hand they are supported by the observation that a whole class of textures (so-called *deterministic textures*) give rise to periodic gray value structures. We will restrict ourselves to the Gabor filter based approaches here. In the following the term texture will always be understood as *image texture* in contrast to *surface texture*. While surface texture is a property of a 3D real-world object, image texture in this context is a property of a 2D intensity image.

In the following sections we analyze in detail the pioneering work of Bovik et al. [11] and in parallel introduce the corresponding quaternionic Gabor filter based approach to texture segmentation. In the final section we discuss our result and make some remarks on other texture segmentation approaches based on Gabor filters.

4.3.1 Bovik's Approach

Bovik et al. [11] introduced a Gabor filter based approach to texture segmentation. As mentioned above, texture segmentation is the task of segmenting an image into uniformly textured regions. According to Bovik's approach a uniform texture is characterized by a dominant frequency and orientation. Here, *characterization* does not mean full characterization of a texture in all its aspects, but "weak characterization" which yields just enough information in order to solve the segmentation task. Thus, different textures occurring in a given image are supposed to differ significantly at least in either the dominant frequency or the dominant orientation.

This assumption leads to the following simple *texture model*. An image containing only one homogeneous texture is modeled as

$$\begin{aligned} f_i(\mathbf{x}) &= c_i(\mathbf{x}) \cos(2\pi(u_i x + v_i y)) + s_i(\mathbf{x}) \sin(2\pi(u_i x + v_i y)) \\ &= a_i(\mathbf{x}) \cos(2\pi(u_i x + v_i y) + p_i(\mathbf{x})), \end{aligned} \tag{4.25}$$

where the amplitude $a_i = \sqrt{c_i^2 + s_i^2}$ and the phase $p_i = -\tan^{-1}\left(\frac{s_i}{c_i}\right)$ are assumed to vary slowly, i.e. in such a way that the dominant frequency component is always well approximated by (u_i, v_i). The characterizing dominant frequency and orientation of the texture f_i are $|\mathbf{u}_i| = \sqrt{u_i^2 + v_i^2}$ and $\alpha_i = -\tan^{-1}(\frac{v_i}{u_i})$, respectively.

A textured image containing n different textures f_i is then given by n textures of the form (4.25) each of which occurring in exactly one connected region $\mathcal{R}_i$ of the image. Defining the characteristic functions z_i of the regions as

$$z_i(\mathbf{x}) = \begin{cases} 1 & \text{if } \mathbf{x} \in \mathcal{R}_i \\ 0 & \text{else,} \end{cases}$$

we can write the texture image f as

$$f(\mathbf{x}) = \sum_{i=1}^{n} f_i(\mathbf{x}) z_i(\mathbf{x}). \tag{4.26}$$

The regions $\mathcal{R}_i$ are assumed to define a partitioning of the domain of f, i.e. $\sum_{i=1}^{n} z_i(\mathbf{x}) \equiv 1$ and $z_i(\mathbf{x}) z_j(\mathbf{x}) \equiv 0$ if $i \neq j$. The set of all possible textures f will be denoted by $\mathcal{T}$. This texture model fits optimally the texture segmentation technique applied by Bovik et al.

The first step in the segmentation procedure is devoted to *filter selection*. In this stage the parameters of a number of Gabor filters that will be used for the segmentation are chosen. In their approach Bovik et al. restrict themselves to filters with aspect ratio $\epsilon = 1$. The bandwidth of the filters is chosen depending on the frequency of the filter by fixing the parameter $c = \sigma\omega$. Thus, only frequency and orientation of the filters (and the number of applied filters) have to be chosen. The authors set the number of filters to two in all experiments. This choice is based on the a priori knowledge that all experiments are performed with images consisting of two uniformly textured regions. The choice of $|\mathbf{u}_i|$ and α_i is performed by a peak-finding algorithm on the power spectrum of the input image, applied to one half of the frequency plane. In this stage human supervision is used. Depending on the type of texture (highly oriented vs. nonoriented) different ways of selecting the "right" peaks are chosen. Hence, the presented method is not a completely unsupervised one. However, the authors propose an unsupervised filter selection scheme, which consists of smoothing the power spectrum of the image with a Gaussian filter, extracting the local maxima of the smoothed image and selecting the filter parameters by applying a threshold to the local maxima image.

The segmentation itself is performed in an unsupervised way. The image f is convolved with the set of selected Gabor filters h_i which yields n filtered images k_i, where n is the number of selected filters. The complex filtered images are transformed into the amplitude/phase-representation according to

$$m_i = |k_i|, \quad \phi = -\mathrm{atan2}\left(\mathcal{I}(k_i), \mathcal{R}(k_i)\right). \tag{4.27}$$

The first level of segmentation is based on the comparison of the channel amplitudes. At this stage each pixel of the image is assigned to one channel. We will denote the region of pixels belonging to channel i by $\mathcal{R}_i$. The classification is simply based on the comparison of the amplitudes m_i at each position in the image:

$$\mathbf{x} \in \mathcal{R}_i \Longleftrightarrow \mathrm{arg}\left(\max_{j\in\{1,\ldots,n\}}(m_j(\mathbf{x}))\right) = i, \tag{4.28}$$

where the function arg returns the index of m. The experiments show that smoother segmentation results are obtained if the local amplitudes m_i are smoothed by convolution with a Gaussian filter before applying (4.28). For smoothing Bovik uses $g_i(\frac{2}{3}\mathbf{x})$, where g_i is the envelope of the Gabor filter h_i.

According to the above view, i.e. that different textures differ in dominant frequency and/or in dominant orientation, the segmentation task is finished at this stage. However, situations occur where two regions contain textures which belong to the same (frequency and orientation) channel but are shifted against each other. Using (4.28) these two textures are assigned to the same region. Using the additional information contained in the phase ϕ obtained by (4.27) the border line between the shifted textures is detectable, since it gives rise to a discontinuity in the phase. This discontinuity is difficult to detect directly because of the natural discontinuities occurring due to the 2π-wrap-around of the phase. Bovik et al. circumvent this difficulty by analyzing the local frequency instead of the local phase. Within a homogeneous textured region the local frequency is assumed to be approximately constant while at the position of a phase-discontinuity there occurs a local-frequency discontinuity as well. These can be detected by the condition $\nabla^2\phi(\mathbf{x}) = 0$ as zero-crossings of the Laplacian of the local phase. As demonstrated in the section on disparity estimation (section 4.2.3) the derivatives of ϕ can be determined analytically to be expressions containing derivatives of k_e and k_o. As before these derivatives are evaluated by convolving the input image by the derivative of the Gabor filter components $\partial_x k = (\partial_x h) * f$. Using this procedure the need for phase unwrapping, i.e. the transformation of the phase into a continuous representation without 2π wraparounds, is circumvented. In the following section we demonstrate how this approach can be extended using quaternionic Gabor filters. A schematic view of Bovik's segmentation procedure is given in figure 4.15.

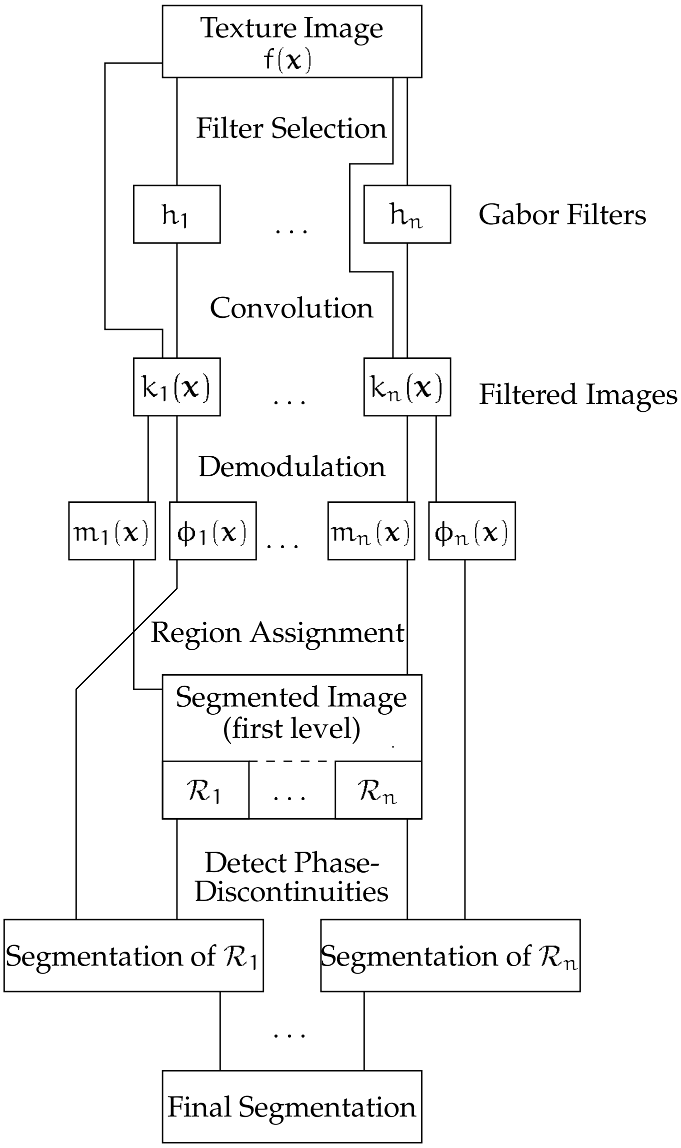

Figure 4.15: Bovik's segmentation procedure. According to the textured input image f a set of Gabor filters h_1 to h_n is selected. The filter responses k_1 to k_n are demodulated into magnitude/phase-representation. The first segmentation step uses the channel amplitude and (4.28) in order to segment f into n regions $\mathcal{R}_1$ to $\mathcal{R}_n$. Phase information is used for the detection of phase-discontinuities, in order to segment the $\mathcal{R}_i$ into subregions where necessary. For further explanation see text.

4.3.2 Quaternionic Extension of Bovik's Approach

The extension of Bovik's approach to texture segmentation using quaternionic Gabor filters is straightforward. Before outlining the segmentation procedure in the quaternionic case we modify the texture model given above. If quaternionic Gabor filters are applied instead of complex filters, the following texture model is more appropriate. A textured image is assumed to consist of homogeneously textured regions

$$f^q(\mathbf{x}) = \sum_{i=1}^{n} f_i^q(\mathbf{x}) z_i(\mathbf{x}), \tag{4.29}$$

where this time the homogeneous textures are of the form

$$\begin{aligned} f_i^q(\mathbf{x}) &= cc_i(\mathbf{x})\cos(2\pi u_i x)\cos(2\pi v_i y) \\ &+ sc_i(\mathbf{x})\sin(2\pi u_i x)\cos(2\pi v_i y) \\ &+ cs_i(\mathbf{x})\cos(2\pi u_i x)\sin(2\pi v_i y) \\ &+ ss_i(\mathbf{x})\sin(2\pi u_i x)\sin(2\pi v_i y). \end{aligned}$$

Again, the functions cc_i, sc_i, cs_i and ss_i are assumed to vary slowly. The set of all possible textures f^q will be denoted by $\mathcal{T}^q$. Obviously, this model is most appropriate for the use of quaternionic filters, since the four terms exactly correspond to the modulation functions of the components of a quaternionic Gabor filter. In figure 4.16 two model textures are shown which demonstrate the difference between the two models.

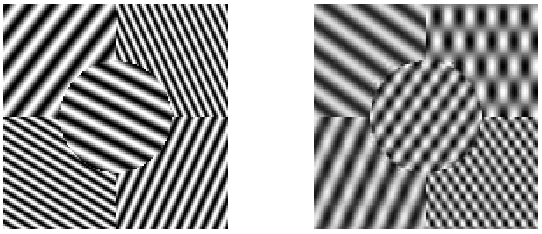

Figure 4.16: Two examples of textured images. Left: A textured image fitting Bovik's texture model (4.26). Right: An image fitting the extended texture model (4.29). For simplicity, in both examples constant coefficients have been chosen.

Note that the quaternionic texture model comprises Bovik's model as a special case, i.e. $\mathcal{T} \subset \mathcal{T}^q$.

The first stages of the segmentation procedure stay basically the same as described in the previous chapter. Only slight modifications have to be made. The filter selection stage is performed by a peak-finding algorithm in the quaternionic power spectrum. The difference is that here the peak finding is only performed over one quadrant of the frequency domain instead of one half in the complex approach. As we have shown when introducing the quaternionic analytic signal in section 3.1.3, one quadrant of the quaternionic frequency domain contains the complete information about the image.

Having selected a set of n quaternionic Gabor filters h_i^q the textured image is convolved with these filters, which yields the filtered images k_i^q. These images are transformed into the polar representation of quaternions introduced in section 2.1.2. This leads to an amplitude/phase-representation $(m_i, \phi_i, \theta_i, \psi_i)$ of the filtered images.

Like in Bovik's approach the first level of segmentation is reached by a channel assignment of each pixel using (4.28), where this time m_i is the magnitude of the quaternionic filter response. In this stage the segmentation results differ only in one aspect from Bovik's algorithm: A real texture with the dominant frequencies $\mathbf{u}_0 = (u_0, v_0)$ with $u_0, v_0 > 0$ contains a component with the negative frequency $\mathbf{u}_1 = (-u_0, -v_0)$ as well, due to the hermitian symmetry of the spectrum. A complex Gabor filter approximately constructs the analytic signal, i.e. it suppresses the redundant negative frequency component. The entire relevant information is contained in one half-plane of the complex frequency domain. Thus, we can choose this half-plane such that $\mathbf{u}_2 = (u_0, -v_0)$ lies in the same half-plane as $\mathbf{u}_0$. If $v_0 \neq 0$, textures with dominant frequency $\mathbf{u}_0$ and $\mathbf{u}_2$ belong to *different* frequency channels, while $\mathbf{u}_0$ belongs to the same channel as $\mathbf{u}_1$ and $\mathbf{u}_2$ to the same channel as $\mathbf{u}_3 = (-u_0, v_0) = -\mathbf{u}_2$. A texture f_0 with dominant frequency $\mathbf{u}_0$ and another texture f_2 with dominant frequency $\mathbf{u}_2$ respond to different Gabor filters and will be assigned to different regions — e.g. $\mathcal{R}_0$ and $\mathcal{R}_2$ — in the first stage of Bovik's method. We assume that f_0 and f_2 carry the same amount of energy. Any superposition $f = a_0 f_0 + a_2 f_2$ will be assigned either to $\mathcal{R}_0$ or to $\mathcal{R}_2$, depending on whether $|a_0| > |a_2|$ or $|a_0| < |a_2|$. If $|a_0| = |a_2|$ the assignment will fail or will be of a random nature. A further segmentation step of detecting phase-discontinuities will not help in this case.

As shown in 3.1.3 the QFT of a real signal contains all non-redundant information in one quadrant of the frequency domain. Thus, a quaternionic Gabor filter will equally well respond to f_0, f_1, f_2, and f_3 as well as to arbitrary linear superpositions. Hence, these textures are not discriminated by the channel assignment step of the quaternionic approach. However, as we will demonstrate later, the textures f_0 and f_2 as well as their linear superpositions are discriminated by the ψ-component of

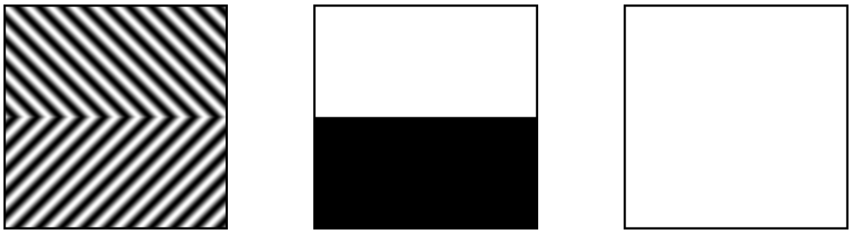

Figure 4.17: A textured image containing two differently textured regions with $(u, v) = (0.05, 0.05)$ pixels^{-1} in the upper half and $(u, v) = (0.05, -0.05)$ pixels^{-1} in the lower half (top), the channel assignment based segmentation using the complex approach (middle) and using the quaternionic approach (right). On this stage the quaternionic approach is apparently inferior. Its superiority will become obvious only in a later stage of the segmentation procedure.

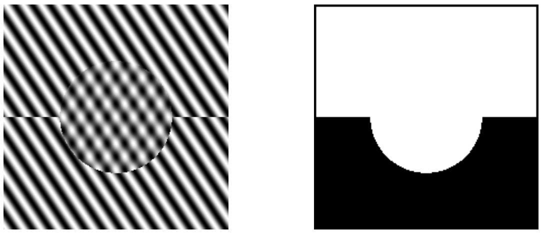

Figure 4.18: Left: A synthetic textured image containing three distinguishable regions which all belong to the same frequency channel. Right: The segmentation result obtained from the detection of the phase discontinuities either in the complex or in the quaternionic case.

the local quaternionic phase.

An example of a textured image containing two differently textured regions and the segmentation results after the channel assignment step in the complex and in the quaternionic case are shown in figure 4.17. All segmentation results shown in this section are schematic and not the results of real experiments. Experimental results will be shown in section 4.3.3. In this first stage the image is segmented into regions belonging to different frequency channels. However, within these regions there may exist subregions which differ either in a phase shift or by a superimposed frequency component with the same frequency $|\mathbf{u}|$ as the dominant component but with orientation $-\alpha$ instead of the dominant orientation α. An example of a synthetic textured image containing only one dominant frequency component but three distinguishable regions is shown in figure 4.18. In order to segment phase-shifted regions belonging to the same frequency channel we use the ϕ- and θ-component of the local quaternionic phase which behave similarly to the complex phase, in that they vary monotonically in general. Thus, phase discontinuities can be detected by $\nabla^2\phi = 0$ and $\nabla^2\theta = 0$ (see explanation in section 4.3.1). In the example of figure 4.18 the image would be segmented into two regions: The upper half containing the whole central disk on the one hand and the rest of the image on the other hand. This segmentation result is the same for either the complex or the quaternionic approach as introduced so far. The complex Gabor filter tuned to the dominant frequency is blind to the superimposed ripples in the central disk of the image in figure 4.18. As shown in section 3.2.4.3 the ψ-component of the phase holds the information about the mixture of two superimposed frequency components like the ones denoted by f_0 and f_2 above. Denoting the mixed texture by $f = (1-\lambda)f_0 + \lambda f_2$ there is a one-to-one mapping of ψ to λ. Thus, it is possible to segment the image in 4.18 into its three regions, based solely on the ψ-component of the local phase.

4.3.3 Experimental Results

The meaning of the ψ-component of the quaternionic phase has been explained in section 3.2.4.3. We demonstrate its segmentation power first on a synthetic texture consisting of three different textures (figure 4.19). This image resembles an image used by Bovik ([11] p. 64, fig. 6), with the difference that in [11] only two different regions are used. The third region (upper right and lower left region), which is the superposition of the two orthogonally oriented sinusoidals, can not be segmented using the complex approach. In contrast, the ψ-component of the quaternionic phase distinguishes not only local frequency and orientation but also local structure as explained in the last section. See also figure 4.21 for clarification. We tested the robustness of ψ for segmentation by adding Gaussian noise to the synthetic texture in figure 4.19. The result is shown in figure 4.20. We added noise with zero mean and variance 1.5 and 5, respectively. The texture itself has zero mean and takes values between -1 and 1. The SNR is -2.7 and -13.2, respectively. Although it is almost impossible for a human observer to segment the image with the strongest noise, by means of ψ more than 78% of the pixels are correctly classified.

4.3.3.1 Detection of Defects in Woven Materials

As a practical application we demonstrate how the quaternionic Gabor segmentation method can be used for the detection of defects in woven materials. We regard this task as a texture segmentation problem, where we want to segment the regular texture from defective regions. However, defects are often so small that they

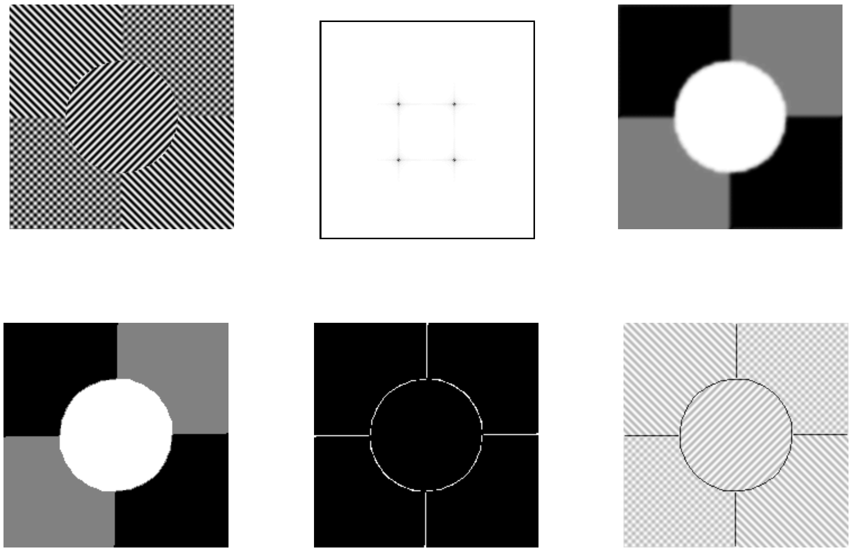

Figure 4.19: The textured image, its QFT-magnitude spectrum (origin at the center, and high values marked dark, low values marked white), and the ψ-component of the local phase (top), and the segmentation result, the pixels which were misclassified (1.22%) and the edges of the ψ-component found by a Sobel filter superimposed to the original texture (bottom).

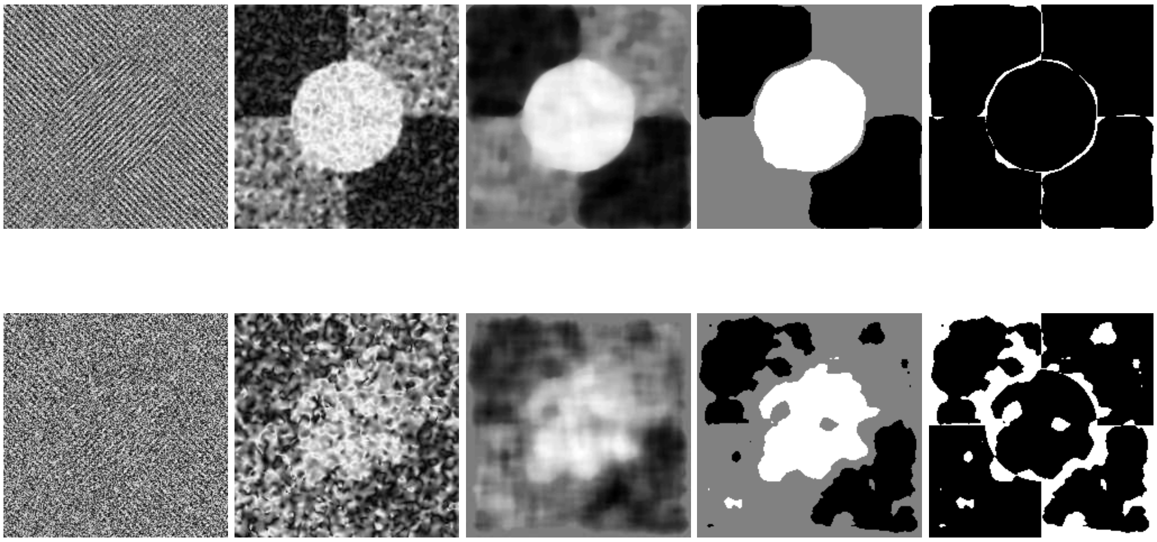

Figure 4.20: The texture from figure 4.19 with added Gaussian noise. In the upper row the SNR is −2.7 dB, and more than 97% of the pixels are classified correctly. In the lower row the SNR is −13.2 dB and about 78% of the pixles are classified correctly. From left to right the rows show the contaminated texture, the ψ-component of the local phase, the median filtered ψ-component, the segmented texture and the wrongly classified pixels.

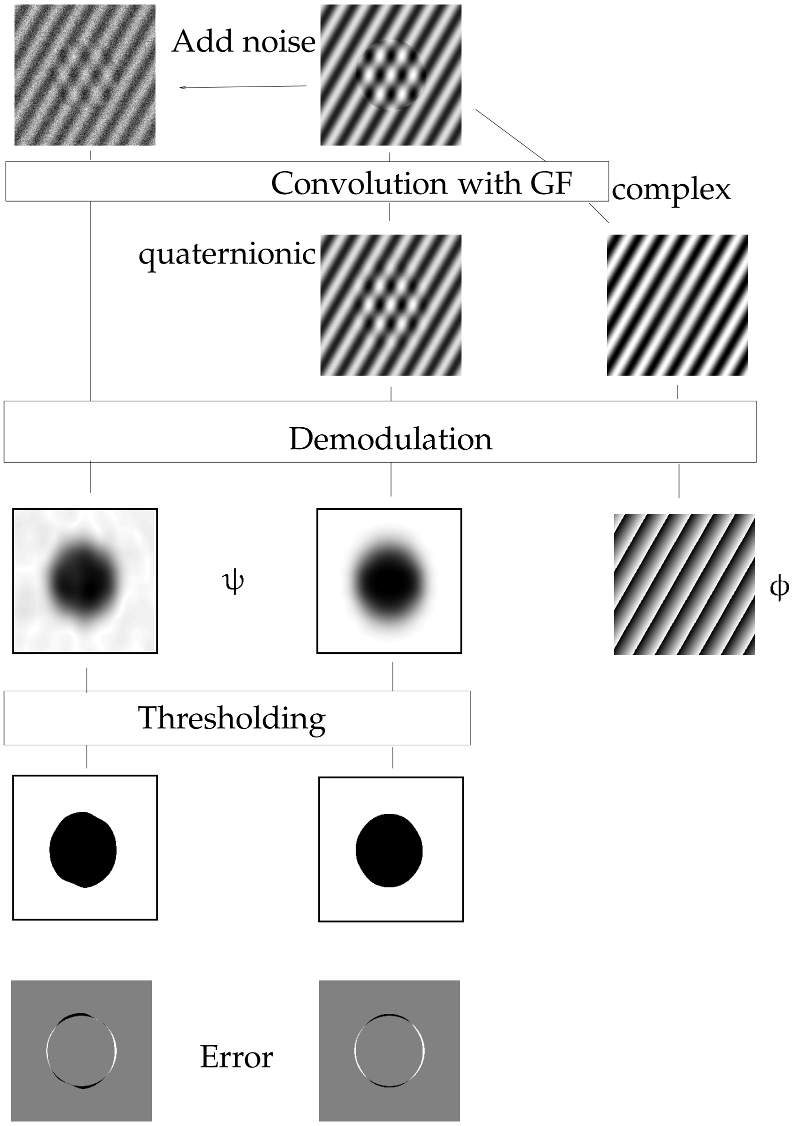

Figure 4.21: Comparison of the complex and the quaternionic segmentation approach. The input image (top) is convolved with an optimally tuned complex (right column) and quaternionic (middle column) Gabor filter. In the second row the real parts of the filter responses are shown. The filtered images are transformed into amplitude/phase-representation. In the complex case the magnitude (not shown) is constant, and the phase ϕ is varying monotonically. No segmentation is possible. In the quaternionic case segmentation based on the ψ-component (magnitude and other phase-components are not shown) is possible. The left column is like the middle column, but with added noise (SNR=0 dB).

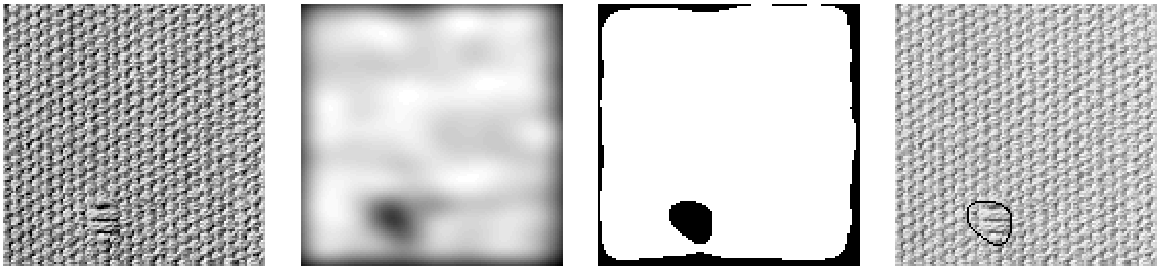

Figure 4.22: From left to right: A subregion of Brodatz' texture D77. The smoothed ψ-component of the local quaternionic phase as intensity image and after applying a threshold. The edges of the thresholded ψ-phase superimposed to the input image.

do not exhibit periodic structure. That makes the defect detection not feasible for a channel assignment method — complex or quaternionic — based on the magnitude of response to a certain channel filter. We test the following method here. Given a homogeneous woven texture we extract the dominant quaternionic frequency component. The image is convolved with the corresponding quaternionic Gabor filter (where the remaining parameters are chosen as $c_h = c_v = 3$) and the ψ-component of the local phase is extracted. A flaw in the texture manifests itself in a change of the local structure, which is what is measured by the ψ-phase. As the experiments show, ψ varies only very modestly within a homogeneously textured region. The mean ψ-value of a homogeneous texture f will be denoted as ψ_f. For the segmentation we chose an interval of acceptance $I_{\mathit{Texture}} = [\psi_f - \delta, \psi_f + \epsilon]$. The defective region will be denoted by $\mathcal{R}_{\mathit{Flaw}}$. The assignment rule is then given by

$$\mathbf{x} \in \mathcal{R}_{\mathit{Flaw}} \Leftrightarrow \psi(\mathbf{x}) \notin I_{\mathit{Texture}}.$$

As a second example we use a subregion of the texture D77 (see figure 4.22 taken from Brodatz' album [16]). We apply one QGF whose central frequencies have been tuned to the main peak in the power (QFT)-spectrum of the image. In this case the frequencies are 21 cycles/image in vertical direction and 12 cycles per image in horizontal direction. In the regular part of the texture we find $\psi \approx 0.5$ while at the irregularity we get $\psi \leq 0$. Before applying a threshold, the ψ-image is smoothed with a Gaussian filter with $\boldsymbol{\sigma}_{\mathrm{Gauss}} = 1.5\boldsymbol{\sigma}_{\mathrm{QGF}}$ where $\boldsymbol{\sigma} = (\sigma_1, \sigma_2)^\top$. This choice is based on an empirical result by Bovik et al. [11]. Since at the flaw the applied filters do not match optimally, also the amplitude of the filter output yields a hint for the defect searched for. However, the amplitude is very sensitive to changing lightning conditions as shown in the following experiments. However, ψ is insensitive to changes in contrast. This is important, because of the fact that the lightning conditions are not necessarily optimal (e.g. not homogeneous) in practical applications [29].

We simulate changing lightning conditions by adding a gray-value ramp with constant slope (figure 4.23) and by changing the contrast inhomogeneously (figure 4.24). In figure 4.25 the amplitude of the filter responses are shown for the different lightning conditions. A segmentation on the basis of the amplitude envelopes is not possible by a thresholding procedure.

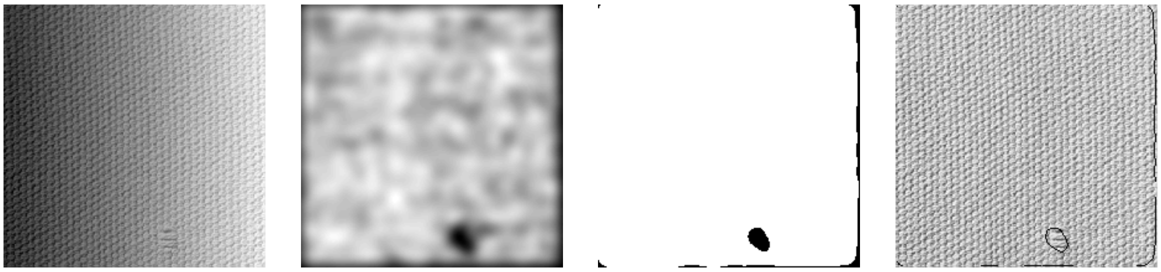

Figure 4.23: As in figure 4.22. To the original image a gray value ramp with constant slope is added.

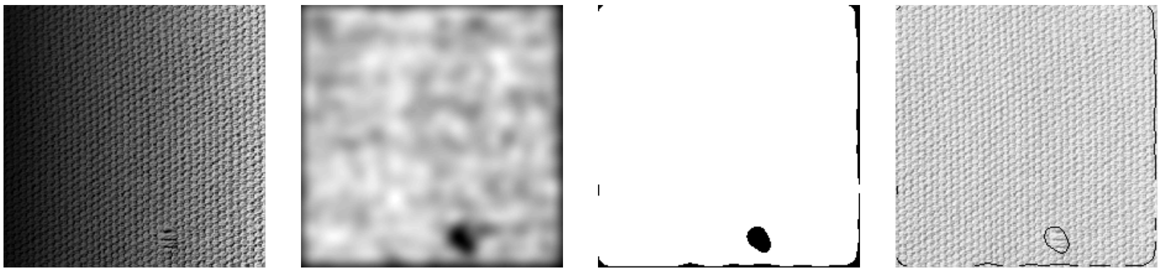

Figure 4.24: As in figure 4.22. The contrast is modified to vary from left (low contrast) to right (high contrast).

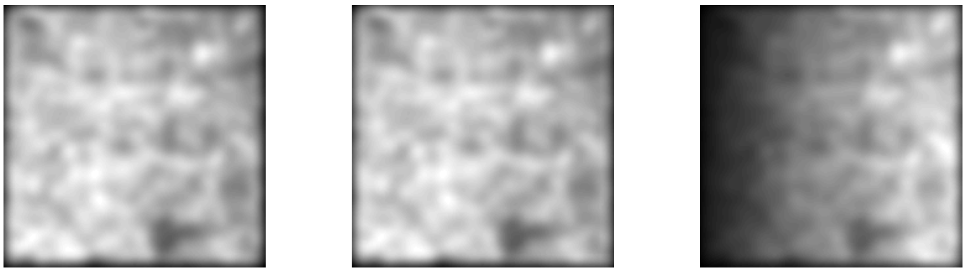

Figure 4.25: The amplitude envelopes of the quaternionic Gabor filter response to the texture D77 under different lightning conditions. Left: Original illumination. Middle: A gray value ramp added. Right: Changing contrast.

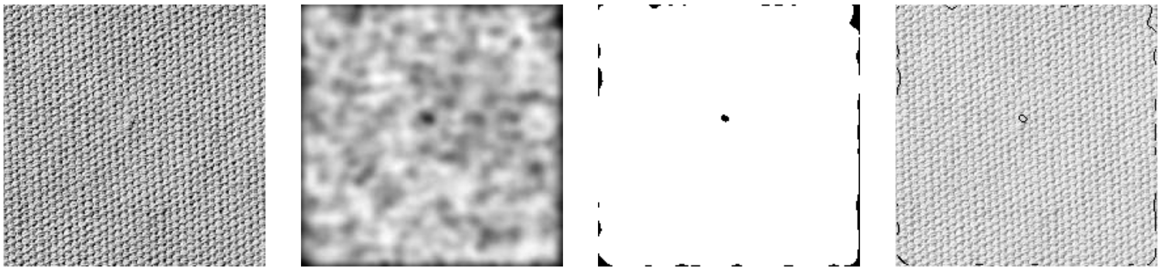

Figure 4.26: Another subregion of D77. As in figure 4.22.

The flaw detection method presented here has the advantage of being fast, since only separable convolutions have to be performed and only the ψ-component of the local phase has to be evaluated which is a pointwise nonlinear operation. The method is robust to changing lightning conditions.

4.3.4 Comparison to Other Approaches and Discussion

In the previous sections we introduced a texture segmentation scheme based on quaternionic Gabor filters. The procedure is based on the one introduced by Bovik et al. [11]. Actually, the quaternionic scheme includes Bovik's method at least if the used Gabor filters have an isotropic Gaussian envelope. This is the case in Bovik's experiments. Thus, we can reproduce all of their results. Additionally, the quaternionic approach provides the ψ-phase as a new entity. In special situations this entity allows a finer segmentation. This is the case when there occur regions which contain the same dominant frequency, once in a pure form and once with another differently oriented frequency component superimposed. These situations which occur often e.g. in woven fabrics can be handled by the ψ-phase. There has been a lot of activity in texture segmentation using Gabor filters. We will comment on some of these approaches here.

Du Buf (1990) [30] uses merely Gabor phase information for texture segmentation, where the applied filters are selected non-automatically from a given filter set covering the whole frequency plane. To the phase component of each filtered image one of two proposed phase demodulation methods is applied. Since global unwrapping schemes are applied, there occur problems whenever the image contains regions with different local frequencies. Overall, this method seems inferior to the local phase-discontinuity detection used by Bovik. Results on synthetic images are provided.

Dunn (1994,'95) [33, 32] introduces a method for finding an optimal 2D Gabor filter for the discrimination of a two-texture image. This filter is designed such that the discontinuity in the magnitude of the filtered image is most significant at the texture boundary. Since examples of the two textures must be known beforehand, this is a so-called supervised segmentation method.

In contrast to directly assigning each pixel to the best-matching channel and detecting phase discontinuities afterwards, many authors apply some clustering algorithm to the extracted Gabor features for segmentation:

Jain et al. (1991): Jain [60] uses a decomposition of the textured image by a set of approximately orthogonal even-symmetric real Gabor filters, which approximates a wavelet transform. For the segmentation only a subset of the filtered images is used: The filtered images are ordered according to the Euclidean distance to the input image in increasing order and the first k images are used for segmentation. The filtered images are subjected a nonlinear transformation from which a feature image is computed. For segmentation a two-phase clustering algorithm is applied to these feature images. The first stage is a k-means algorithm, the result of which is improved in a second stage. The clustering algorithm also takes into account the pixel coordinates (in addition to the feature images), which accounts for the fact that neighboring pixels tend to belong to the same texture.

Teuner et al. (1995) point out that the dominant frequencies do not necessarily coincide with the ones that are important for segmentation [91]: A dominant frequency is only helpful for segmentation when it does not occur everywhere in the textured image. The authors provide a measure called the spectral feature contrast, which indicates the discriminatory power of a Gabor feature. The same authors use the feature contrast for the reduction of the dimensionality of the feature space [82].

Our approach to texture segmentation is directly based on Bovik's method. In this stage we have shown that the quaternionic Gabor approach is more powerful than the complex Gabor filter approach, since the texture model is extended by using quaternionic filters. This extension of the texture model is realized without any additional computational effort since quaternionic Gabor filters are separable. The other methods mentioned here have not been applied to quaternionic Gabor filters yet. However, there seem to be no fundamental problems in an extension of e.g. the feature contrast to quaternionic Gabor filter. Quaternionic Gabor filters show their efficiency in the first stage, and it seems probable that this can be improved by combining the approach presented here with more recent methods developed for texture segmentation using complex Gabor filters.

4.4 Summary

We have applied quaternionic Gabor filters and the local quaternionic phase to two practical tasks, namely disparity estimation and texture segmentation. One class of methods for disparity estimation comprises the so-called phase-based approaches. These approaches use the property of the local phase of being equivariant with spatial position. We have extended an existing approach which is based on complex Gabor filters to the use of quaternionic Gabor filters. The complex approach considered here is restricted to the evaluation of the horizontal disparity. According to the shift theorem of the quaternionic Fourier transform the first two components of the quaternionic phase are equivariant with the spatial position. We have shown how the full disparity field can be estimated on the basis of the first two components of the local quaternionic phase.

It was shown in chapter 3 that each quaternionic Gabor filter corresponds to two complex Gabor filters. In addition to the disparity information found from the quaternionic phase we have used the phase of these complex filters. This yields a higher density of the estimated disparity field than each of the two methods alone. Experiments on two real image pairs are provided.

As a second application of quaternionic Gabor filters we have presented their use in texture segmentation. A pioneering approach for the usage of local amplitude and phase in texture segmentation has been provided by Bovik [11]. Bovik's approach uses complex Gabor filters. We have modified this approach to the use of quaternionic Gabor filters. We were able to show that the class of textures which are separable according to Bovik's model is considerably extended by the use of quaternionic filters. It is especially worth noting that we do not have to increase the computational load in order to achieve the additional segmentation power of the quaternionic approach. It has been shown that the third component ψ of the local quaternionic phase provides an important new feature for segmentation which is not contained in Bovik's approach when complex Gabor filters are used.

Chapter 5

Conclusion

The main goal of this thesis was to establish a correspondence between the local phase and the local structure of intrinsically two-dimensional signals. For one-dimensional signals this correspondence is well-known. In 2D, generic filters had to be introduced which make accessible an extended local phase concept. This was accomplished by introducing Gabor filters with values in Clifford algebras. In 1D, Gabor filters can be regarded as an approximation of quadrature filters. Such filters are defined via the analytic signal, which is most easily constructed in the Fourier domain. Thus, in order to lay the theoretical foundation for the introduction of hypercomplex Gabor filters, we had to introduce the notions of a hypercomplex Fourier transform and of the hypercomplex analytic signal. These concepts have been developed in this thesis, with the main emphasis on two-dimensional signals. However, all concepts can easily be extended to n-dimensional signals.

The original contributions of this thesis, and the articles upon which it is based, are the following:

- We have presented the Clifford Fourier transform (CFT). A hypercomplex Fourier transform (HCFT) based on a commutative 2^n-dimensional algebra has been introduced and compared to the n-dimensional Clifford Fourier transform. It turns out that the CFT and the HCFT of a real n-dimensional signal are related by a simple mapping which we call *switching*.

- We were able to show that the quaternionic Fourier transform (QFT) builds the highest level of a natural three-level hierarchy of two-dimensional harmonic transforms. The principle on which this hierarchy is based is the symmetry selectivity of the transform with respect to real signals. The first and second level are made up by the Hartley transform and the Fourier transform, respectively. This hierarchy can be extended to an $(n + 1)$-level hierarchy of n-dimensional harmonic transforms, on the top of which stands the Clifford Fourier transform. In 2D, the QFT comprises the Fourier transform and the Hartley transform. The Fourier transform and the Hartley transform are simply linear combinations of QFT components.

- We defined the quaternionic analytic signal based on the quaternionic Fourier transform, and compared it to existing approaches. The most recent of these approaches is the complex signal with single quadrant spectrum, proposed by Hahn [48, 49]. This approach suffers from the fact that the original signal is not contained in its analytic or complex signal. It has been shown that this can be cured by replacing the complex Fourier transform by the quaternionic Fourier transform, which leads to the quaternionic analytic signal. The reason for the superiority of the QFT in this context lies in the fact that the QFT of a real signal is quaternionic hermitian, a property which we introduced in this thesis.

- On the basis of the QFT, we introduced quaternionic Gabor filters. In 1D, the numerical similarity of Gabor filters and derivatives of the Gaussian has been analyzed by Michaelis [78]. We were able to extend this to 2D as a similarity between quaternionic Gabor filters and (mixed) partial derivatives of a 2D Gaussian. Furthermore we showed that quaternionic Gabor filters fulfill the two-dimensional version of the uncertainty principle of communication theory in an optimal manner. Quaternionic Gabor filter masks are separable and therefore convolution can be implemented very efficiently. This can be used in order to speed up convolution even with complex Gabor filters, since these are linear combinations of quaternionic Gabor filter components.

- The quaternionic Gabor filters allow the definition of an extended concept of the local phase consisting of three real components. This generalizes the relation of the local phase of a signal to the local structure, which is well known in 1D, to intrinsically two-dimensional signals. Applications in the two areas of texture segmentation and disparity estimation have been performed. Especially in texture segmentation tasks the local quaternionic phase shows high discriminatory power. It is an important fact that this additional feature comes without any additional computational cost.

Developing the theory of hypercomplex spectral signal representations, we were able to construct linear filters which have the possibility of capturing the intrinsically two-dimensional signal structure. Their intrinsic two-dimensional structure is a fundamental property of images. Images contain regions of intrinsically zero-dimensional and one-dimensional structure as well, but these structures can equally well be described by one-dimensional signals.

The possibility of capturing intrinsically two-dimensional structure is the main feature of the hypercomplex signal representations. The value of the representation lies in the fact that it contains the symmetry information of a signal in a way which is more directly accessible by a linear method than in other linear representations. Of course, the full signal information is as well contained in the pixel representation or in the complex Fourier representation. However, the information is presented in very different ways. It has been shown that the QFT and quaternionic Gabor filters make accessible intrinsically two-dimensional structure more directly than the other mentioned representations. Future research will be concerned with extensions of the applications sketched in this thesis. On the other hand, there remain open theoretical questions like the existence of a phase concept in dimensions $n > 2$.

Surely, the methods presented here are only a first step in using hypercomplex methods in image processing. It should be possible to construct hypercomplex filters which capture other symmetries than the reflectional symmetries with respect to the coordinate axes, which were used here. Thus, we have the hope of having opened a door to future research in multidimensional signal processing using representations in hypercomplex algebras.

Bibliography

[1] I. Ahrns and H. Neumann. Improving phase-based disparity estimation by means of filter tuning techniques. In P. Levi et al., editor, *Mustererkennung 1998*, pages 357–364. Springer Verlag, Berlin et al., 1998.

[2] J.L. Barron, D.J. Fleet, and S.S. Beauchemin. Performance of optical flow techniques. *International Journal of Computer Vision*, 12:43–78, 1994.

[3] E. Barth. *Geometrische Analyse und iterative Synthese von Bildern*. VDI-Verlag, Düsseldorf, 1995.

[4] E. Barth, T. Caelly, and Chr. Zetzsche. Image encoding, labeling, and reconstruction from differential geometry. *Graphical Models and Image Processing*, 55(6):428–446, 1993.

[5] E. Barth, Chr. Zetzsche, and G. Krieger. Curvature measures in visual information processing. *Open Sys. and Information Dyn.*, 5:25–39, 1998.

[6] M.J. Bastiaans. Gabor's expansion of a signal into Gaussian elementary signals. *Proceedings of the IEEE*, 68(4):538–539, 1980.

[7] E. Bayro-Corrochano and S. Buchholz. Geometric neural networks. In G. Sommer and J.J. Koenderink, editors, *Algebraic Frames for the Perception–Action Cycle*, volume 1315 of *Lecture Notes in Computer Science*, pages 379–394. Int. Workshop AFPAC'97, Kiel, Springer-Verlag, Heidelberg, 1997.

[8] E. Bayro-Corrochano and J. Lasenby. A unified language for computer vision and robotics. In G. Sommer and J.J. Koenderink, editors, *Algebraic Frames for the Perception–Action Cycle*, volume 1315 of *Lecture Notes in Computer Science*, pages 219–234. Int. Workshop AFPAC'97, Kiel, Springer-Verlag, Heidelberg, 1997.

[9] E. Bayro-Corrochano, J. Lasenby, and G. Sommer. Geometric algebra: A framework for computing point and line correspondences and projective

structure using n uncalibrated cameras. In *Proc. 13th Int. Conf. on Pattern Recognition*, volume A, Vienna, pages 334–338. ICPR, 1996.

[10] W. Blaschke. *Kinematik und Quaternionen*. VEB Deutscher Verlag der Wissenschaften, Berlin, 1960.

[11] A.C. Bovik, M. Clark, and W. Geisler. Multichannel texture analysis using localized spatial filters. *IEEE Trans. Pattern Analysis and Machine Intelligence*, 12(1):55–73, 1990.

[12] R. Bracewell. *The Fourier Transform and its Applications*. McGraw Hill, 1986.

[13] R.N. Bracewell. The discrete Hartley transform. *J. Opt. Soc. Amer.*, 73:1832–1835, 1983.

[14] R.N. Bracewell. Affine theorem for the Hartley transform of an image. *Proceedings of the IEEE*, 82:388–390, 1994.

[15] R.N. Bracewell. Aspects of the Hartley transform. *Proceedings of the IEEE*, 82:381–387, 1994.

[16] P. Brodatz. *Textures: A photographic Album for Artists and Designers*. New York: Dover, 1966.

[17] J. Bruske and G. Sommer. Intrinsic dimensionality estimation with optimally topology preserving maps. *IEEE Transactions on Pattern Analysis and Machine Intelligence*, 20(5):572–575, May 1998.

[18] Th. Bülow and G. Sommer. Algebraically extended representations of multidimensional signals. In *Scandinavian Conference on Image Analysis, Lappeenranta*, volume 2, pages 559–566, 1997.

[19] Th. Bülow and G. Sommer. Das Konzept einer zweidimensionalen Phase unter Verwendung einer algebraisch erweiterten Signalrepräsentation. In *E. Paulus, F. M. Wahl (Eds.), 19. DAGM Symposium Mustererkennung, Braunschweig*, pages 351–358. Springer-Verlag, 1997.

[20] Th. Bülow and G. Sommer. Multi-dimensional signal processing using an algebraically extended signal representation. In *G. Sommer, J.J. Koenderink (Eds.), Proc. Int. Workshop on Algebraic Frames for the Perception-Action Cycle, Kiel, LNCS vol. 1315*, pages 148–163. Springer-Verlag, 1997.

[21] Th. Bülow and G. Sommer. Lokale Signalanalyse mittels quaternionischer Gaborfilter. In *1. Tübinger Wahrnehmungskonferenz*, page 147, 1998.

[22] Th. Bülow and G. Sommer. Quaternionic Gabor filters for local structure classification. In *14th International Conference on Pattern Recognition, August 17-20 1998, Brisbane, Australia*, 1998. 808-810.

[23] K.R. Castleman. *Digital Image Processing*. Prentice-Hall, 1996.

[24] V.M. Chernov. Discrete orthogonal transforms with data representation in composition algebras. In *Scandinavian Conference on Image Analysis, Uppsala, Sweden, 1995*, pages 357–364, 1995.

[25] M.A. Chichyeva and M.V. Pershina. On various schemes of 2d-DFT decomposition with data representation in the quaternion algebra. *Image Processing and Communications*, 2(1), 1996.

[26] K. Daniilidis. Hand-eye calibration using dual quaternions. *International Journal of Robotics Research*, 1999. To appear.

[27] J. G. Daugman. Two-dimensional spectral analysis of cortical receptive field profiles. *Vision Res.*, 20:847–856, 1980.

[28] J. G. Daugman. Uncertainty relation for resolution in space, spatial frequency, and orientation by two-dimensional visual cortical filters. *Journal Opt. Soc. Am. A*, 2(7):1160–1169, 1985.

[29] Ch. Daul and et al. A fast image processing algorithm for quality control of woven textiles. In *Levi, P. and et al. (Eds.), 20. DAGM Symposium Mustererkennung, Stuttgart*, pages 471–479. Springer-Verlag, 1998.

[30] J. M. H. du Buf. Gabor phase in texture discrimination. *Signal Processing*, 21:221–240, 1990.

[31] P. Duhamel and M. Vetterli. Improved Fourier and Hartley transform algorithms: Application to cyclic convolution of real data. *IEEE Trans. Acoust. Speech Signal Process.*, ASSP-35:818–824, 1987.

[32] D. Dunn and W.E. Higgins. Optimal Gabor filters for texture segmentation. *IEEE Trans. Image Processing*, 4:947–964, 1995.

[33] D. Dunn, W.E. Higgins, and J. Wakeley. Texture segmentation using 2-d Gabor elementary functions. *T-PAMI*, 16:130–149, 1994.

[34] T.A. Ell. *Hypercomplex Spectral Transformations*. PhD thesis, University of Minnesota, 1992.

[35] T.A. Ell. Quaternion Fourier transforms for analysis of 2-dimensional linear time-invariant partial-differential systems. In *Proc. 32nd IEEE Conf. on Decision and Control, San Antonio, TX, USA, 15-17 Dec.*, pages 1830–1841, 1993.

[36] H.-D. Ebbinghaus et al. *Zahlen*. Springer, Berlin, 1988.

[37] O.D. Faugeras. What can be seen in three dimensions with an uncalibrated stereo rig? *ECCV*, 92:563–578, 1992.

[38] O.D. Faugeras. Stratification of three-dimensional vision: projective, affine, and metric representation. *Journal Opt. Soc. Am. A*, 12:465–484, 1995.

[39] M. Felsberg. Fast quaternionic Fourier transform. Student project, Christian-Albrechts-Universität Kiel, Germany, 1997.

[40] M. Felsberg. Signal processing using frequency domain methods in Clifford algebra. Master's thesis, University of Kiel, 1998.

[41] D.J. Field. Relations between the statistics of natural images and the response properties of cortical cells. *Journal Opt. Soc. Am. A*, 5(12):2379–2394, 1987.

[42] D. J. Fleet, A. D. Jepson, and M. R. M. Jenkin. Phase-based disparity measurement. *CVGIP: Image Understanding*, 53(2), 3 1991.

[43] D.J. Fleet and A.D. Jepson. Computation of component image velocity from local phase information. *IJCV*, 5:77–104, 1990.

[44] D. Gabor. Theory of communication. *Journal of the IEE*, 93:429–457, 1946.

[45] G.H.Granlund and H. Knutsson. *Signal Processing for Computer Vision*. Kluwer Academic Publishers, 1995.

[46] H.G. Gröndahl and K. Gröndahl. Subtraction radiography for the diagnosis of periodontal bone lesions. *Oral Surg.*, 55:208–213, 1983.

[47] L. Haglund. *Adaptive Multidimensional Filtering*. PhD thesis, Linköping University, 1992.

[48] S. L. Hahn. Multidimensional complex signals with single-orthant spectra. *Proc. IEEE*, 80(8):1287–1300, 1992.

[49] S. L. Hahn. *Hilbert Transforms in Signal Processing*. Artech House, Boston, London, 1996.

[50] W.R. Hamilton. *Elements of Quaternions*. Longmans Green, London 1866. Chelsea, New York, 1969.

[51] M. Hansen. *Stereosehen. Ein verhaltensbasierter Zugang*. PhD thesis, Christian-Albrechts-Universität Kiel, Germany, 1998.

[52] M. Hansen, K. Daniilidis, and G. Sommer. Optimization of stereo disparity estimation using the instantaneous frequency. In *G. Sommer et al. (Ed.), Proc. Int. Conf. Computer Analysis of Images and Patterns CAIP, Kiel, Springer LNCS vol. 1296*, pages 321–328. Springer Verlag, Berlin et al., 1997.

[53] R.M. Haralick. Statistical and structural approaches to texture. *Proceedings of the IEEE*, 67:786–804, 1979.

[54] R.V.L. Hartley. A more symmetrical Fourier analysis applied to transmission problems. *Proc. IRE*, 30:144–150, 1942.

[55] W. Hein. *Struktur- und Darstellungstheorie der klassischen Gruppen*. Springer Verlag, Berlin et al., 1990.

[56] D. Hestenes and G. Sobczyk. *Clifford Algebra to Geomertic Calculus: A Unified Language for Mathematics and Physics*. D. Reidel, Dortrecht, 1984.

[57] B.K.P. Horn. Robot Vision, Mcgraw-Hill. *New York*, 1986.

[58] B. Jähne. *Digitale Bildverarbeitung*. Springer Verlag, Berlin et al., 4th edition, 1993.

[59] B. Jähne. Spatio-temporal image processing-theory and scientific applications, springer. *BERLIN*, 94:1993, 1993.

[60] A.K. Jain and F. Farrokhnia. Unsupervised texture segmentation using Gabor filters. *PR*, 24:1167–1186, 1991.

[61] A.D. Jepson and M.R.M. Jenkin. Recovering local surface structure through local phase difference measurement. *CVGIP: Image Understanding*, 59(1):72 – 93, 1 1994.

[62] B. Julesz. Binocular depth perception of computer-generated patterns. *Bell Syst. Techn. J.*, 39:1125–1162, 1960.

[63] B. Julesz. Textons, the elements of texture perception, and their interpretations. *Nature*, 290(12):91–97, 1981.

[64] I.L. Kantor and A.S. Solodovnikov. *Hypercomplex Numbers*. Springer Verlag, Berlin et al., 1989.

[65] H. Knutsson. Representing local structure using tensors. In *Scandinavian Conference on Image Analysis, Oulu, Finland*, pages 244–251, 1989.

[66] J. J. Koenderink. Mapping formal structures on networks. In T. Kohonen, K. Mäkisara, O. Simula, and J. Kangas, editors, *Artificial Neural Networks*, pages 93–98. Elsevier Science Publishers B.V., 1991.

[67] J. J. Koenderink, A. Kappers, and A. van Doorn. Local operations: The embodiment of geometry. In *Artificial and biological vision systems*. ESPRIT Basic Research Series, 1992.

[68] J. J. Koenderink and A. van Doorn. Representation of local geometry in the visual system. *Biological Cybernetics*, 55:367–375, 1987.

[69] J. J. Koenderink and A. van Doorn. Generic neighborhood operators. *IEEE Trans. Pattern Analysis and Machine Intelligence*, 14(6):597–605, 1992.

[70] A. Korn and M. Korn. *Mathematical Handbook for Scientists and Engineers*. McGray-Hill Book Company, 1968.

[71] A.I. Kostrikin and I.R. Shafarevich (Eds.). *Algebra II*. Springer Verlag, Berlin et al., 1991.

[72] G. Krieger and Chr. Zetzsche. Nonlinear image operators for the evaluation of local intrinsic dimensionality. *IEEE Trans. Image Processing*, 5(6):1026–1042, 1996.

[73] P. Kube and P. Perona. Scale-space properties of quadric feature detectors. *IEEE Trans. Pattern Analysis and Machine Intelligence*, 18(10):987–999, 1996.

[74] K. Langley, T.J. Atherton, R.G. Wilson, and M.H.E. Larcombe. Vertical and horizontal disparities from phase. In *Proc. 1st ECCV*, pages 315–325, 1990.

[75] Th.M. Lehmann. A two-stage algorithm for model-based registration of medical images. In *14th International Conference on Pattern Recognition, August 17-20 1998, Brisbane, Australia*, pages 344–351, 1998.

[76] P. Lounesto. *Clifford Algebras and Spinors*. Cambridge University Press, 1997.

[77] A. Maki, L. Bretzner, and J.-O. Eklundh. Local Fourier phase and disparity estimation: An analytical study. In *V. Hlavac et al. (Ed.), Proc. Int. Conf. Computer Analysis of Images and Patterns CAIP, Prag*, pages 868–874, 1995.

[78] M. Michaelis. *Low level image processing using steerable filters*. PhD thesis, Kiel University, 1995.

[79] K.J. Olejniczak and G.T. Heydt. Scanning the special section on the Hartley transform. *Proceedings of the IEEE*, 82:372–380, 1994.

[80] A.V. Oppenheim and Lim J.S. The importance of phase in signals. *Proc. IEEE*, 69(5):529–541, 1981.

[81] A. Papoulis. *Systems and Transforms with Applications in Optics*. McGraw-Hill, New York, 1968.

[82] O. Pichler, A. Teuner, and B. J. Hosticka. An unsupervised texture segmentation algorithm with feature space reduction and knowledge feedback. *IEEE Trans. Image Processing*, 7(1):53–61, 1998.

[83] W. Press et al. *Numerical Recipes in C*. Cambridge University Press, 1994.

[84] T.D. Sanger. Stereo disparity computation using Gabor filters. *Biol.Cybernetics*, 59:405–418, 1988.

[85] S.J. Sangwine. Fourier transforms of colour images using quaternion or hypercomplex numbers. *Electronics Letters*, 32(21):1979–1980, 1996.

[86] S.J. Sangwine. Colour image edge detector based on quaternionic convolution. *Electronics Letters*, 34(10):969–971, 1998.

[87] H.W. Schüßler. *Netzwerke, Signale und Systeme*. Springer Verlag, Berlin et al., 1991.

[88] G. Sommer. Bivariant signal representations. In R. Klette and W. Kropatsch, editors, *Theoretical Foundations of Computer Vision*, pages 119–130. Akademie Verlag, Berlin, 1992.

[89] G. Sommer. Algebraic aspects of designing behavior based systems. In G. Sommer and J.J. Koenderink, editors, *Algebraic Frames for the Perception and Action Cycle*, volume 1315 of *Lecture Notes in Computer Science*, pages 1–28. Proc. Int. Workshop AFPAC'97, Kiel, Springer–Verlag, Heidelberg, 1997.

[90] H. Stark. An extension of the Hilbert transform product theorem. *Proc. IEEE*, 59:1359–1360, 1971.

[91] A. Teuner, O. Pichler, and B.J. Hosticka. Unsupervised texture segmentation of images using tuned matched gabor filters. *T-IP*, 4:863–870, 1995.

[92] S. Venkatesh, J. Cooper, and B. White. Local energy and pre-envelope. *Pattern Recognition*, 28(8):1127–1134, 1995.

[93] S. Venkatesh and R. Owens. On the classification of image features. *Pattern Recognition Letters*, 11:339–349, 1990.

[94] J.D. Villasenor. Optical Hartley transforms. *Proceedings of the IEEE*, 82:391–399, 1994.

[95] J. Weng. Image matching using the windowed Fourier phase. *International Journal of Computer Vision*, 11(3):211–236, 1993.

[96] A. Wenzel, K. Warrer, and T. Karring. Digital subtraction radiography in assessing bone changes in periodontal defects following guided tissue regeneration. *J. Clin. Periodontol.*, 19:208–213, 1992.

[97] R. Wilson and G.H. Granlund. The uncertainty principle in image processing. *IEEE Trans. Pattern Analysis and Machine Intelligence*, 1984.

[98] R. Wilson and H. Knutsson. Uncertainty and inference in the visual system. *IEEE SMC*, 1988.

[99] C. Zetzsche and E. Barth. Fundamental limits of linear filters in the visual processing of two-dimensional signals. *Vision Research*, 30(7):1111–1117, 1990.

Index